MICROCOPY RESOLUTION TEST CHART

NATIONAL BUREAU OF STANDARDS-1963-A

AFIT/GEP/PH/82D-10

INVESTIGATION OF THE FEASIBILITY OF USING LASER
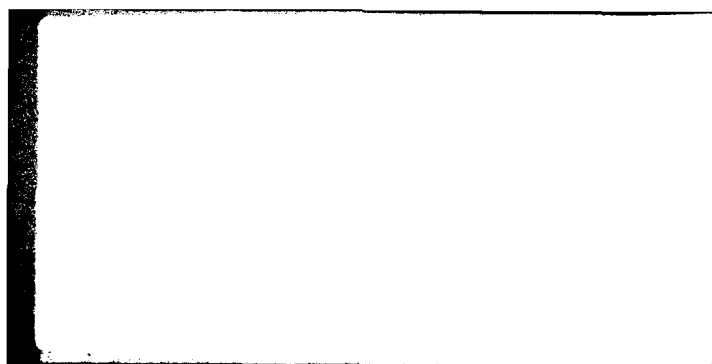
INDUCED FLUORESCENCE FOR

CONCENTRATION MEASUREMENTS OF DIATOMIC SULFUR

THESIS

AFIT/GEP/PH/82D-10 William D. Harris, Jr.
         Captain   USAF

DTIC
ELECTE
E

Approved for public release; distribution unlimited

INVESTIGATION OF THE FEASIBILITY OF USING LASER

INDUCED FLUORESCENCE FOR

CONCENTRATION MEASUREMENTS OF DIATOMIC SULFUR

THESIS

Presented to the Faculty of the School of Engineering

of the Air Force Institute of Technology

Air University

in Partial Fulfillment of the

Requirements for the Degree of

Master of Science

by

William D. Harris, Jr.

Captain   USAF

Graduate Engineering Physics

December 1982

Accession For	
NTIS GRA&I	X
DTIC TAB	☐
Unannounced	☐
Justification	
By	
Distribution/	
Availability Codes	
Dist	Avail and/or Special
A	

Approved for public release; distribution unlimited

Preface

This thesis presented a rare opportunity and a formidable challenge.
From start to finish there were daily learning experiences and situations,
some which discouraged, but many which motivated. I am thankful for
these experiences and feel I can begin to appreciate laboratory work.

I am grateful to the Air Force Institute of Technology for
maintaining its good standing within the Air Force's scientific community
and therefore allowing students access to the remarkably vast facilities
and resources of that community. In particular, my most sincere thanks
go to Dr. Won B. Roh of the Air Force Institute of Technology Physics
Department for the guidance, advice and consistent interest he invested
in this project.

Special thanks also go to the Aero Propulsion Laboratory for the
expertise and friendship of its people. I am especially thankful to
Sig Kizirnis for his encouragement, advice and timely procurement of
critical equipment. Special thanks also go to Don Linder for constructing
several essential parts of the experimental set up, Bob Brecha of
Wright State University for hour after hour of valuable assistance
during excitation scans and to Harold Norris of the University of
Dayton for helping with the initial experimental set up.

Finally, I am most grateful to my wife Laura for her understanding,
patience, and encouragement during this past year and for her typing
and improvements of the manuscript.

ii

Contents

List of Figures

List of Symbols

Roman Letters

E	Energy
exp	Exponential of the quantity following
h	Planck's constant
k	Boltzmann's constant
°K	Degrees Kelvin
P	Pressure
q	Franck-Condon factor
T	Temperature
UV	Ultraviolet
v'	Vibrational quantum number – excited electronic state
v"	Vibrational quantum number – ground electronic state
pps	Pulses per second

Greek Letters

ν	Frequency (Hz)
Σ	Summation of the quantity following

Units of Measure

Length

m	Meter
cm	Centimeter
mm	Millimeter
μ	Micron (micrometer)
nm	Nanometer

$\overset{o}{A}$ Angstrom (10^{-10} meter)

<u>Time</u>

min	Minute
sec	Second
msec	Millisecond
μsec	Microsecond
nsec	Nanosecond

<u>Voltage</u>

V	Volt
mV	Millivolt

Note: Other specific symbols are defined where they first occur in Sections II and III.

Abstract

The feasibility of using laser induced fluorescence to measure total S_2 number densities in a laboratory environment is studied. A rate equation analysis modeling transitions within the $B^3\Sigma_u^- \text{-} X^3\Sigma_g^-$ system of S_2 is developed and applied to model the $v'=9$, $v''=6$ transition at 3214.6 Å. Excitation spectra were obtained over the range of 2890 to 2810 Å clearly showing the $v''=0$, $v'=8$ and $v''=0$, $v'=9$ absorption bands. Fluorescence scans of the $v'=8$, $v''=1$ through 24 and $v'=9$, $v''=1$ through 25 were taken. After these broad spectra were identified, further investigations of the $v'=9$, $v''=6$ transition included fluorescence intensity versus temperature, laser power, and pressure. Additional measurements of quenching, radiative lifetime and self absorption are made.

ix

INVESTIGATION OF THE FEASIBILITY OF USING LASER

INDUCED FLUORESCENCE FOR

CONCENTRATION MEASUREMENTS OF DIATOMIC SULFUR

I   Introduction

Background

There is widespread interest in the development of efficient,
tunable, visible and ultraviolet lasers. In April 1977, S.R. Leone
and K.G. Kosnik (Ref 1:346) reported lasing in the $B^3\Sigma_u^- \leftarrow X^3\Sigma_g^-$
transition of S_2. The characteristics, they stated, of this dimer's
electronic lasing transition indicate the S_2 is capable of nondegradable
operation, is tunable over almost the entire ultraviolet and visable
regions of the spectrum, is scalable, has potential for efficient operation,
and offers promise for successful pumping by other excitation schemes.

Because of this potential, S_2 has been the subject of several
investigations since Leone and Kosnik's report (Refs 2, 3, 4). In
1978, D.A. Peterson (Ref 2:1-5) achieved stable glow discharges in
pure sulfur and He-sulfur at operating temperatures between 0°C
and 250°C. Spectrum analysis of this electrical pulse produced discharge
indicated only S_2 spectra in the 2800-7000 Å region. The 600°C
temperature used by Leone and Kosnik in order to increase S_2 concentrations
by thermally dissociating S_8 in the polymeric sulfur vapor, it was shown,
was not required when electrical excitation was used. Peterson's
results indicated that S_8 molecules are broken directly into S_2 molecules
and thus enhances the promise of a highly efficient discharge pumping
of the $(B-X)S_2$ laser transition at much lower temperatures than

1

previously thought.

To quantitatively determine the lasing potential of this electrically pumped S_2 discharge, or an S_2 discharge p. duced by other means, the number densities of the individual levels of interest must be found. The rate equations can be used to determine these individual level populations provided the total number density is known. The population difference between upper and lower laser levels can then be calculated and the strength of lasing determined, hence, the need for concentration measurements to determine the total number density of S_2.

'Several methods of determining number densities and species concentrations exist. Some traditional methods use material probes which disturb the discharge's flow and have limited spatial and temporal resolution. With the advent of the laser, several optical diagnostic techniques have been developed which could be used to measure species concentrations without many of the problems of traditional methods. Of these techniques, laser induced fluorescence was selected because fluorescence cross sections and resulting emission signals are generally many orders of magnitude stronger than those from the spontaneous Raman method, sensitivity is higher than that obtainable from the CARS method, nonresonance or shifted fluorescence wavelengths can be examined to avoid interference from laser scattering or competing mechanisms, and the fluorescence signal is linearly dependent on the state species concentration corresponding to the particular fluorescence transition wavelength observed (Ref 5:4).

Laser induced fluorescence (LIF) is the process of pumping molecules to higher energy levels using an excitation laser tuned through or parked on an appropriate absorption frequency, and then observing the radiation emitted in their decay to lower energy levels. LIF technique consists of two methods of spectroscopic data acquisition, excitation and fluorescence scans (Ref 6:446).

In laser induced <u>excitation</u> spectroscopy the wavelength of the excitation source is varied over a range in which the molecule or atom being studied has one or more absorption lines. As the excitation wavelength is scanned, the detector, which has been chosen and positioned so that fluorescence from <u>any</u> excited level is detected, responds whenever an absorption line is passed. This is illustrated in Figure 1.

Schematic diagram of an excitation scan showing the potential curves (electronic states) and some levels involved. The detection system measures fluorescence (downward arrow) from any excited level; this will occur each time the laser is tuned to match the frequency of some absorption line (upward arrows). As the laser is tuned through the series of absorption lines, an excitation scan results.
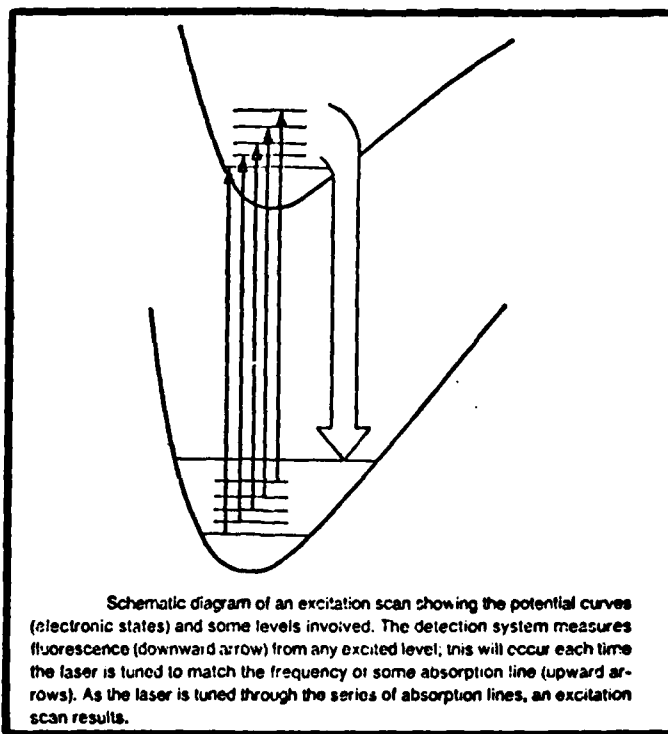
Figure 1.   Schematic Diagram of an
            Excitation Scan.   (Ref 6:446)

3

Since the intensity of each line is proportional to the ground state

level responsible for that absorption, excitation spectra can be used to

measure populations in the ground state of the molecule. Because fluores-

cence occurs each time an absorption line is crossed, an excitation

spectrum reflects an absorption spectrum. The major difference between

the two is the sensitivity which can be achieved. In absorption

spectroscopy the detector is usually positioned on line with the exciting

beam. A drop in transmitted signal corresponds to an absorption line.

Compared to the transmitted signal, the dip caused by absorption is small.

In LIF technique the signal is normally collected at 90° to the excitation

beam and a positive signal on an almost zero background results. For

this reason LIF is much more sensitive and total absorptions of 10^{-6}

or less can provide easily measured signals (Ref 6:446).

In laser induced fluorescence spectroscopy, the excitation wavelength

is tuned to a particular absorption line frequency so that molecules

are excited to a single upper state level. This is illustrated in Figure 2

on the next page. If the excitation source has a linewidth larger than

the spacing between adjacent absorption lines, more than one line will be

excited, and the linewidth would limit the resolution possible. In

contrast to ground state populations deducible from excitation scan

intensities, excited state populations can be deduced from fluorescence

spectra because the intensity of each fluorescence line is proportional

to the number density of molecules in the excited state. In the idealistic

case where there are no collision processes which populate difference

levels, the fluorescence emitted will be only that from the single

excited state. This contrasts with emission spectroscopy in which

4

Schematic diagram for a fluorescence scan. Here the laser is set at some wavelength so as to pump a specific level in the excited state. Fluorescent lines emitted by the pumped level and/or by other levels populated by collisions are separated by a scanning monochromator.
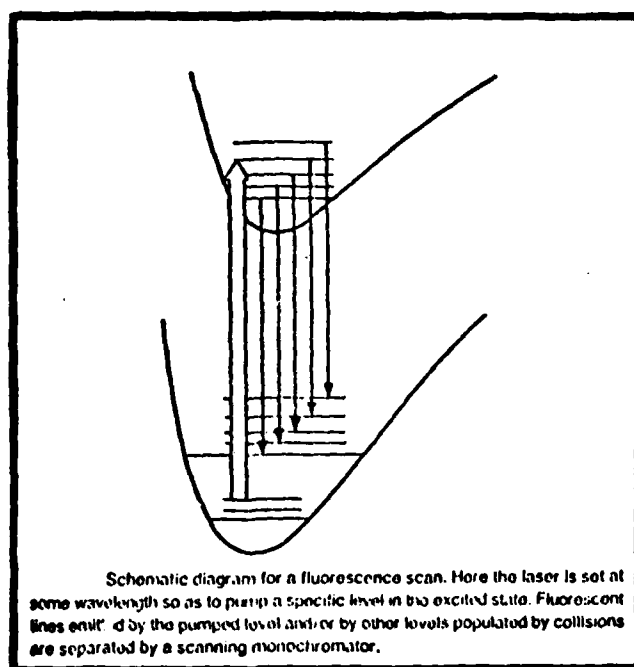
Figure 2.   Schematic Diagram of a
            Fluorescence Scan.   (Ref 6:447)

many upper state levels are populated and the resulting fluorescence

spectra can be very congested as shown in Figure 3 on the next page.

In most LIF experiments there is a colliding species which transfers energy

from the excited level to other levels through nonradiative processes.

In this case, other fluorescence lines appear in the spectra, but

overall it is still much less congested than emission spectra under

similar circumstances.

In LIF technique the emitted signal is often affected by nonradiative

processes.   These processes complicate data analysis and collection

because they reduce fluorescence intensity and reduce decay times.

Collectively they are called quenching, and include: dissociation,

chemical reactions, energy transfer to other molecules through collisions,

and energy transfer to other internal states within the molecule of

EMISSION SPECTRUM OF S_2 REGION OF (4,2) BAND

MICROWAVE DISCHARGE   SELECTIVE EXCITATION OF v'=4, N'=40, J'=41

Left, Emission spectrum from the $B^3\Sigma_u^- - X^3\Sigma_g^-$ system of the S_2 molecule excited in an electrodeless discharge, in a small wavelength region. The zero of intensity is at the bottom of the figure; the apparent offset is due to the blending of many individual lines (above 50 of which can be distinguished) emitted by many upper state levels. *Right*. The fluorescence spectrum in the same region following excitation of the single level $v' = 4$, $N = 40$, $J = 41$ of the B-state. The lines are all emitted by this level and are (in order of increasing wavelength) the $R_1(39)$, $P_1(41)$, $^rR_{13}(41)$, and $^NP_{13}(43)$.

Figure 3.   Emission and Fluorescence
Spectra.   (Ref 6;447)

interest (Ref 4:9). The techniques of saturation or near saturation laser induced fluorescence are often used to minimize the impact of quenching processes (Ref 7, 8, 9, 10 and 11).

Objective

The objective for this thesis effort is to investigate the feasibility of using laser induced fluorescence to measure total S_2 number densities in a laboratory environment. This represents the second investigation of this kind, the first having been by Robbins (Ref 4). In his investigation, Robbins used an N_2 laser to excite the (2+4) band of the $B^3\Sigma_u^- - X^3\Sigma_g^-$, S_2 electronic system. (The notation (2+4) has been introduced here to

indicate the transition from $v''=4$ to $v'=2$, i.e., $(v'{\leftarrow}v'')$. This notation will be used hencefore.) Because the N_2 laser available to Robbins ($\lambda = 3371$ $\overset{o}{A}$) was not tunable, only the $(2{\leftarrow}4)$ band of S_2 could be excited. Robbins performed broad band spectrum identification, fluorescence intensity versus temperature and laser power, effective lifetime measurements, and total S_2 number density calculations using $(2{\rightarrow}v'')$ band data. His experimentally determined number densities were too large in the low pressure region, but generally within one order of magnitude over the pressure range examined (0.31 to 12.58 torr). Differences between the known and calculated number densities were attributed to the complexity of S_2, quenching and radiation trapping, difficulties in measuring the effective lifetime, and inadequacies in the theoretical analysis (Ref 4:55).

In the present work, an experimental system was developed for making concentration measurements. This versatile experimental set up incorporated a tunable dye laser and an autotracking frequency doubler which permitted the operator a choice of excitation beam frequencies. Because $N_o \approx 1.16 \times 10^2 N_4$ at an operating temperature near 600°C, many more ground state molecules were available for excitation in this work than in Robbins. (Note: N_o represents the population of S_2 molecules in the ground vibrational level of the $X^3\Sigma_g^-$ lower electronic state, and N_4 the fourth.) By making the proper choice of dye, in this case Rhodamine 590, the $(8{\leftarrow}0)$ and $(9{\leftarrow}0)$ bands of S_2 were easily excited. The fluorescence resulting from these bands was analyzed to provide measurements of the quenching and self absorption which occurred, and insight to the

7

complex S_2 molecule. Effective lifetime measurements were obtained that were consistent with theory, unlike the previous study (Ref 4:50), and the affect of absorption was incorporated to improve the theoretical analysis.

II Theory

T. Robbins (Ref 4:11-30) provided a detailed derivation of a quanti-
tative relationship giving the total number of S_2 molecules as a function
of the observed fluorescence intensity. In this section, Robbin's
treatment is modified and condensed to model the present experimental
situation. Because of absorption of the excitation beam by S_2 molecules
prior to the beam's reaching the observed fluorescing volume, an absorption
analysis is added. The theoretical treatment will be presented in the
following order: (1) rate equations, (2) assumptions and approximations,
(3) solution to the rate equation, (4) observed fluorescence intensity
and (5) sulfur vapor composition.

Rate Equations

As stated in the introduction, the radiant power from a given fluorescence
transition, $\Phi_{f_{v'v''}}$ is proportional to the number of molecules in the
excited state, $N_{v'}$. Although the excited state population can be found
once the proportionality constant has been calculated, determination of the
total number density, N_T, from the knowledge of $N_{v'}$ requires a mathematical
model which describes changes in level populations and energy transfers
that occur in the LIF technique experiment employed. Although rigorous
models, such as the quantum mechanical density matrix approach could be
applied at this point (Ref 14:249), they are beyond the scope of this thesis.
The rate equations, which can be used for simple two-level to multilevel
models, provide the mathematical model which will be employed. To discuss
the rate equations further, the transitions and energy levels involved
in this LIF experiment need to be described.

9

Figure 4 shows the potential energy curves for the ground state and three excited states of S_2. The $B^3\Sigma_u^-$ - $X^3\Sigma_g^-$ transition was chosen
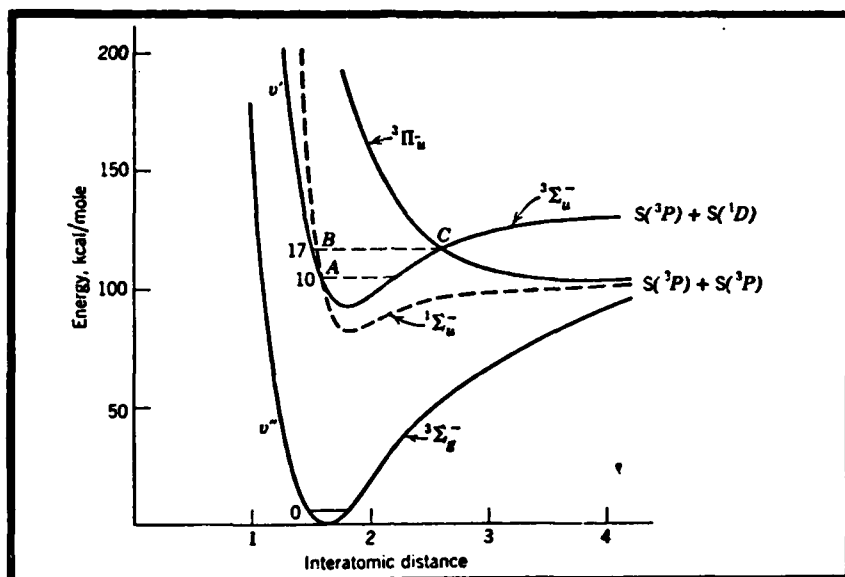
S_2 Potential Energy Curves. (Ref 12:186)

for investigation because it has Franck-Condon factors as high as 0.1 for many bands, making it the most prominent transition. According to Peterson and Schlie (Ref 3:1553), the ground molecular state $X^3\Sigma_g^-$ is formed from two ground state atoms while the $B^3\Sigma_u^-$ state originates from one excited ^1D sulfur atom and one ground state atom. (Interactions between S_2 potential energy curves will be further discussed in the results section.) Within this $B^3\Sigma_u^-$ - $X^3\Sigma_g^-$ system the (9→6) transition was selected for total S_2 concentration measurements.

Figure 5 illustrates the three level model employed in this analysis where

B_{09} = integrated Einstein B coefficient for stimulated absorption ($m^3/_{joules-sec}^2$)

B_{90} = integrated Einstein B coefficient for stimulated emission ($m^3/_{joules-sec}^2$)

10

A_{96} = Einstein A coefficient for spontaneous emission

from the v'=9 to v"=6 energy level $(\sec^{-1})$

A_{91} = Einstein A coefficient for spontaneous emission

from the v'=9 to v'=1 energy levels $(\sec^{-1})$

A_{9j} = collisional rate constant $(M^3/_{\sec})$

D_f = diffusion coefficient $(\sec^{-1})$
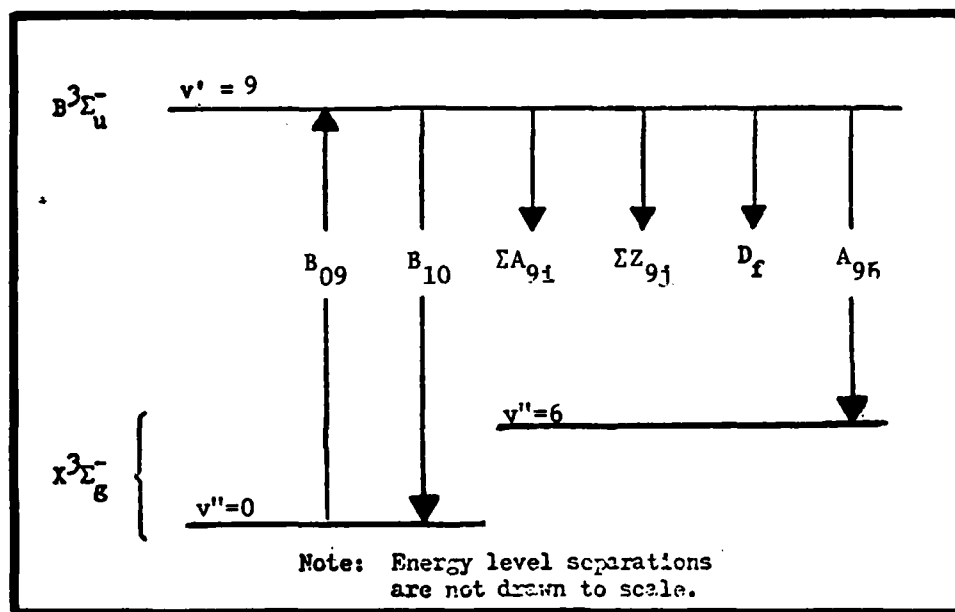
Figure 5. Three-level Model

The rotational sub-structure of each vibrational level has not been
included because the bandwidth of the excitation laser beam available
was believed to be too large to provide the resolution needed to
selectively excite and distinguish individual rotational levels.
(The excitation beam bandwidth was measured using a Fabry-Perot etalon
to be .04 $\overset{o}{A}$ at 2850 $\overset{o}{A}$ or 0.5 cm^{-1}.)

11

By referring to Figure 5, the change in population with time for the v'=9 level is given by:

$$\frac{dN_9(t)}{dt} = B_{09}\rho(\nu)N_o(t) - B_{90}\rho(\nu)N_9(t) - A_{96}N_9(t) \tag{1}$$

$$-\Sigma A_{9i}N_9(t) - Q_{9j}N_9(t)N_j(t) - D_f\nabla^2 N_9(t)$$

where

$N_o(t)$ = number density of molecules in the v''=0 vibrational

level (m^{-3})

$N_9(t)$ = number density of molecules in the v'=9 vibrational

level (m^{-3})

$N_j(t)$ = colliding molecule number density for each of the

j species (m^{-3})

$\rho(\nu)$ = laser energy density (joules/m^3-Hz)

Equation (1) can be simplified by letting

$$\sum_{\substack{i \\ i\neq 6}} A_{9i} = A_9 \text{ and } \sum_{j} Z_{9j}N_j(t) = Q_9 \tag{2}$$

where A_9 represents the total spontaneous decay rate from the upper

level to all lower levels except the one being studied in detail, and

Q_9 represents the total quenching or nonradiative relaxation rate.

Equation (1) now becomes

$$\frac{dN_9(t)}{dt} = B_{09}\rho(\nu)N_o(t) - B_{90}\rho(\nu)N_9(t) \tag{3}$$

$$-(A_{96}+A_9+Q_9)N_9(t) - D_f\nabla^2 N_9(t)$$

12

In modeling a system containing M different energy levels, the rate equations are first developed for each level in the above manner. From these a set of M coupled differential equations are formed of which M-1 are linearly independent. The additional Mth equation: $\sum_i N_i(t) = N_{Total}$ completes the set. The populations can then in theory be obtained by solving the coupled set of rate equations. The general solutions of these coupled equations are at best algebraically involved even for three-level systems and become rapidly more complicated as more levels are considered (Ref 14:254). To allow the use of each rate equation individually, simplifying assumptions and approximations are needed. This model can then be applied without solving the entire system of equations. A discussion of these simplifications follows.

Assumptions and Approximations

If certain assumptions can be made the rate equations become easier to apply. A most frequently valid assumption is steady state operation in which all time derivatives are set equal to zero. The rate equations are then solved algebraically as a system of M linear equations and M unknowns. The steady state assumption, however, is not valid for this experiment. When the laser pulse was turned on $N_9(t)$ increased: when the pulse was turned off it decreased exponentially. Because of the dynamic behavior of $N_9(t)$ the time dependence had to be retained in Equation (3).

When using lasers with high spectral intensity it is sometimes possible to saturate an absorbing transition. Saturation is the condition in which stimulated absorption and emission completely dominate other processes (Ref 15:77). Daily and Piepmeir have shown that under

saturation conditions the observed fluorescence intensity is independent of both quenching and laser power (Refs 10 and 11). Under near saturation conditions, Baronavski and McDonald have shown, fluorescence intensity versus laser power measurements will give the total quenching rate and upper level number density (Refs 7, 8). To determine if saturation conditions exist, fluorescence intensity versus laser power is experimentally measured. In Section V the results of this measurement are shown. A linear, straight line relationship resulted, indicating even near saturation was not reached.

Although neither steady state or saturation conditions were exhibited, consideration of thermal equilibrium does provide some simplification of Equation (3). Before the laser pulse occurs, the sulfur molecules are in thermal equilibrium near 600°C. Under these conditions the Boltzmann equation

$$\frac{N_j}{N_i} = \exp\left[-(E_j - E_i)/KT\right] = \exp\left[\frac{-\Delta E}{KT}\right] \tag{4}$$

can be applied to determine the relative populations N_j and N_i of any two energy levels E_j and E_i (Ref 17:18). The thermal energy KT at near 600°C corresponds to an energy gap of approximately 606 cm^{-1}, while the energy difference ΔE between the $X^3\Sigma_g^-$ ground electronic state and the $B^3\Sigma_u^-$ excited state in S_2 is roughly 3.2×10^4 cm^{-1}. Under these conditions $\Delta E \gg KT$, implying that almost all molecules are in the ground electronic state. Since experimental results indicated neither saturation or near saturation and since the laser energy density is a small number, only a small fraction of these ground electronic state molecules will be pumped to the $v'=9$ level compared to those in $N_o(t)$.

14

In addition, $B_{9,0}(\nu)N_9(t)$, the stimulated emission term, will be even smaller as it contains the product of $N_9(t)$ and $\rho(\nu)$. As a result, compared to spontaneous emission and the processes of quenching, stimulated emission will be negligible and can be disregarded for this analysis.

Still on the microscopic scale, molecules of the $v''=0$ level are in thermal equilibrium with molecules in the other vibrational levels of the ground electronic state. Compared to the thermal distribution, the processes of spontaneous emission and stimulated absorption will not appreciably affect the total population of $v''=0$. Therefore, $N_0(t)$ can be approximated as a constant, N_0. N_0 can be related to the total number of S_2 molecules, N_T, by the following argument. Using the earlier approximation $N_T=N_{e''}$,

$$N_T = N_0 + N_1 + N_2 + N_3 \ldots = N_0 Z_{v''} \tag{5}$$

where

$$Z_{v''} = \sum_{i=0}^{\infty} \exp\left[\frac{E_i - E_0}{KT}\right] \equiv \text{vibrational partition function of the lower electronic state.}$$

The relationship, then, is

$$N_0 = \frac{N_T}{Z_{v''}} . \tag{6}$$

For calibration purposes, N_T can be calculated from the amount of solid sulfur placed in the sample tube and the percentage that exists as S_2 at near 600°C. This is discussed more fully later in this section.

On the macroscopic scale, the gas within the sample tube will be in overall thermal equilibrium after the temperature stabilizes near 600°C.

Since the tube is completely sealed and heated uniformly, no temperature or pressure gradients exist within. Under these circumstances, the diffusion term $D_f \nabla^2 N_9(t)$ will be nearly zero and can be neglected.

Based on thermal equilibrium, Equation (3) can now be simplified. Letting $N_o(t)$ equal N_o and dropping the $B_{90}\rho(\nu)N_9(t)$ and $D_f \nabla^2 N_9(t)$ terms yields:

$$\frac{dN_9(t)}{dt} = B_{09}\rho(\nu)N_o - (A_{96} + A_9 + Q_9)N_9(t) \tag{7}$$

or rearranging,

$$\frac{dN_9(t)}{dt} + (A_{96} + A_9 + Q_9)N_9(t) = B_{09}\rho(\nu)N_o \tag{8}$$

Equation (8) is a first order linear differential equation that can be solved readily.

Solution to the Rate Equation

The mathematical solution to the rate equation must accurately describe the real physical phenomena if it is to be valuable. As mentioned in the discussion on approximations, two separate events occur. First, the laser pulse is on and $N_9(t)$ grows due to stimulated absorption from the $v''=0$ level. When the pulse ceases, $B_{09}\rho(\nu)N_o(t)$ vanishes because $\rho(\nu) = 0$. This situation is illustrated in Figure 6, where t_o represents the laser pulse width (6-7 msec). Equation (8), then, has two solutions. The first is valid when the laser pulse is on, during time $t=0$ to $t=t_o$, and the second after the laser pulse ends, $t \geq t_o$. When the approximate boundary conditions are used, the solution to Equation (8) becomes
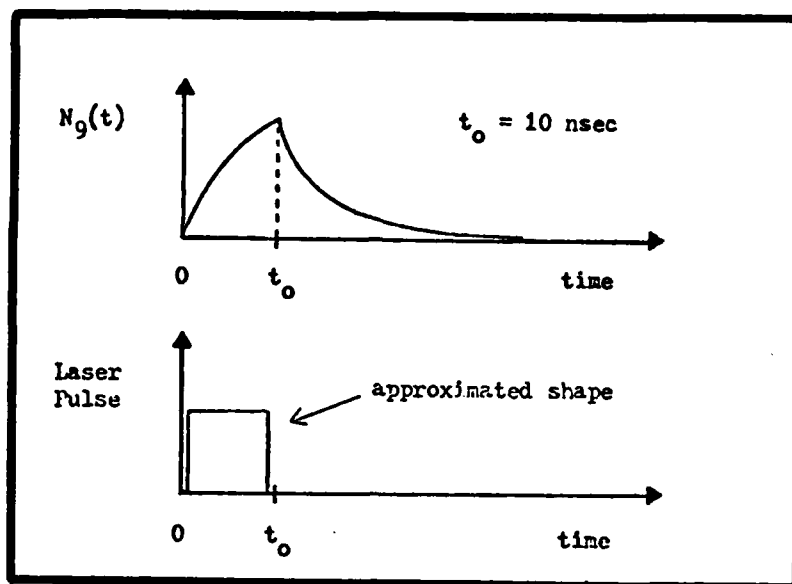
16

Figure 6. Variation of $N_9(t)$ with Time.

$$N_9(t) = \begin{cases} \tau_{eff} B_{09} \rho(\nu) N_o \left\{ 1 - \exp\left[-t/\tau_{eff} \right] \right\} & , \ 0 < t < t_o \\[3mm] \tau_{eff} B_{09} \rho(\nu) N_o \left\{ \exp\left[t_o/\tau_{eff} \right] - 1 \right\} \exp\left[-t/\tau_{eff} \right] & , \ t > t_o. \end{cases} \qquad (9)$$

where

$$\tau_{eff} = (A_{96} + A_9 + Q_9)^{-1}.$$

Substitution of Equation (6) into Equation (9) yields

$$N_9(t) = \begin{cases} \dfrac{\tau_{eff} B_{09} \rho(\nu) N_T}{Z_{v''}} \left\{ 1 - \exp\left[-t/\tau_{eff} \right] \right\} & , \ 0 < t < t_o \\[5mm] \dfrac{\tau_{eff} B_{09} \rho(\nu) N_T}{Z_{v''}} \left\{ \exp\left[t_o/\tau_{eff} \right] - 1 \right\} \exp\left[-t/\tau_{eff} \right] & , \ t > t_o. \end{cases} \qquad (10)$$

17

Because of absorption, $\rho(\nu)$ in Equation (10) is a function of
a ($a = z - z_o$, see Figure 7), the distance from the inside of the sample
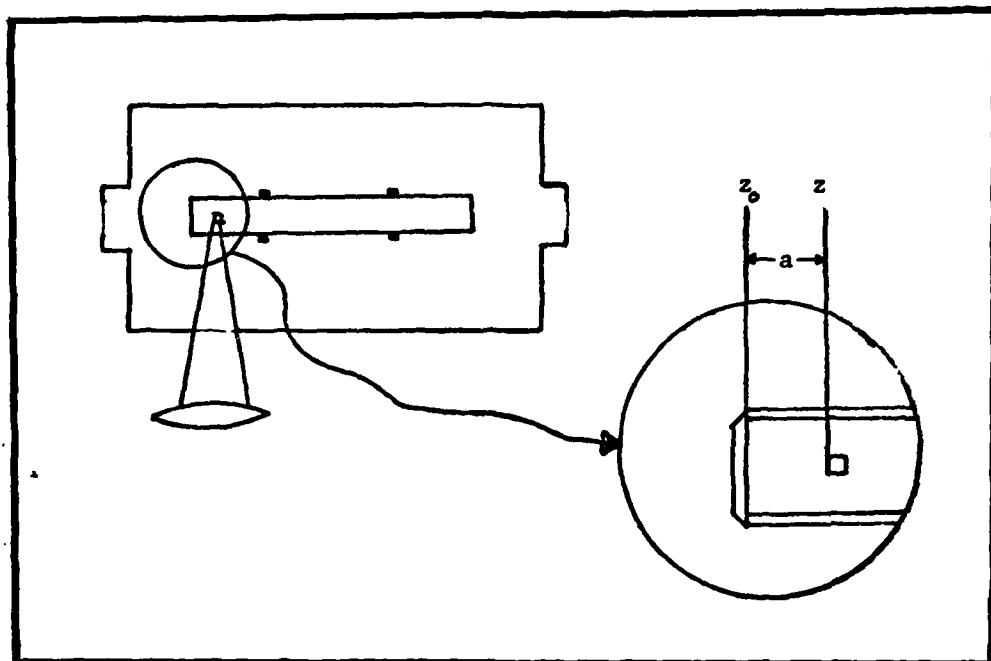

Figure 7. Absorption Considerations

tube's front window to the observed fluorescing volume, $\rho(a, \nu)$. To

consider these absorption effects quantitatively, it is convenient,

at this point, to introduce the spectral irradiance, $E_e(a, \nu)$, in

place of the radiant energy density $\rho(a, \nu)$. Use of $E_e(a, \nu)$ instead of

$\rho(a, \nu)$ changes the units associated with the Einstein B coefficients

used up to now (Ref 16:2-14). The units for B change from $\left[\dfrac{m^3}{joules-sec^2}\right]$

to $\left[\dfrac{m^2}{Watt\ sec^2}\right]$ when the relationship (Ref 17)

$$c\ \rho(a, \nu) = E_e(a, \nu) \qquad\qquad (11)$$

18

is introduced. Beer's law can now be used to give an expression for the spectral irradiance at the observed fluorescing volume

$$E_e(a, \nu) = E_e(z_o, \nu) \exp\left[-\alpha(\nu)a\right] \qquad (12)$$

where $\alpha(\nu)$ is the frequency dependent absorption coefficient. The energy density becomes

$$p(a, \nu) = \frac{E_e(z_o, \nu)}{c} \exp\left[-\alpha(\nu)a\right] \qquad (13)$$

and Equation (10) becomes

$$\dot{N}_9(t) = \begin{cases} \dfrac{\tau_{eff}B_{09}N_T E_e(z_o,\nu)}{Z_{v''}C} \exp\left[-\alpha(\nu)a\right] \left\{1 - \exp\left[-t/\tau_{eff}\right]\right\}, \\ \qquad\qquad\qquad\qquad\qquad\qquad 0 < t < t_o \\[10pt] \dfrac{\tau_{eff}B_{09}N_T E_e(z_o, \nu)}{Z_{v''}C} \exp\left[-\alpha(\nu)a\right] \\[6pt] \qquad \left\{\exp\left[t_o/\tau_{eff}\right] - 1\right\} \exp\left[-t/\tau_{eff}\right], \quad t > t_o \end{cases} \qquad (14)$$

where $\left[B_{09}\right] = \left[\dfrac{m^2}{W\ sec^2}\right]$ and $E_e(z_o, \nu)$ is the spectral irradiance measured just inside the sample tube's front window.

Observed Fluorescence Intensity

The fluorescent power associated with the $(9 \rightarrow 6)$ transition scattered in a solid angle Ω can be written as

$$\Phi_f(t) = h\ \nu\ A_{96}N_9(t)\ V\left[\frac{\Omega}{4\pi}\right] \qquad (15)$$

19

where

$\Phi_f(t)$ = the observed fluorescence power (watts)

ν = the observed transition frequency (Hz)

V = the observed volume (m^3)

The observed fluorescence power can also be related to the boxcar output in volts by the formula (Ref 4:24)

$$I_{fb}(t) = K_1 \Phi_f(t) = K_1 h \nu A_{96} N_9(t) V \left[\frac{\Omega}{4\pi} \right] \qquad (16)$$

where K_1 is a parameter with units of volts/watts that represents the effects of the spectrometer, PMT, and boxcar. As $\Phi_f(t)$ is proportional to $N_9(t)$, the observed fluorescence will exhibit the same dependence as $N_9(t)$ does, as shown in Figure 6. Therefore the total fluorescence signal will also be a combination of two functions, one for each region in time.

To properly relate the boxcar output to $\Phi_f(t)$, the observed fluorescence power, Equation (16) must be modified because the boxcar integrates the observed fluorescence signal over the aperture time, A_t. The boxcar output is then given by

$$I_{fb} = \int_o^{A_t} I_{fb}(t)dt = K_1 \int_o^{A_t} \Phi_f(t)dt \qquad (17)$$

The time dependence of $N_9(t)$ requires two integrals, one for each region of time

$$I_{fb} = K_1 \int_o^{t_o} \Phi_f(t)dt + K_1 \int_{t_o}^{A_t} \Phi_f(t)dt \qquad (18)$$

20

where $A_t > t_o$ has been assumed. By substituting the expression for $\phi_f(t)$ and $N_9(t)$ into Equation (18), carrying out the integration, and combining terms, the intermediate step below is obtained

$$I_{fb} = \frac{K_1 \, h \, \nu \, A_{96} \, V \, \Omega \, \tau_{eff}^2 \, B_{09} \, N_T \, E_e(z_o, \nu) \, \exp\left[-\alpha(\nu)a\right] C_t}{Z_{v''} \, C \, 4\pi} \quad (19)$$

where

$$C_t = \left\{ t_o/\tau_{eff} - \exp\left[(t_o - A_t)/\tau_{eff} \right] + \exp\left[-A_t/\tau_{eff} \right] \right\}$$

Upon rearranging terms,

$$N_T = \frac{Z_{v''} \, C \, 4\pi}{K_1 \, h \, \nu \, A_{96} \, V \, \Omega \, \tau_{eff}^2 \, B_{09} \, E_e(z_o, \nu) \, \exp\left[-\alpha(\nu)a\right] C_t} I_{fb} \quad (20)$$

It might appear that the desired result has been obtained at this point; however, realizing that

$$\alpha(\nu) = N_o(t) \, \sigma(\nu) \quad (21)$$

or using Equation (6)

$$\alpha(\nu) = \frac{N_T \, \sigma(\nu)}{Z_{v''}(T)}$$

it is clear that more analysis of Equation (20) is necessary. The transcendental Equation (20) can be written as

$$N_T = \frac{Z_{v''}(T) \, C \, 4\pi \, \exp\left[\dfrac{N_T \, \sigma(\nu) \, a}{Z_{v''}(T)} \right]}{K_1 \, h \, \nu \, A_{96} \, V \, \Omega \, \tau_{eff}^2 \, B_{09} \, E_e(z_o, \nu) C_t} I_{fb} \quad (22)$$

21

where Table I below summarizes the nature of each parameter.

Table I

Summary of Parameters in Equation (22)

Constants		Sulfur Data		Determined from Set Up and Equipment		Measured during Experiment	
4π	h	A_{96}	B_{09}	V	Ω	τ_{eff}	I_{fb}
k	K_1	ΔE_1	ν	T	t_o	C_t	
C		$Z_{v''}(T)$	$\sigma(\nu)$	a	$E_e(z_o, \nu)$		
				A_t			

Experimental Considerations

Once the equipment is set up for an experiment, all the parameters in Equation (22) become constant except τ_{eff}, $E_e(z_o, \nu)$, C_t and I_{fb}. τ_{eff} and C_t vary with the amount of S_2 present, while $E_e(z_o, \nu)$ will vary because the laser output varies from run to run. Based on this, Equation (22) can be written in the more basic form

$$N_T = \frac{K \exp N_T \beta}{\tau_{eff}^2 E_e(z_o, \nu) C_t} I_{fb} \qquad (23)$$

where

$$K = \frac{Z_{v''}(t) \ C \ 4\pi}{K_1 \ h \ \nu \ A_{96} \ V \ \Omega \ B_{09}}$$

$$\beta = \frac{\sigma(\nu) \ a}{Z_{v''}(T)}$$

are constants that combine the effects of all other parameters. If

22

Equation (23) is written as

$$N_T(n) = \frac{K \exp\left[N_T(n-1) \; \beta\right]}{\tau_{eff}^2 E_e(z_o, \nu) C_t} \; I_{fb} \tag{24}$$

then repeated iterations until $N_T(n) - N_T(n-1) < \varepsilon$, where ε is some

acceptable deviation, will give the desired result. The process of

iterating using Equation (24) will give the total S_2 number density as

a function of observed fluorescence power for the (9→6) transition,

based on the assumptions made in this analysis. If a precalibrated

sample cell with a known S_2 number density, N_T, is available, Equation (24)

can be solved for K by measuring τ_{eff}, $E_e(z_o, \nu)$, C_t and I_{fb}. This

K value could then be used to determine N_T under other conditions by

measuring the fluorescence intensity in addition to τ_{eff}, $E_e(z_o, \nu)$

and C_t. When precalibrated cells are not available, N_T can be calculated

from the amount of solid sulfur placed in the sample tube. Before this

can be done, the percentage of S_2 which exists under the operating

conditions of the experiment must be known. The calculated value of

N_T can then be used to determine K and other number densities as

described above.

Sulfur Vapor Composition (Ref 18:125-160)

The molecular composition of sulfur is complex and often not under-

stood, especially while in the vapor phase. In this phase sulfur is

known to exist as S_8, S_7, S_6, S_5, S_4, S_3 and S_2 molecules, the concen-

tration of each depending on the temperature and pressure. At room tempera-

tures, sulfur exists as an orthorhombic solid. It melts into a low

viscosity, yellow liquid consisting primarily of S_8 molecular rings at

about 113°C and shows no other characteristic behavior up to about
159°C. At this transition temperature, it is believed, the S_8 rings begin
to break up and form S_8 chains or polymers causing the observed sudden
increase in viscosity. Temperatures above 160°C thermally dissociate
the S_8 chains through different polymers until S_2 becomes a dominate
percentage of the sulfur vapor at near 600°C. Low pressures must be
used to completely vaporize solid sulfur for operating temperatures
below the 445°C boiling point. Figure 8 below gives a plot of total
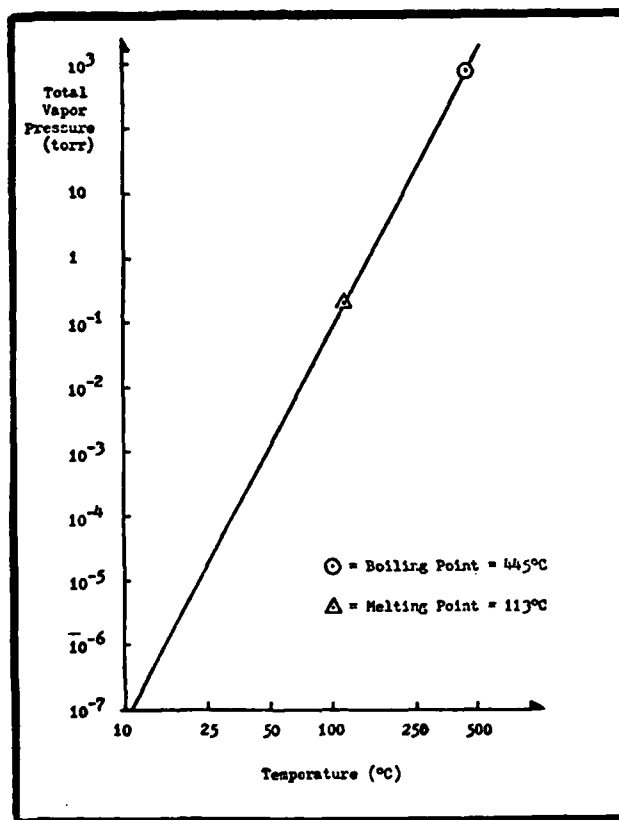sulfur vapor pressure versus temperature.

Figure 8. Sulfur Vapor Pressure versus
Temperature (from Ref 19:4-300)

In determining the reference concentration of S_2 for calibration of a sample cell, the S_2 number density can be calculated from the amount of soild sulfur placed within the sample tube. In converting from grams of sulfur to molecules of S_2 there is still some uncertainty in the percentage of S_2 existing near 600°C. Researchers have reported that over 98% is S_2 near this temperature (Ref 20:822). Other sulfur molecular species can be ignored if this percentage is accepted and the overall chemical equilibrium equation approximated by

$$S \rightleftarrows (.5)S_2 \tag{25}$$

From this equation theoretical S_2 number densities can be calculated based on the sulfur sample's weight in grams.

In contrast to this result, Braune, Peter and Neveling experimentally determined that approximately 78% of the sulfur vapor exists as S_2 near 600°C and have reported spectroscopic evidence of other molecular species at this temperature (Refs 21:33-37 and 12:149-150). If Braune's data is used to modify Equation (25) the new equilibrium equation can be written

$$S \rightleftarrows (.337)S_2 + (.065)S_4 + (.010)S_6 + (.0004)S_8 \tag{26}$$

based on measurements made at a total pressure = 92.5 torr (Ref 16:30). As measurements taken in the present experiment used pressures of 12.58 torr or less and since molecular proportions in Equation (26) are pressure dependent, the theoretical conversion of Equation (25) was used to calculate total S_2 number densities used as a standard reference throughout the results section.

25

III Experimental Apparatus

The equipment used in this experiment is described below under
the subheadings of: (1) sample chamber, (2) excitation source, (3) optical
system and (4) electronics. The experimental set up for the various
experiments performed is illustrated in Figure 9 on the following page.

Sample Chamber

The oven and the sulfur tubes described below were the same as
those used by T. Robbins (Ref 4:31). The three sample tubes, fabricated
in the laboratory, were constructed from quartz tubing and windows, and
were evacuated to approximately 10^{-7} torr. After known amounts of solid
sulfur were measured and placed in the evacuated tubes they were sealed
off. The amounts of the 98% pure Eagle-Picher of Oklahoma sulfur were
controlled to insure desired pressures at operating temperatures.
The pressures used to characterize each sample tube were calculated
at 590°C. The locally fabricated oven was constructed out of sheet metal
and lined with fiberfax insulation, was 22 cm wide, 45 cm long, and
28 cm tall. It was heated electronically with nichrome wire filaments
strung in four loops along the inside walls. Temperature inside the
oven was regulated by a Fenwal Model 199 digital temperature gauge and
Type K thermocouple. One and three quarter inch diameter (38mm)
Amersil-Supersil circular quartz windows on each end of the oven permitted
the ultraviolet laser beam to pass through. A one and one-half inch
(32mm) diameter circular quartz window on one side of the oven allowed
sampling of the fluorescence signal. The quartz windows were necessary
for high temperature operation and maximum transmission of the ultraviolet
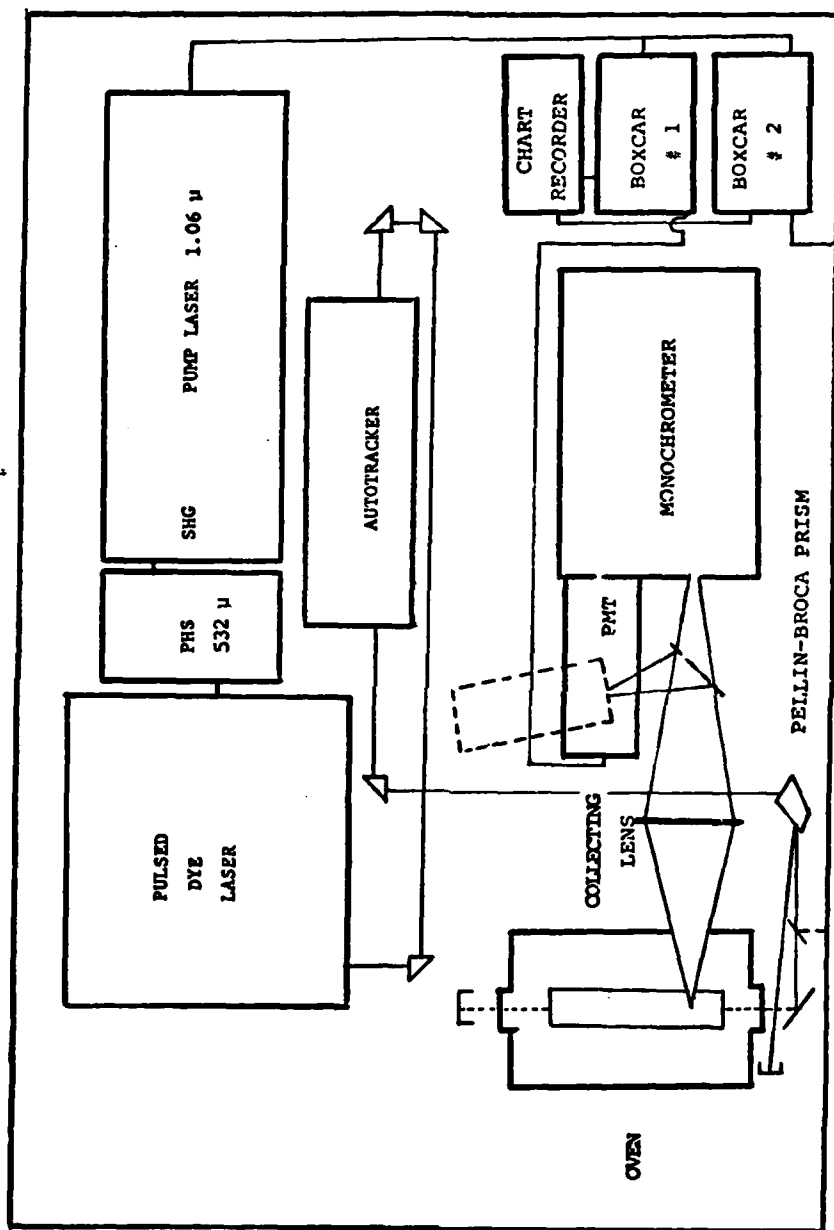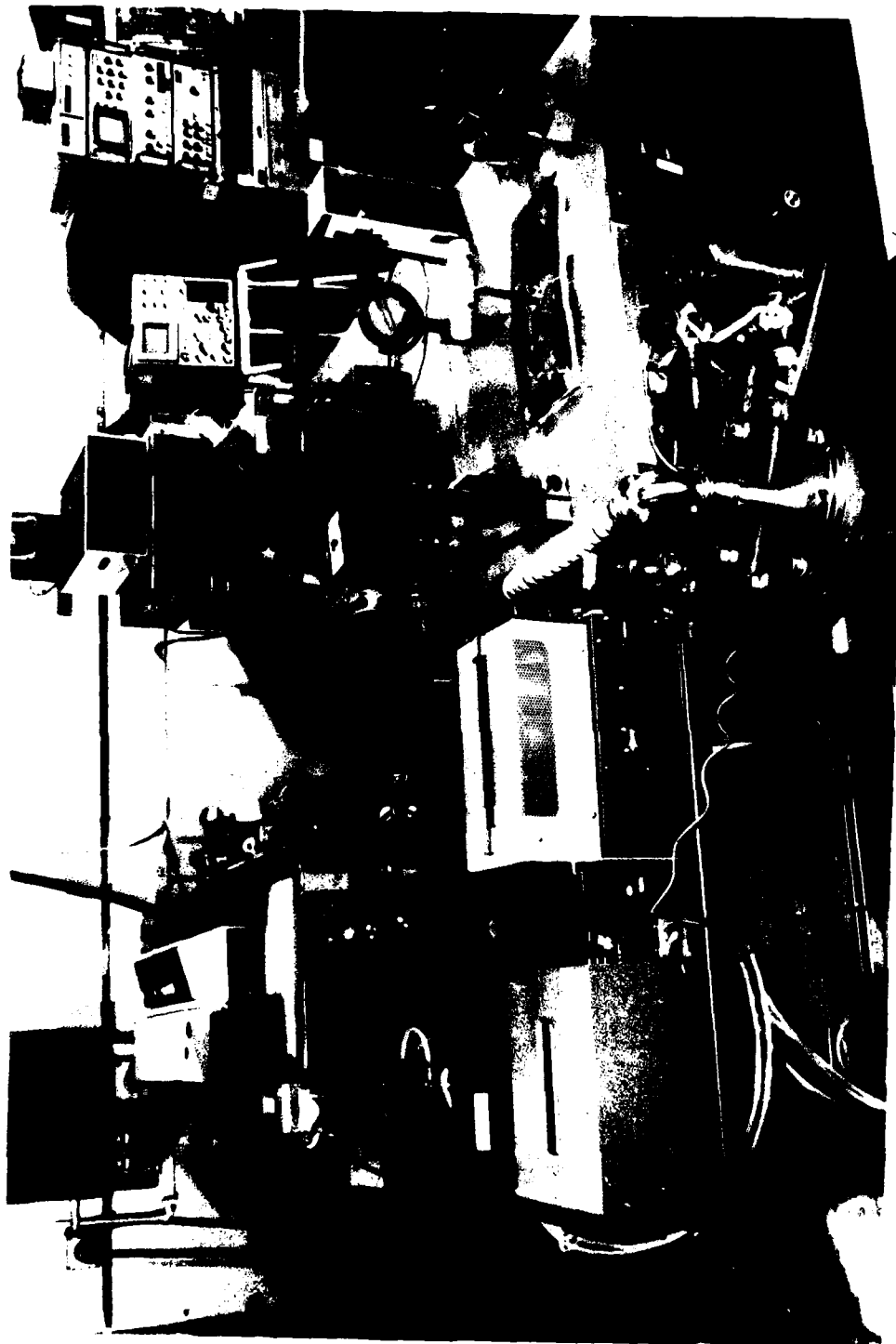
26

Figure 9. Experimental Set-up

Figure 10. Experimental Set Up (Photo)

28

laser beam, Sample tubes were placed inside the oven through an opening in the top and rested on a "v" shaped cradle. The cradle was oriented such that the axis of the sample tube very nearly coincided with that of the ultraviolet beam. In addition to the temperature regulator, an Omega Engineering Model 199 K Chromel Alumel provides continuous digital temperature readings.

Excitation Source

A Quanta Ray Nd:YAG laser Model DCR-2A-10 Head diffraction centered resonator (DCR) operating at 10 pps produced the fundamental 1.06 micron infrared beam which was frequency doubled, using Quanta Ray type II second harmonic generating crystals (SHG), to 532 nm. A Quanta Ray HG-2 temperature controller maintained the SHG in proper alignment after initial optimization of the 532 nm beam. Both the fundamental and second harmonic beams then passed into the prism harmonic separator (PHS) in which the 1.06 micron beam was directed into a beam dump. The 532 nm beam passed through the PHS and was used to pump the Quanta Ray Model PDL-1 tunable pulsed dye laser (PDL). The Rhodamine 590 molecular dye concentrations used in the PDL were optimized for a dye laser beam of 560 nm or 280 nm after a second frequency doubling.

Energies for the DCR oscillator and amplifier flashlamps of 60 joules were generally used. In Q-switched mode the frequency doubled laser pulse duration was 5 or 6 nsec. Because of the limited spectral response of the ScienTech Model 3600 detector available and the unavailability of a calibrated detector with a response in the ultraviolet region, absolute power measurements were not performed on the UV beam.

29

The variable Q-switch sync pulse out of the DCR was used for triggering the detection device/devices being used. Jitter between the variable Q-switch sync pulse and the actual Q-switch was specified .25 nsec or less. The laser linewidth of the dye laser beam determined from measurements taken using a Fabry-Perot etalon was 0.5 cm^{-1}. For most applications the PDL grating was used in fifth order. A reversible stepping motor with gear train was used to drive the dye laser grating at various speeds. An Inrad Model 5-12 autotracker was used to frequency double the green-yellow dye beam from the pulsed dye laser while the grating of the PDL scans over wavelengths of interest. The dye laser beam was turned and then aligned to the autotracker using three 90° prisms mounted on adjustable bases.

Optical System

After the pulsed dye laser beam was doubled by the autotracker the ultraviolet portion was directed to the input window of the oven by a quartz turning prism, a Pellin-Broca prism, and an aluminum mirror. The dispersion of the Pellin-Broca was used to separate and direct the visible portion of the dye laser beam, which could not be doubled by the autotracker, into a beam dump. This method of separating the fundamental dye beam from the harmonic dye beam provided greater intensities than using a filter to absorb the visible light. Since the ultraviolet beam had a clean profile an aperture was not needed to limit its size. To monitor the ultraviolet beam power, a pelicle was often placed between the Pellin-Broca prism and the aluminum mirror to pick off a small constant fraction of the UV beam and direct it

30

to a vacuum photo diode or other detector whose output was used to monitor or normalize the collected signal.

For excitation scans, the monitoring detector was an RCA 8850 photomultiplier tube. Since this PMT had the same spectral response as the RCA 8850 used to detect the fluorescence signal, its trace was used to normalize the detector spectral response out of the signal. For fluorescence scans an ITT F4000 model Vacuum Photodiode with an S-1 cathode with a spectral response ranging from 2000 $\overset{o}{A}$ to 10,000 $\overset{o}{A}$ was the UV monitoring detector.

The fluorescence signal was collected at right angles to the laser beam in the tube by a 9 cm diameter circular lens with a 20 cm focal length. This signal was focused into the entrance slit of a Jarrell-Ash Model 82-000 half-meter Ebert scanning spectrometer. This spectrometer contains a 52 mm by 52 mm grating ruled at 30,000 groves per inch (approximately 1180 groves per millimeter) and blazed for 4000 $\overset{o}{A}$ in the first order. The plate factor or reciprocal linear dispersion at the exit slit is 16 $\overset{o}{A}$ per millimeter under these conditions. After passing through the spectrometer, a 14 stage linear dynode chain Emi-Tronics (EMI) Model 9816B PMT with an S-20 spectral response was used as the detector.

For excitation scans the spectrometer was not used. A first surface aluminum mirror, reflected the fluorescence signal converging toward the spectrometer onto a slit attached to the RCA 8850 detection PMT housing. The mirror was positioned such that the distance from the observed fluorescing volume to the spectrometer slit and that to the slit of the RCA PMT were the same to within $\pm$ .5". Care was taken that

31

the mirror did not become the aperture stop of the detection optical system. The RCA 8850 PMT has twelve dynode stages and an RCA 116 spectral response. The peak response is as with the EMI PMT at 4000 $\overset{o}{A}$ with a quantum efficiency of approximately 30% at that wavelength. Both PMTs were operated at 2000 volts.

Electronics

The signals from the detector PMT and the UV monitor were averaged by means of a pair of PAR 160 boxcar integrators. As shown in Figure 11, the triggering of the boxcars occurs approximately 280 nsec prior to the UV monitor and fluorescence detection signals reach the boxcars circuitry. This is possible because of a variable Q-switch sync pulse from the Quanta Ray DCR. A Tektronix Model 7104 oscilloscope was used to check the jitter between the Q-switch sync pulse of the DCR, which has a specified jitter of less than .25 nsec, and the variable Q-switch sync pulse. No significant jitter between the two was observed.

Output from the boxcars was recorded on a Hewlett-Packard Model 7132 A chart recorder. Special events were marked by applying a brief voltage to the UV monitor's chart recorder pen.
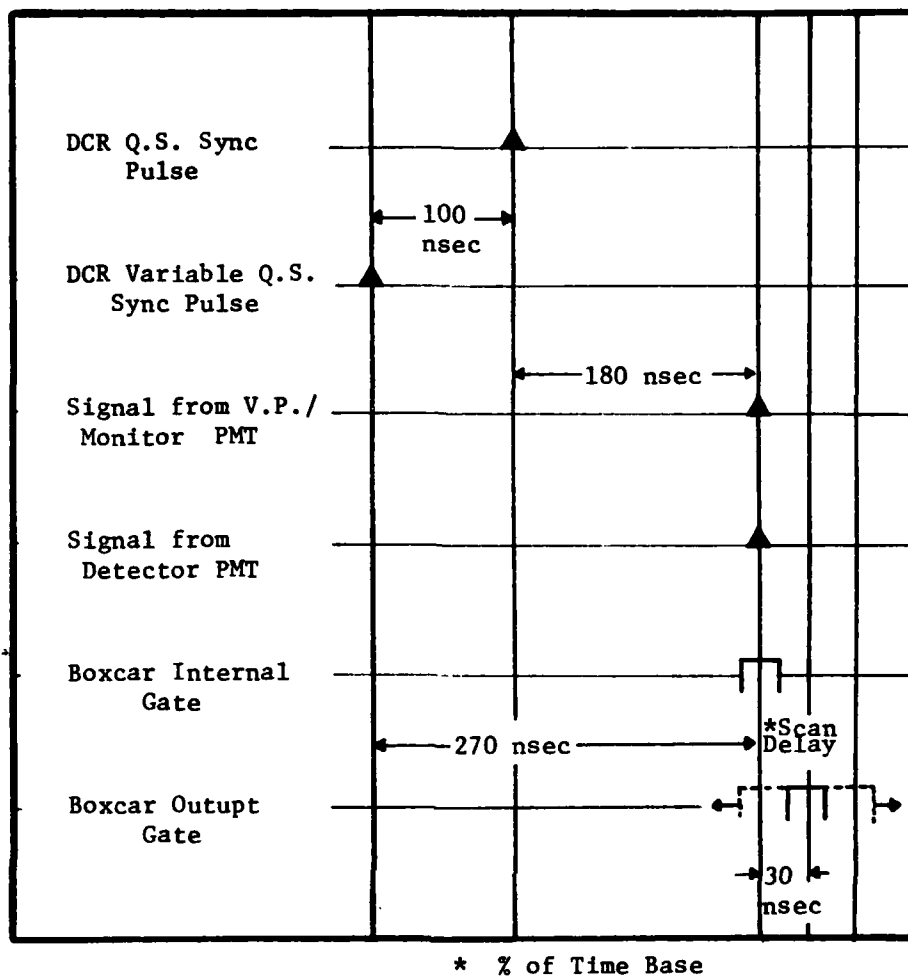
32

Figure 11.   Triggering Scheme

IV Procedure

In this section, the experimental method is described in detail and the idiosyncrasies of the technique briefly explained. The subheadings are (1) excitation scans, (2) broad band fluorescence spectra, (3) fluorescence intensity measurements, (4) fluorescence lifetime measurements, (5) self absorption and (6) concentration measurements.

Excitation Scans

During an excitation scan, the excitation wavelength from the PDL changes. As a result, the phase matching direction of the doubling crystal continuously changes, and constant retuning is required throughout the scan. Attempts were made to retune the crystals by monitoring the strength of a split portion of the beam with the Tektronix 7104 oscilloscope and manually adjusting the phase matching micrometer on the crystal's turret. This method proved insufficient because the phase matching direction changed faster than the crystal could be manually retuned. Time constraints and PDL grating motor drive speeds available prevented slowing down the process. To remedy this situation an Inrad autotracker was employed which could detect wavelength changes in the incident beam and then properly align the crystals before a significant drop in output beam intensity occurred.

The change in excitation beam wavelength referred to above, is produced by the grating drive motor turning the grating of the PDL. Since the distribution of fluorescence intensity with wavelength of the Rhodamine 590 dye changes considerably over the wavelength region scanned, the excitation beam irradiance changes. To account for these changes

in the dye laser's irradiance with wavelength, or spectral irradiance, a beam splitter was used to direct a small portion of the excitation beam to a monitoring detector. Since the monitoring RCA 8850 PMT was identical to the RCA 8850 PMT used to detect the fluorescence signal, the trace on the chart recorder from the monitoring PMT output could be used to normalize out laser power dependence.

Another consequence of the change in excitation beam wavelength during an excitation scan was peculiar to the experimental set up used. Since the dispersion from the Pellin-Broca prism changed with the incident beam's wavelength, "beam walking" of the primary excitation beam and the portion split off for monitoring was observed. Figure 12 illustrates this beam walking.

Although using a filter which could absorb the visible beam would have eliminated the beam walking, it would have reduced the UV beam irradiance considerably more than the Pellin-Broca. This would have decreased the possibility of saturating the transitions being investigated.

To compensate for the monitor's beam walking, a spherical first surface aluminum mirror reflected and focused the relatively low intensity ultraviolet light onto a neutral density placed in front of the PMT's slit. The slit was opened to approximately 2.5 mm while the spot diameter of the focused beam at the neutral density filter as checked using a fluorescence card was less than 1 mm. Although the beam was incident upon the spherical mirror at slightly different angles during a scan, the focused spot showed no perceptible movement.
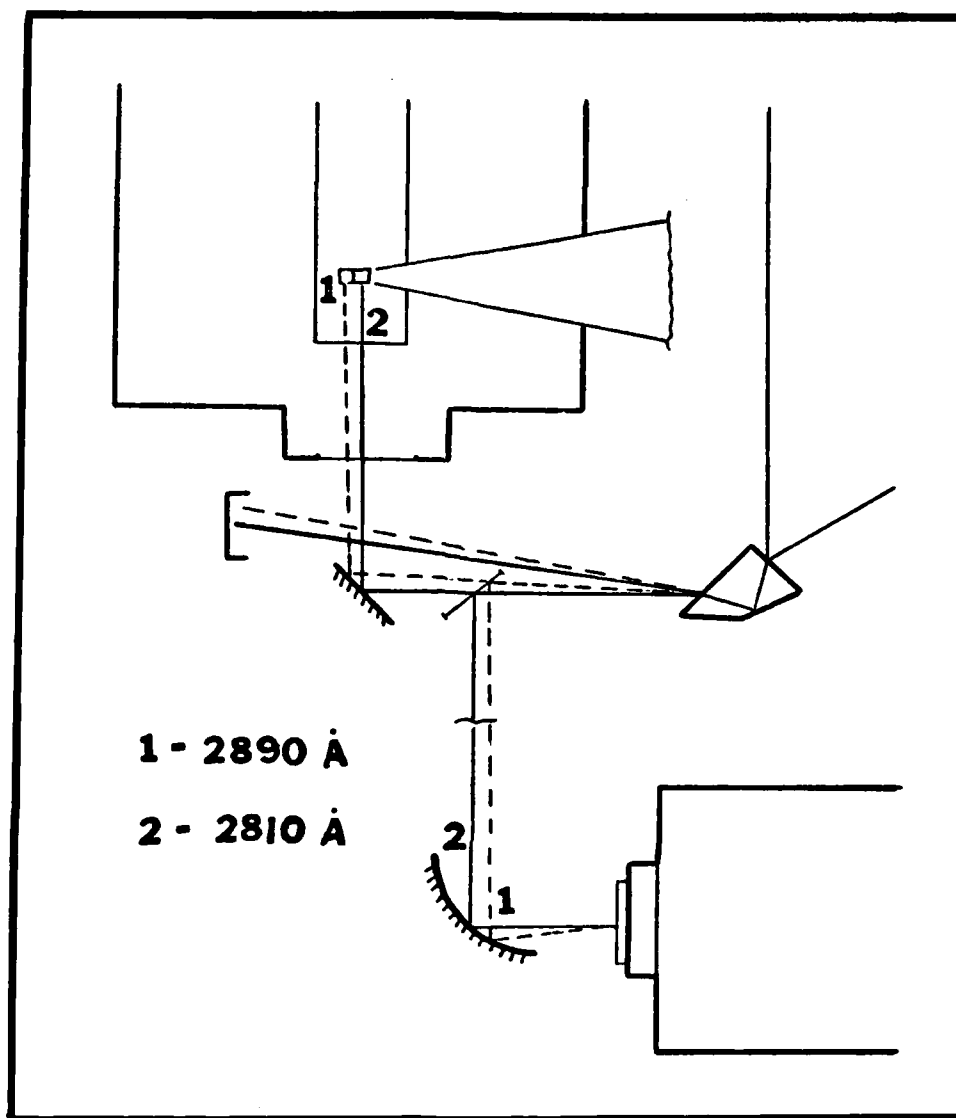
35

Figure 12. Beam Walking

Beam walking of the excitation beam was minimized by reducing the
distance from the Pellin-Broca prism to the observed fluorescence volume.
While this did not eliminate it, the same "walking" occurred for each
run so the error caused was systematic. At the fluorescing volume the
beam diameter measured using a fluorescence card was 5 mm. The total
travel of the walking beam during a scan from 2890 to 2810 $\overset{o}{A}$ was 4 mm.

Prior to a set of scans, the aluminum mirror which directed the beam
into the oven was aligned such that the center of the 5 mm beam at the
fluorescence volume was pierced, by the beam of an HeNe laser back-
lighting the spectrometer through the collection optics, when the PDL was
set at mid-scan wavelength. This assured maximum exposure of the ob-
served fluorescence volume to the excitation beam as it walked. No
beam intensity profiles of excitation beam were made.

Excitation scans were taken at $590° \pm 5°C$ for each of the three
pressures (i.e., sample tubes) available, and ranged from 2890.0 $\overset{\text{o}}{\text{A}}$
to 2810.0 $\overset{\text{o}}{\text{A}}$. The RCA 8850 fluorescence detecting PMT was operated at
2000.volts with a slit width of 11.5 microns while the monitoring RCA
8850 PMT was operated at 900 V and had 2.5 mm slits. A filter was
secured to the front of the detection PMT to prevent the green-yellow,
scattered and reflected, dye laser light from causing strong background
noise.

Broad Band Fluorescence Spectra

Since changing sample tubes (i.e., pressures) required approximately
one and one-half hours cooling and heating time, fluorescence scans
followed each excitation scan. The excitation wavelength was parked at
the wavelength corresponding to the maximum excitation scan fluorescence
signal. Since there were two separate vibrational bands being excited
over the range of the excitation scans, two maxima occurred, and two
fluorescence scans were taken at each pressure. One scan was of fluores-
cence from the $v'=8$ level and the other from the $v'=9$.

After setting the appropriate excitation beam wavelength using
the PDL, the monochrometer was scanned from 5300 $\overset{\text{o}}{\text{A}}$ to 2800 $\overset{\text{o}}{\text{A}}$ at 50 $\overset{\text{o}}{\text{A}}$/min.

For pressures of 3.47 and 12.58 torr the monochrometer slits were set at 50μ, while because of the weaker fluorescence signal 350μ slits were used with 0.31 torr. (Slit widths were not varied during fluorescence intensity measurements but were allowed to vary during scans because of the improved resolution which resulted in the 3.47 and 12.58 torr spectra.) Since the EMI Model 9816 B PMT with S-20 spectral response had the proper mount for maring with the Jerrel Ash half meter monochrometer, it was used for fluorescence scans. As another PMT with S-20 response was not available (and was not as critical as with excitation scans), either the RCA 8850 PMT or an ITT Model F4000 vacuum photodiode were used for monitoring the laser power. The spherical mirror set up was not normally used during fluorescence scans because beam walking did not occur. The monochrometer scanned the fluorescence signal but the excitation beam wavelength was static. Since the monochrometer separated out most of the extraneous light, a filter was not placed in front of the detection PMT during fluorescence scans as it was for excitation scans.

The monochrometer was calibrated using a mercury lamp prior to the fluorescence scans. Although the slit widths were not the same as those used in the fluorescence scans, the calibration was sufficient to permit identification of the various peaks observed by comparing values with tables in Peterson and Schlie's work (Ref 3:1559-1561). A qualitative comparison of the individual peak's intensity with Franck-Condon factors was also made.

Fluorescence Intensity Measurements

After identifying the S_2 spectra, prominent lines were selected for further study. The (8→4) at 3114 $\overset{\circ}{A}$ and the (9→6) at 3215 $\overset{\circ}{A}$ transitions

38

were among the strongest in intensity, taking the spectrometer's blaze

wavelength (4000 $\overset{o}{A}$) and the EMI PMT spectral response into account.

Having zeroed in on these two prominent peaks, further measurements

were made. The spectrometer was set to the appropriate wavelength and

once again, as with the excitation scans, the excitation wavelength

scanned over the vibrational absorption band (2890 – 2850 $\overset{o}{A}$ for the

(8→4) peak and 2850 – 2810 $\overset{o}{A}$ for the (9→6) peak). Since time did not

permit further investigation of both fluorescence transitions, the (9→6)

line was selected for detailed study and the excitation wavelength

parked at the value corresponding to maximum (9→6) fluorescence.

For fluorescence intensity versus laser power measurements the

(9→6) transition was optimized using all parameters except laser power.

Then, using the flash lamp potentiometer dial on the laser head of the

DCR, the laser power was varied over the available range. Although,

saturation is not a function of number density this procedure was

completed for each tube. Because the optimized fluorescence peak

had moderate intensity fluctuations, the high resolution time constant

of the detector's boxcar was increased and the chart recorder ran for

approximately two minutes at each power after sufficient time was allowed

for the slower boxcar output to fully respond. An average value and an

estimate of the noise was taken for each sampled power. After the

fluorescence scans, the monochrometer slits were maintained at 250μ.

Although smaller slits could have been used (and were for the fluorescence

scans) for 3.47 and 12.58 torr pressures, the fluorescence from the 0.31 torr

tube was too weak to be detected when more narrow slits were used.

Fluorescence intensity versus temperature measurements of the (9→6)
transition were made by gradually heating the oven from room temperature
to near 600°C, while stopping to take intensity measurements at a
variety of temperatures above 250°C. The Fenwal Model 199 temperature
regulator allowed temperatures to oscillate ± 8°C from the set value.
Sufficient time for the temperature to stabilize and the effects of
quartz's thermal inertia to be neglected was allowed at each value
selected. Four measurements were obtained using the 3.47 torr tube.

A single fluorescence intensity versus pressure measurement trial
involved three separate intensity measurements. In a single intensity
measurement, one of the sample tubes was heated to 590°C without stopping at
intermediate temperatures. After the temperature stabilized at 590°C,
the (9→6) transition fluorescence intensity was measured. The oven was
then allowed to cool so one of the remaining two tubes could be heated
and another intensity measurement taken. Seven fluorescence intensity
versus pressure measurement trials were accomplished so an estimate of
the random error could be made. Sometimes fluorescence intensity versus
pressure measurements were taken concurrently with fluorescence intensity
versus laser power measurements. This proved to be a more efficient use
of time. Incorporating a fluorescence versus temperature measurement
would have taken longer and it would have been difficult to insure the
same laser power from pressure to pressure.

All fluorescence intensity versus pressure measurements were made
using the same parameters from sample tube to sample tube for a given
single trial but not necessarily from measurement trial to measurement
trial. Parameters which were allowed to vary from trial to trial were

laser power (because of the tendency of the dye to weaken), input
sensitivities, and neutral density filters. These should not have
effected the intensity versus pressure relationship.

As described in Section II, absorption is a function of number
density, therefore its influence was greater for higher pressure tubes.
In an effort to reduce spectral absorption effects the observation volume
was kept as close as possible to the front window of the sample tube.

Fluorescence Lifetime Measurements

(9→6) S_2 fluorescence lifetime measurements at specific temperatures
and pressures were made directly from the oscilloscope display using
the Tektronix camera. Usually ten single sweeps were exposed on a single
photograph to provide an average profile. The effective lifetime of this
transition's fluorescence was obtained by measuring the time required
for the observed fluorescence signal to drop to 1/e of the value displayed
the instant the laser pulse ended. Effective lifetime measurements
were then used to determine the radiative lifetime and the quenching rate
constant using a Stern-Volmer plot.

Self Absorption

As with fluorescence intensity versus temperature, measurements
were made at various temperatures after sufficient time had been allowed
for temperatures to stabilize. Spectrometer scans were then made
from 3300 $\overset{o}{A}$ to 2800 $\overset{o}{A}$ showing the (9→6) through (9→1) transitions. The
relative intensities of the (9→6) through (9→1) fluorescence bands as
a function of temperature was determined in order to see if self absorption
was evident. In doing so all the band intensities were normalized to

41

that of the (9→6) band, which was expected to be least affected by self absorption in view of the negligible thermal population in v"=6.

Concentration Measurements

Concentration measurements were essentially fluorescence intensity versus pressure measurements in which the excitation beam's absolute power is known. Measurements of the ultraviolet excitation beam were made with a Scientech Model 362 power/energy meter and a Model 3600 detector and the ITT F4000 vacuum photodiode. No response was obtained from the Scientech power meter to the 2830.7 $\overset{\circ}{\text{A}}$ excitation beam so an attempt to calibrate the vacuum photodiode was made.

V Results and Discussion

The experimental results are presented in this section. The data
and analyses are discussed under the subheadings of (1) excitation spectra,
(2) broad band fluorescence spectra, (3) fluorescence intensity measure-
ments, (4) fluorescence lifetime measurements, (5) self absorption and
(6) concentration measurements.

Excitation Spectra

Initial excitation spectra were taken for each of the three pressures
available with the fluorescing volume near tube center. These spectra
are shown in Figures 13 through 15 on pages 44 through 46. After
modifying the set up to reduce the affect of spectral absorption, excitation
spectra were once again taken for each pressure. These are presented
in Figures 16 through 18 on pages 47 through 49.

Although the detector PMT slit was 115μ for the initial excitation
scans and 11.5μ for the later arrangement, no other parameter of conse-
quence varied significantly (initial scan temperature was 590°C while
in later scans the oven reached only 585°C because of the new window
position). Both sets of scans clearly show two absorption bands, one
(8←0) and the other from (9←0). Generally the (8←0) band showed a
broader intensity distribution while the (9←0) showed a more narrow
intensity distribution. Reproducibility runs of these spectra showed
that the structure on the large bands is real and not noise. Each
partially resolved peak results from a rotational level being excited.
The intensity displayed by each peak is theoretically related to the
rotational level's population. With improved laser power normalization,

43
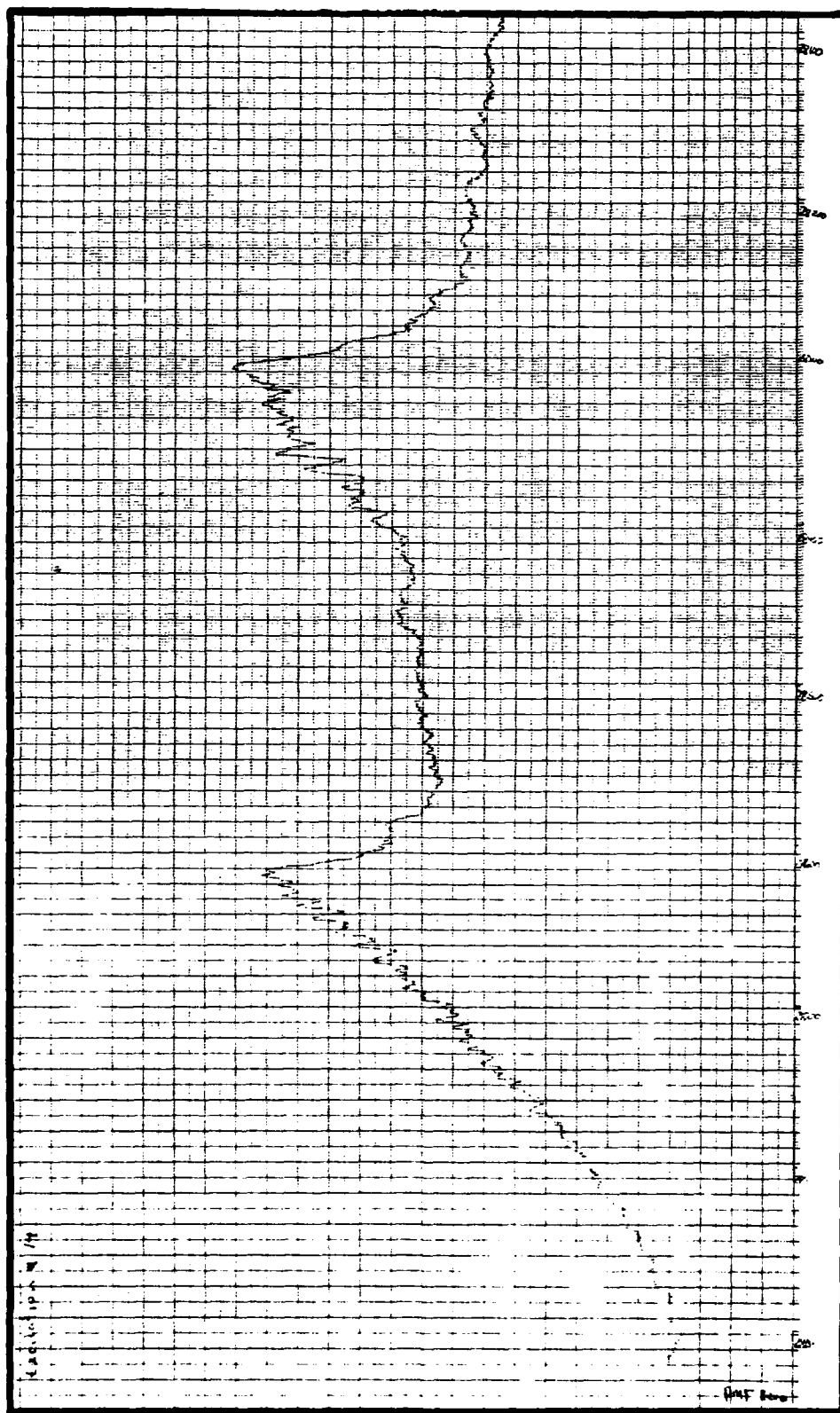
Figure 13, Excitation Spectrum, Center Tube Observed
Fluorescence Volume (0,31 torr)
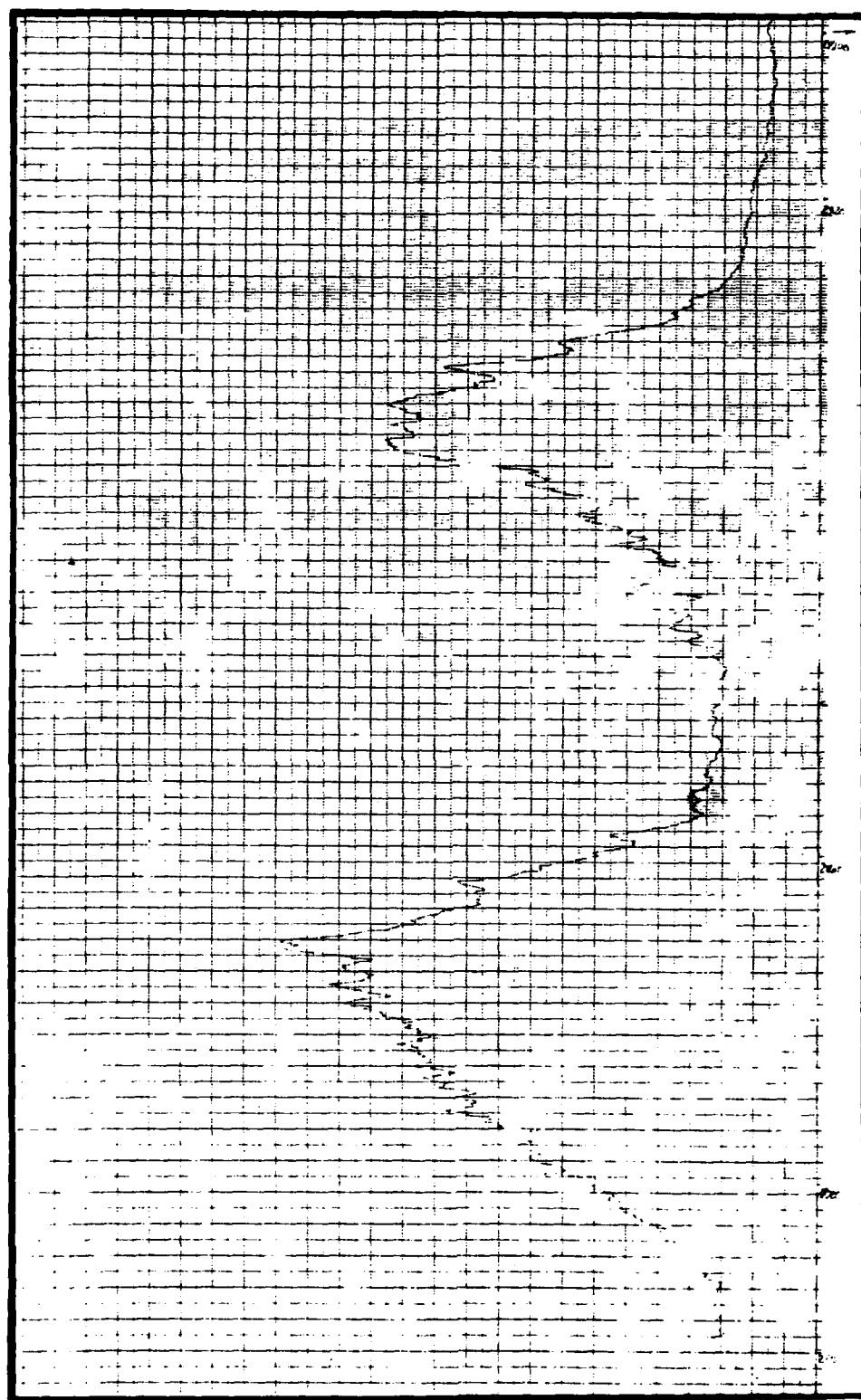
Figure 14. Excitation Spectrum, Center Tube Observed
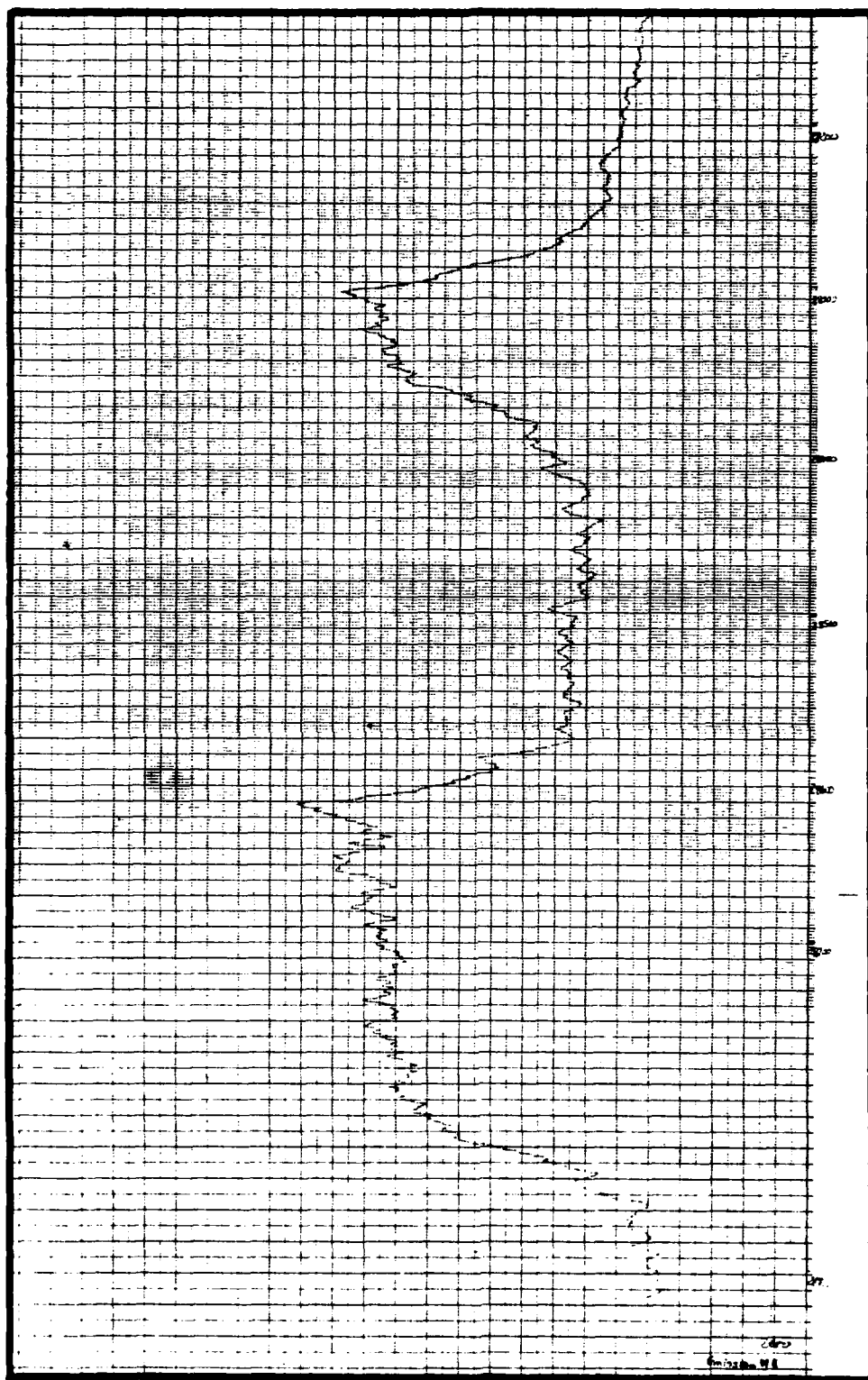Fluorescence Volume (3.47 torr)

Figure 15. Excitation Spectrum, Center Tube Observed
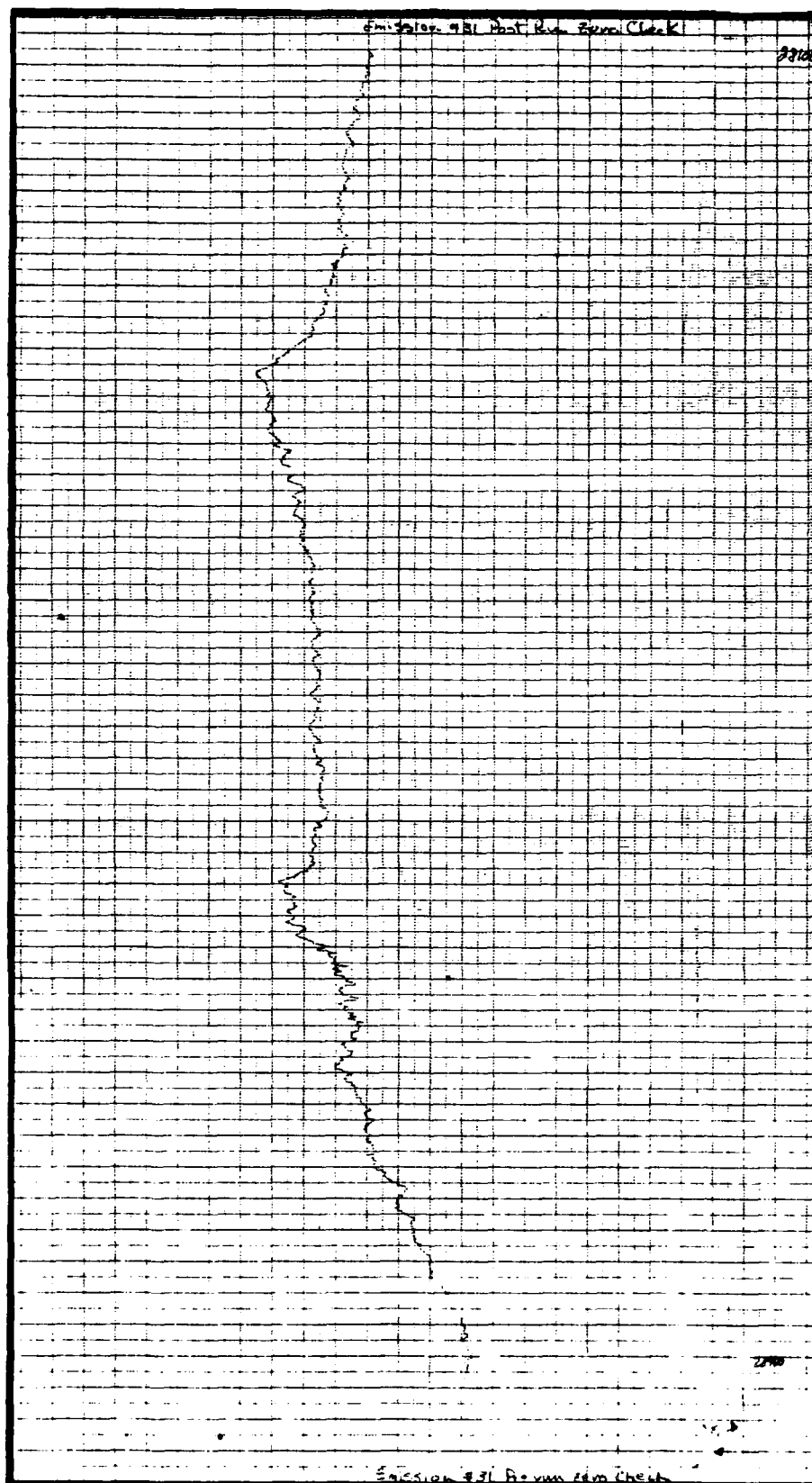Fluorescence Volume (12.58 torr)

Figure 16. Excitation Spectrum, Observed Fluorescence
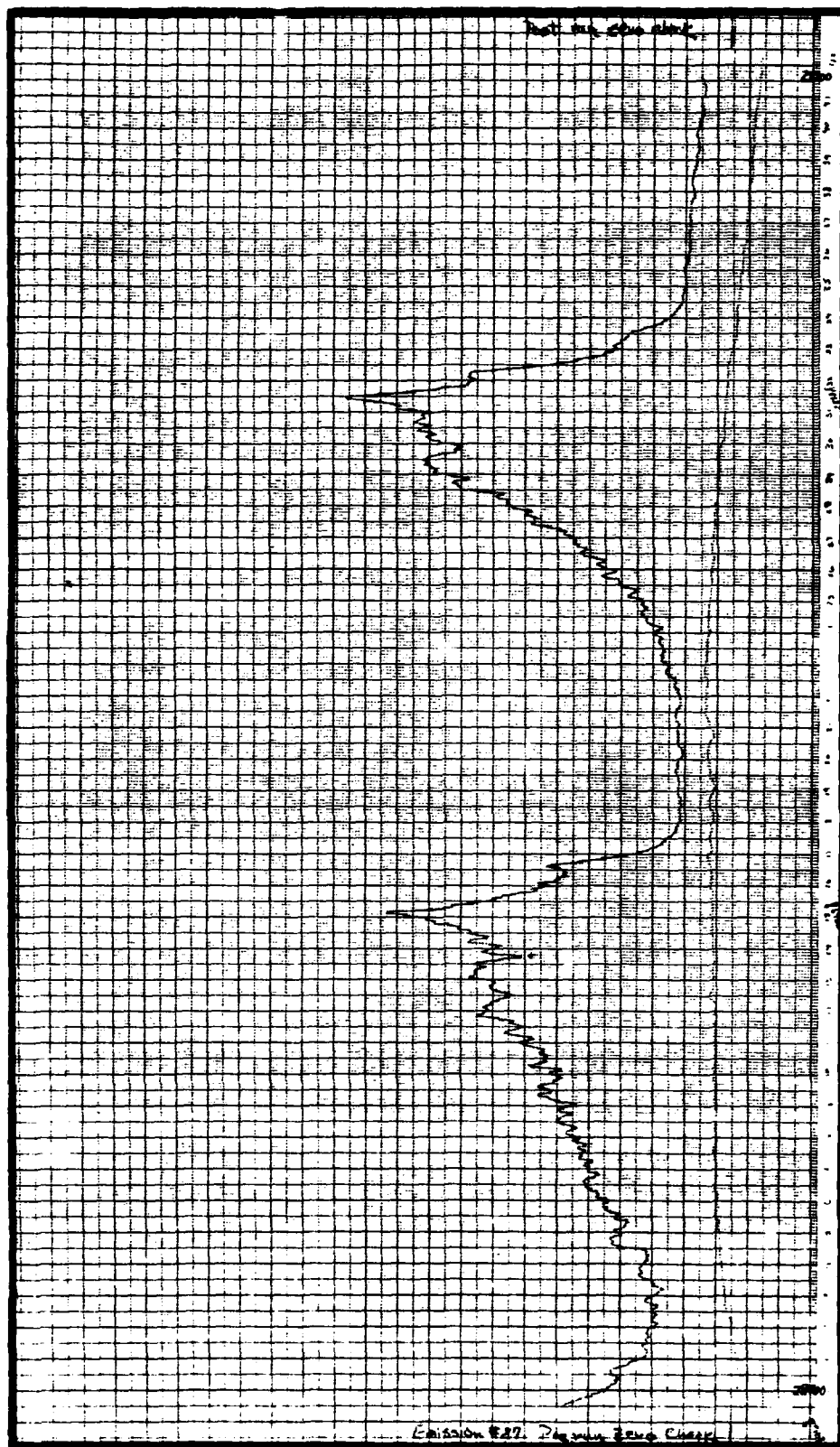Volume near Front Tube Window (0.31 torr)

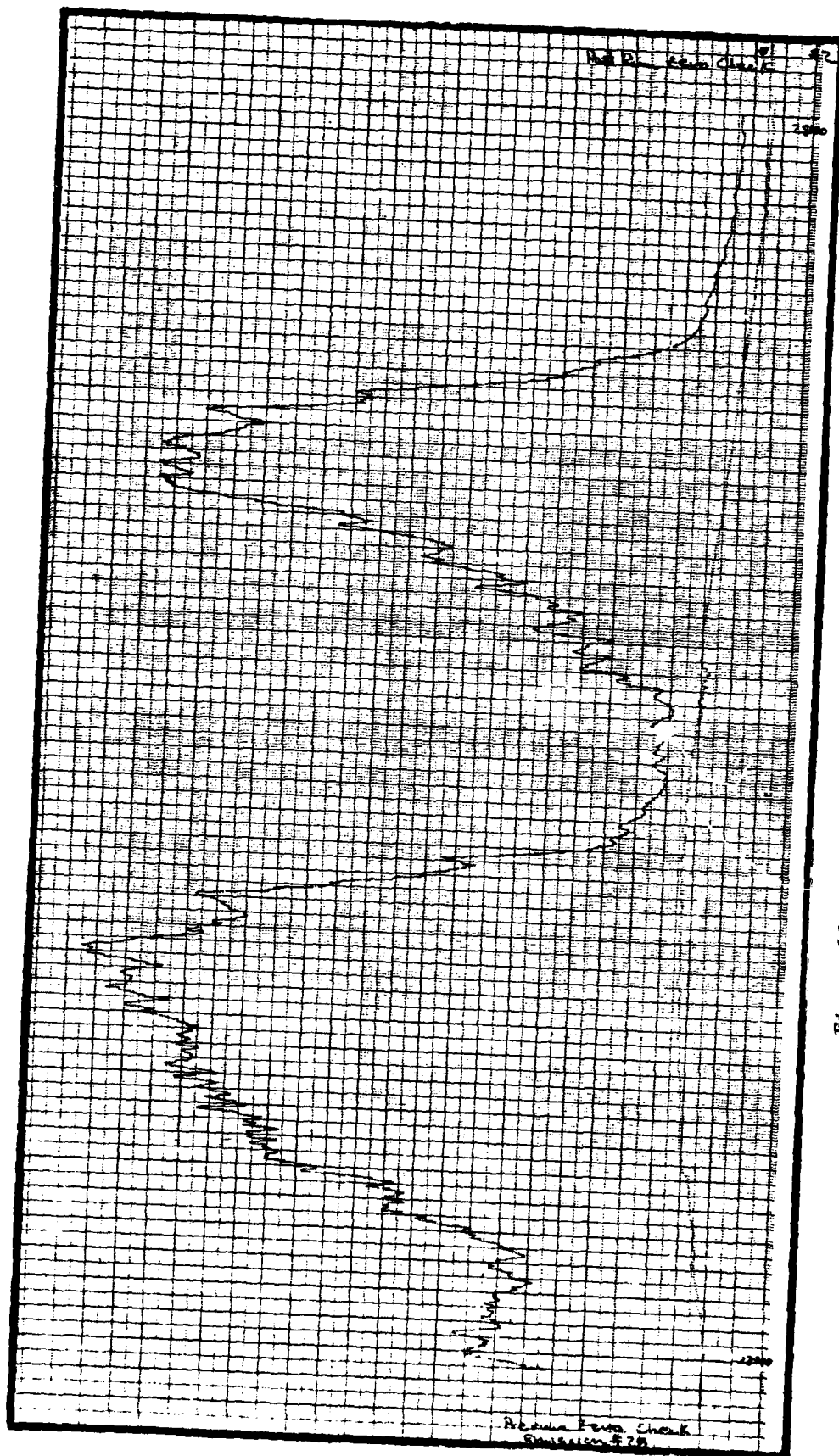Figure 17. Excitation Spectrum, Observed Fluorescence Volume near Front Tube Window (3.47 torr)

Figure 18. Excitation Spectrum, Observed Fluorescence Volume near Front Tube Window (12.58 torr)

quantitative measurements from spectra such as these could be made.

Broad Band Fluorescence Spectra

The broad band fluorescence spectra from the eighth vibrational level
of the upper electronic state $B^3\Sigma_u^-$ is shown in Figures 19 through 21
on pages 55 through 57. The transitions include those to the ground
electronic vibrational levels $(8\rightarrow0)$ through $(8\rightarrow24)$. Table II on page 52
summarizes the important data from these spectra. The relative inten-
sity of each line, after the convolution of the monochrometer's spectral
response and detector response are considered, is related to the Franck-
Condon factor for the transition through the equation (Ref 20:821 and
13:200):

$$I_{v'v''} = \frac{64\pi^4 \nu^4}{3c^2} (\bar{R}e)^2 N_{v'} q_{v'v''} \tag{27}$$

where

$\quad I_{v'v''}$ = the observed fluorescence intensity

$\quad \bar{R}e$ = the average electronic transition moment

$\quad N_{v'}$ = the excited state population

$\quad q_{v'v''}$ = the Franck-Condon factor for the v'-v'' transition

Equation (27) neglects rotational effects which would have to be included
under a more detailed analysis. $N_{J,v'}$, from Equation (28) below (Ref 13:123-125),
can replace $N_{v'}$ in a first order approximation to such an analysis. With
this substitution, changes produced by the rotational distribution could
be estimated.

$$N_{J,v} = N_e \left[\frac{g_v}{Z_v} \exp \left(\frac{-E_v}{KT} \right) \right] \left[\frac{(2J+1)}{Z_J} \exp \left(\frac{-E_J}{KT} \right) \right] \qquad (28)$$

Vibrational   Rotational
Distribution   Distribution

where

$N_{J,v}$ = the number of molecules in a particular rotational-vibrational state

N_e = total number density for a given electronic state

g_v = vibrational degeneracy (g_v=1 for a diatomic molecule)

Z_v = vibrational partition function

The broad spectra from the ninth vibrational level of the upper electronic state $B^3\Sigma_u^-$ is shown in Figures 22 through 24 on pages 58 through 60. The transitions include those to the ground electronic vibrational levels v"=0 through v"=25. Table III on page 53 summarizes the important data from these spectra. As with the broad band spectra from v'=8, more structure was observed on the highest pressure (12.58 torr) tube spectrum than on the lower pressures. By contrasting Figures 19 and 20 to Figure 21, and Figures 22 and 23 to Figure 24; the extra structure on and near each (v'→v") line, especially those above 3500 Å or v"=9 of the highest pressure (12.58 torr) tube, becomes apparent.

It should be noted that, as stated in the procedures section, prior to each fluorescence scan the excitation wavelength was tuned approximately to, and left on, the wavelength corresponding to maximum fluorescence from any level. Since these maxima varied slightly from pressure to pressure the fluorescence spectra from v'=8 and v'=9 were not all excited at exactly the same frequency. Table IV lists the pressures and

Table II

Data from v'=8 Broad Spectrum

v'=8→v"=	Actual Wavelength (Å) (Ref 14)	Franck-Condon Factor $q_{v'v''}$ (Ref 14)	Observed Wavelength (Å)
0	2860.1	.043	2855.0
1	2920.4	.072	2915.0
2	2982.7	.004	2979.0
3	3047.3	.038	3043.0
4	3114.1	.051	3109.0
5	3183.2	<.001	
6	3255.0	.044	3251.0
7	3329.3	.038	3325.0
8	3406.5	.001	3402.0
9	3886.6	.044	3483.0
10	3569.8	.025	3566.0
11	3656.3	.003	3654.0
12	3746.4	.046	3743.6
13	3840.1	.024	3838.0
14	3937.7	.002	3936.6
15	4039.5	.039	4037.8
16	4145.7	.028	4144.0
17	4256.7	<.001	
18	4372.6	.029	4371.8
19	4493.9	.047	4493.2
20	4621.0	.009	4619.0
21	4754.2	.006	4753.0
22	4893.9	.042	4893.2
23	5040.8	.046	5041.0
24	5195.2	.013	5195.0

Fluorescence scan from 3.47 torr tube was used.

Table III

Data from v'=9 Broad Spectrum

$v'=9\rightarrow v''=$	Actual Wavelength ($\overset{o}{A}$) (Ref 14)	Franck-Condon Factor $q_{v'v''}$ (Ref 14)	Observed Wavelength ($\overset{o}{A}$)
0	2828.9	.083	2825.0
1	2887.9	.070	2885.0
2	2948.8	.001	2947.0
3	3011.9	.058	3008.7
4	3077.1	.023	3073.7
5	3144.6	.015	3142.1
6	3214.6	.053	3210.1
7	3287.1	.002	3285.1
8	3362.3	.035	3359.1
9	3440.3	.040	3437.2
10	3521.3	<.001	
11	3605.5	.039	3602.6
12	3693.0	.023	3690.2
13	3784.0	.004	3781.2
14	3878.8	.043	3875.3
15	3977.5	.019	3975.3
16	4080.5	.004	4079.3
17	4187.9	.038	4185.3
18	4300.1	.026	4298.4
19	4417.3	.001	
20	4540.1	.032	4539.4
21	4668.6	.040	4675.5
22	4803.3	.005	4801.5
23	4944.7	.011	4943.5
24	5093.2	.042	5091.6
25	5249.3	.036	5255.6

Fluorescence scan from 3.47 torr tube was used.

the excitation wavelength used for both the v'=8 and v'=9 fluorescence scans.

Table IV Excitation Scan Data

Pressure (torr)	Excitation Wavelength (Å)	
	v'=8	v'=9
0.31	2863.10	2830.44
3.47	2860.72	2829.02
12.58	2864.08	2831.48

It should be also noted that, although the excitation wavelength was not exactly the same for each pressure, there was additional structure on both the v'=8 and v'=9 spectra. This would tend to indicate the structure was due to the higher pressures and not to different excitation wavelengths.

Various explanations for this were proposed. First, it was thought that cross relaxation within the $B^3\Sigma_u^-$ upper electronic state were occurring, but comparisons of structure wavelength with Table III-V in Peterson and Schlie's work (Ref 3:1559-1561), did not show any correspondence. A second possibility is that cross relaxation between two different rotational levels within a single vibrational band was occurring. Yet another possible explanation is induced predissociation described by Calvert and Pitts (Ref 12:185-189). This induced predissociation is the result of interactions between the $^1\Sigma_u^-$ and $B^3\Sigma_u^-$ electronic states which are allowed to occur at higher pressures.
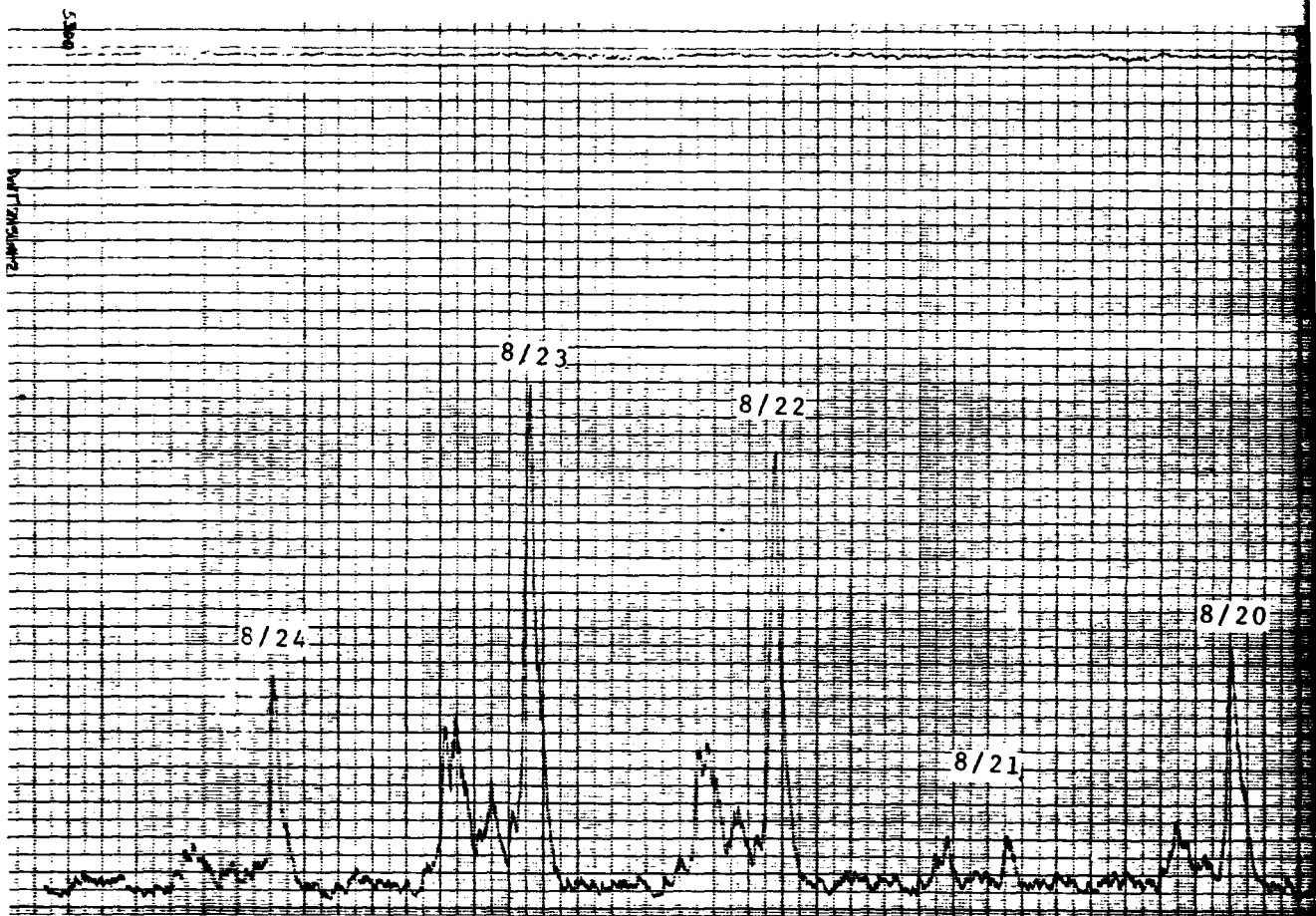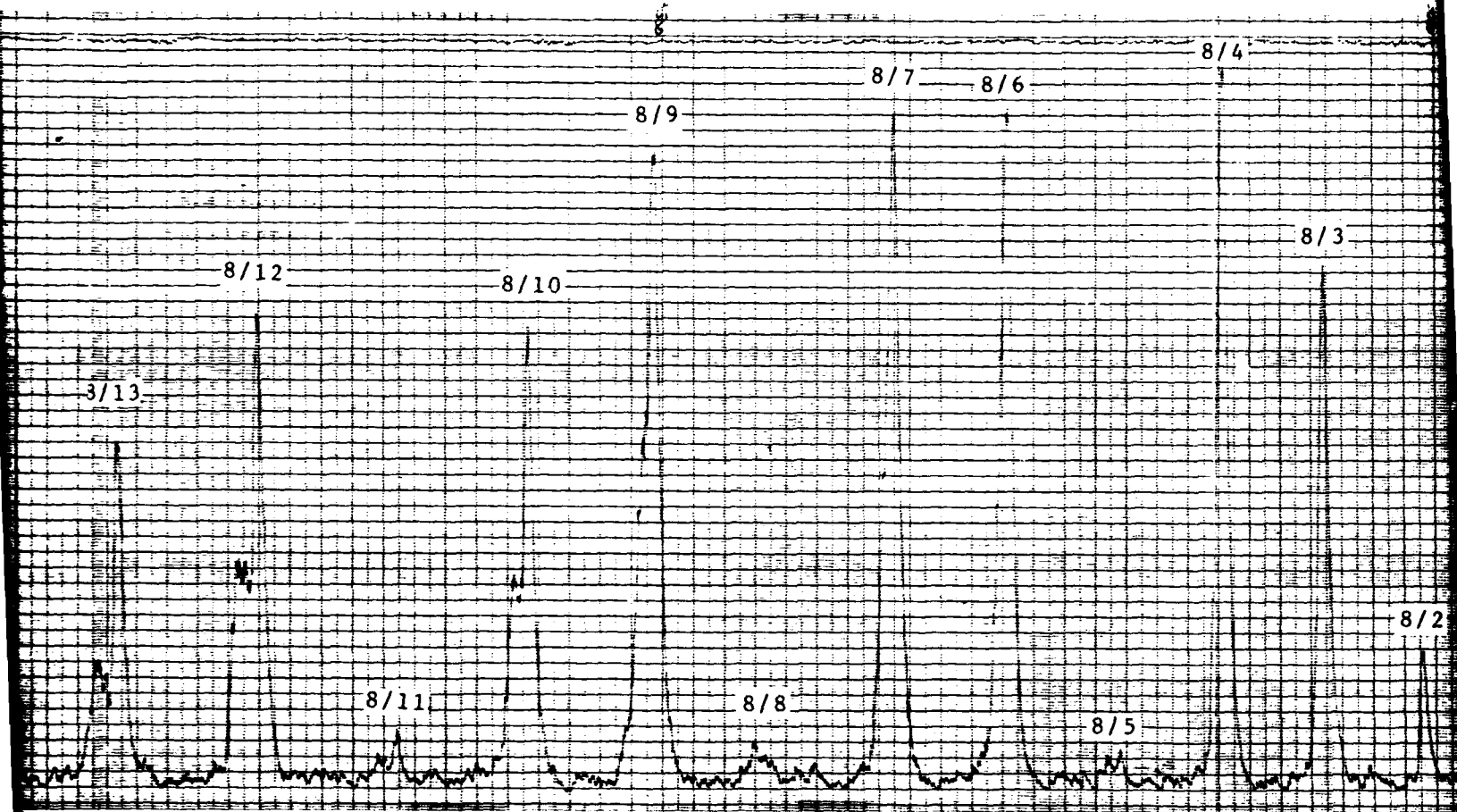
54

55
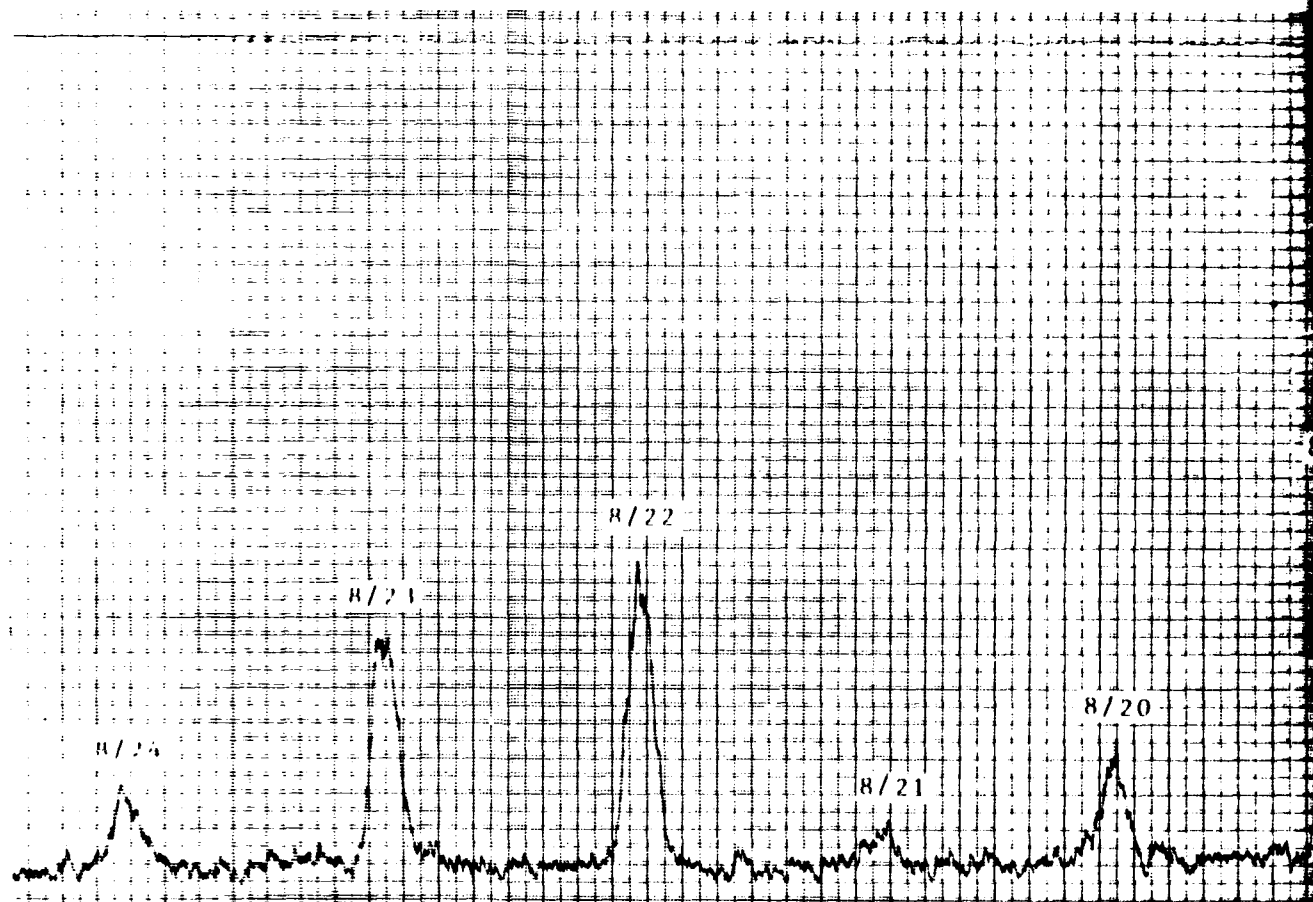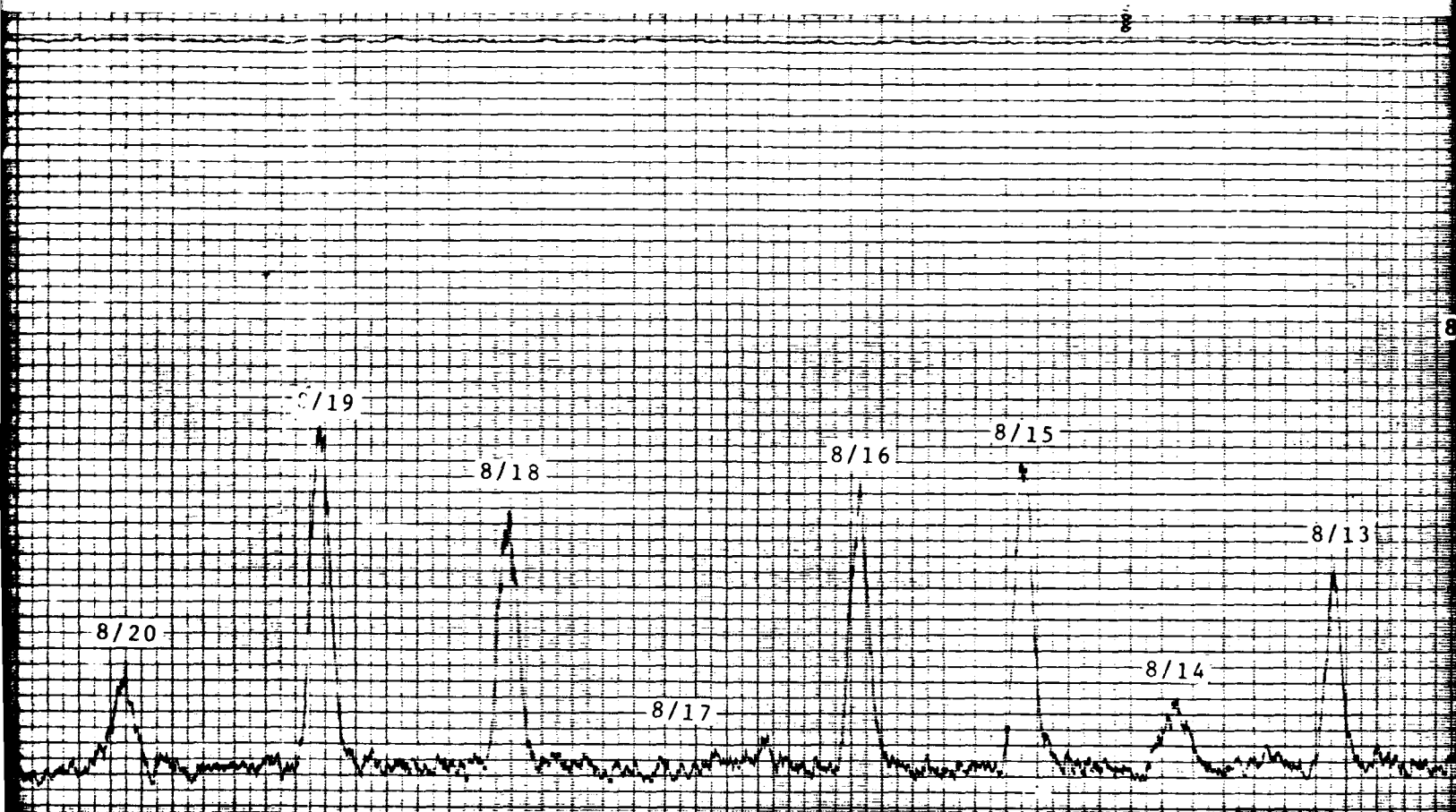
Figure 19. Fluorescence Spectrum $v'=8, v''=0 \rightarrow 24$ (0.31 torr)

136

8/4

8/6

8/12   8/9

8/7   8/3

8/13   8/10

8/11   8/8   8/5

orr)

3

8/1

8/4

8/6

8/7

8/3

8/2

8/5

56
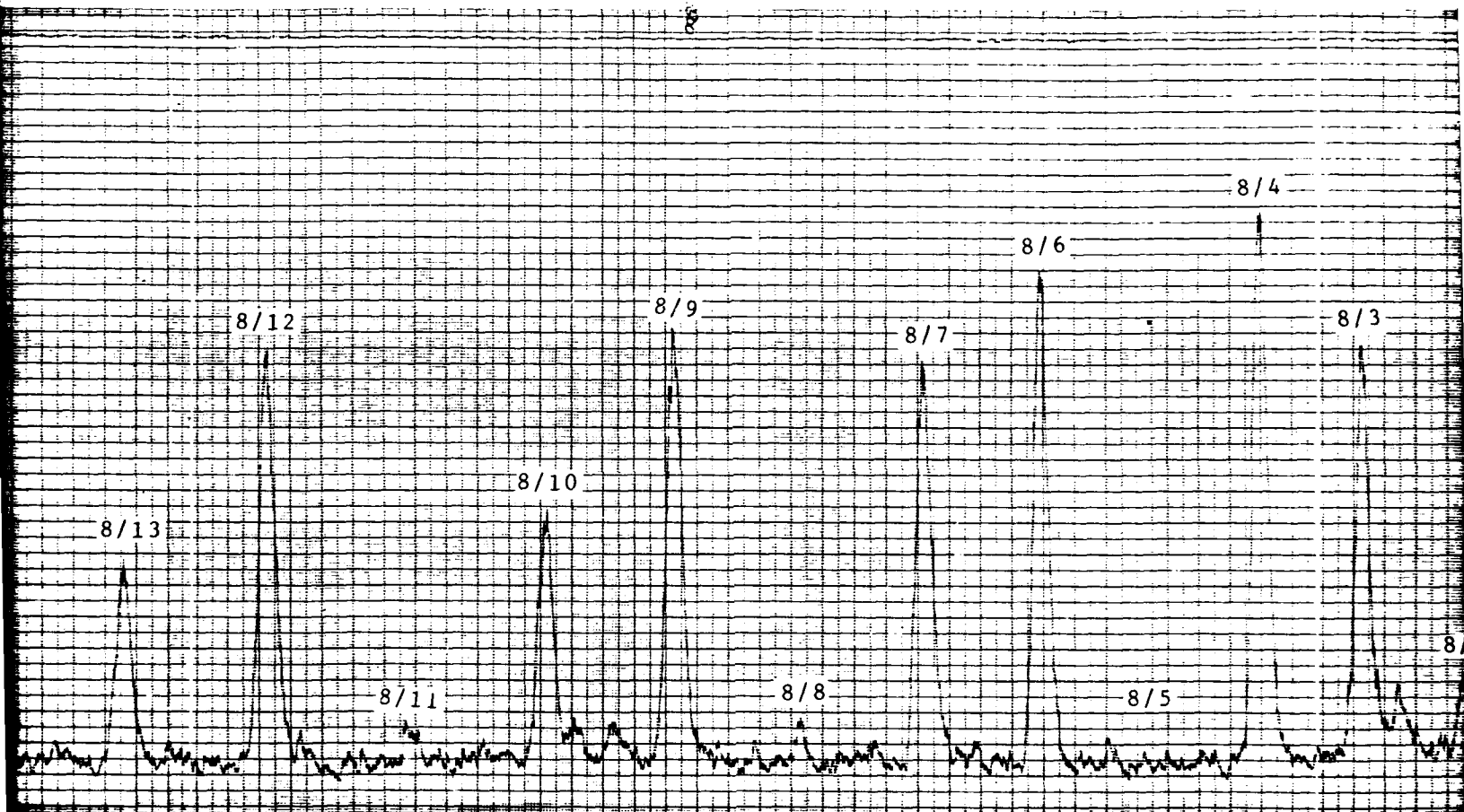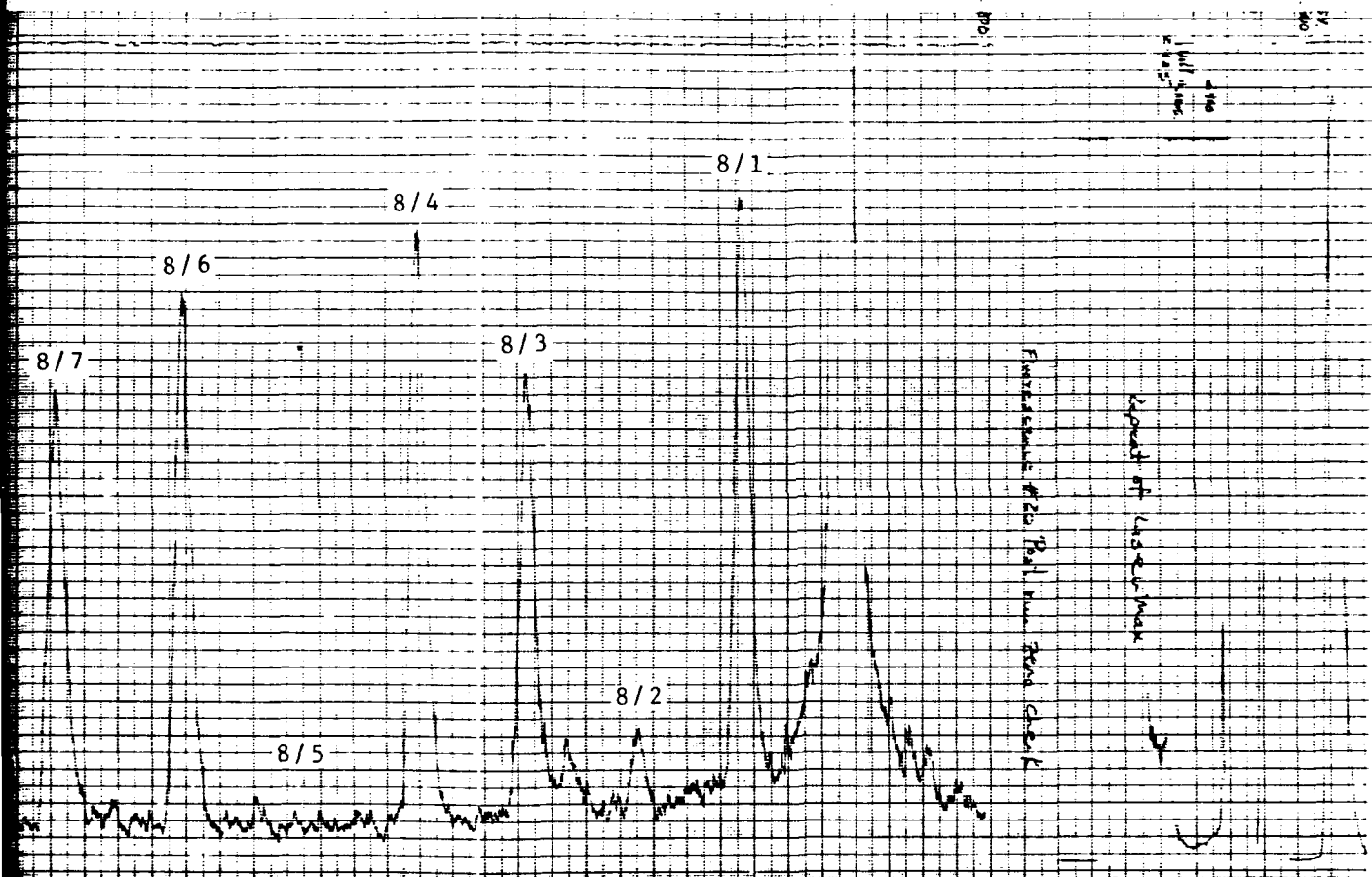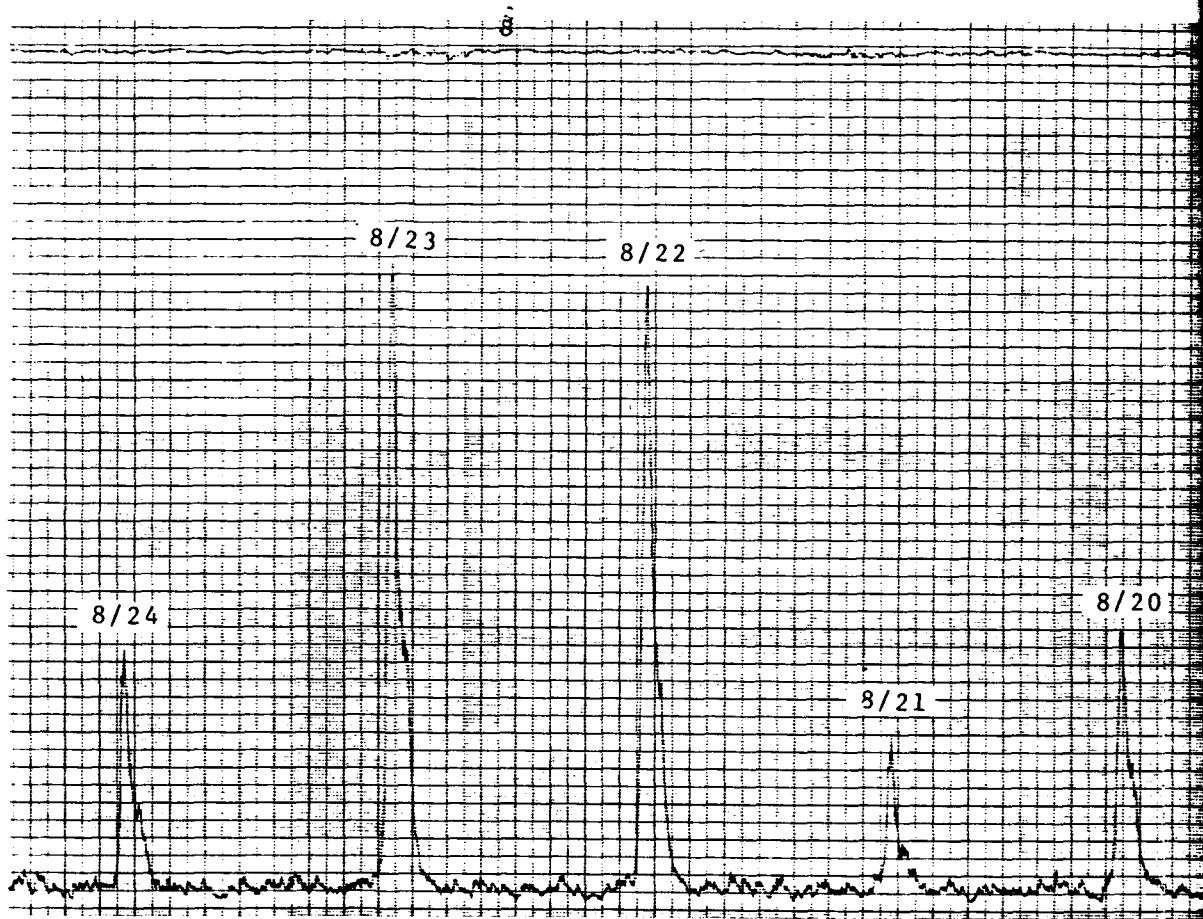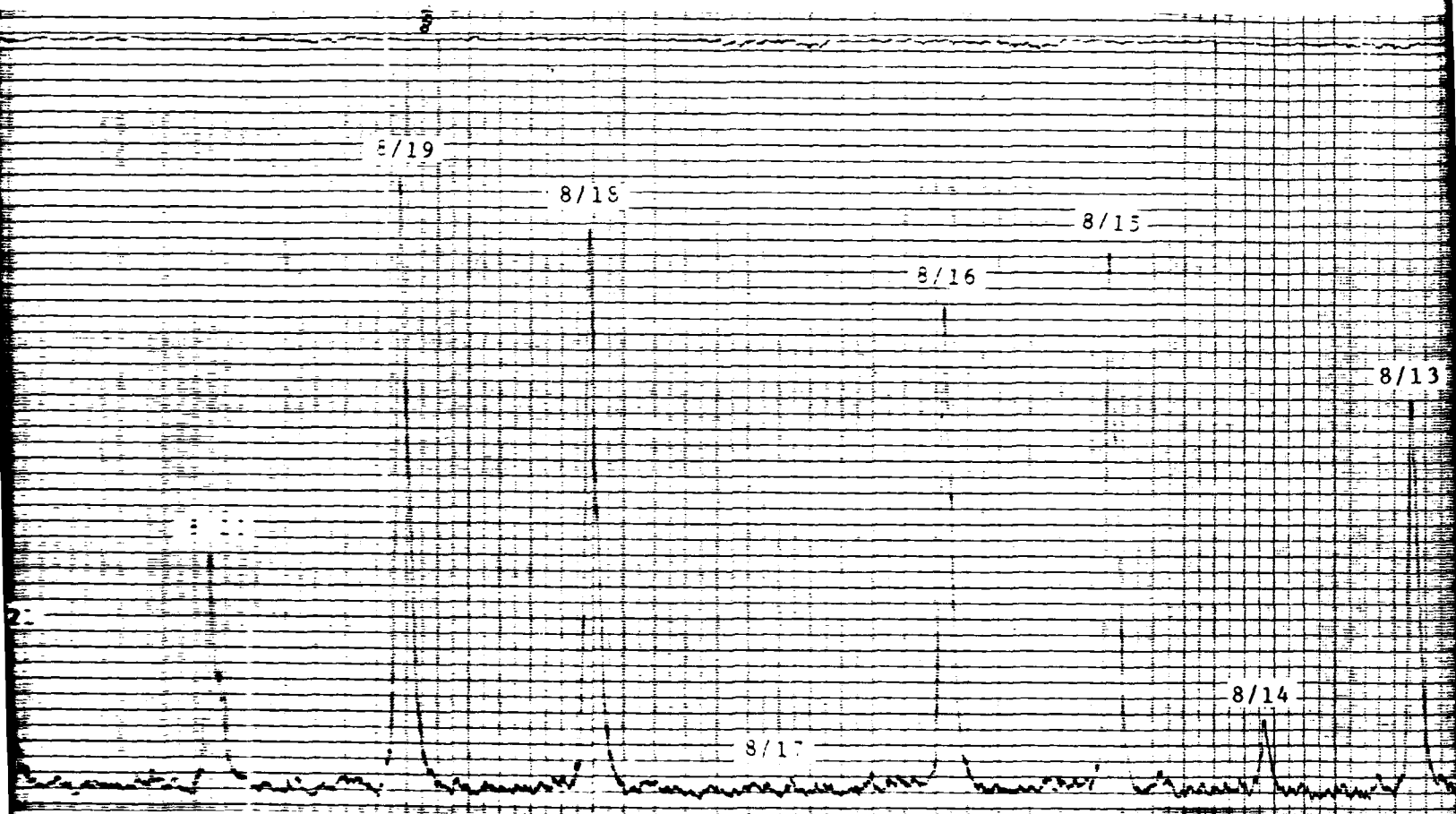
Figure 20. Fluorescence Spectrum $v'=8, v''=0 \rightarrow 24$ (3.47 torr)

8/4

8/6

8/9
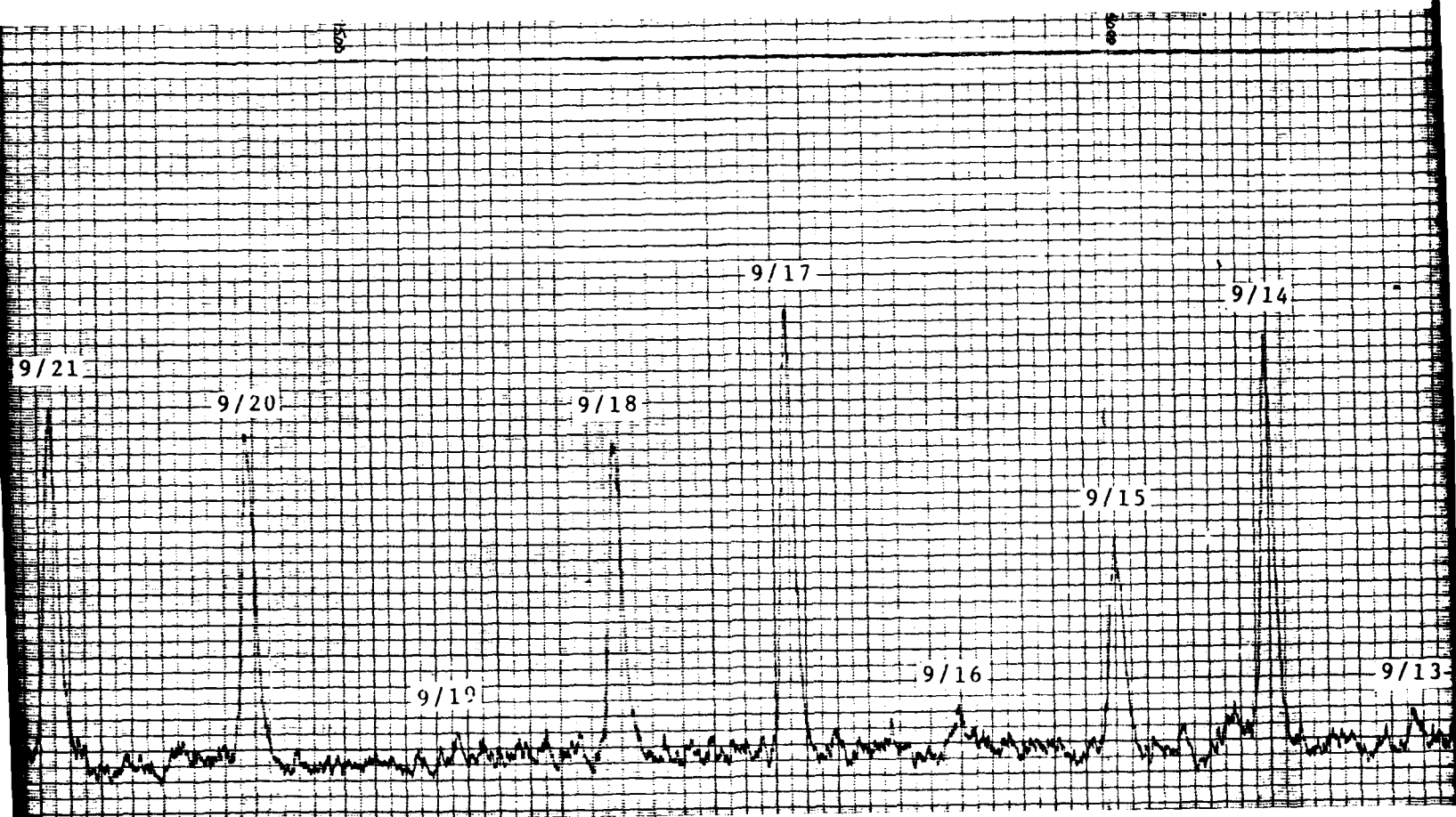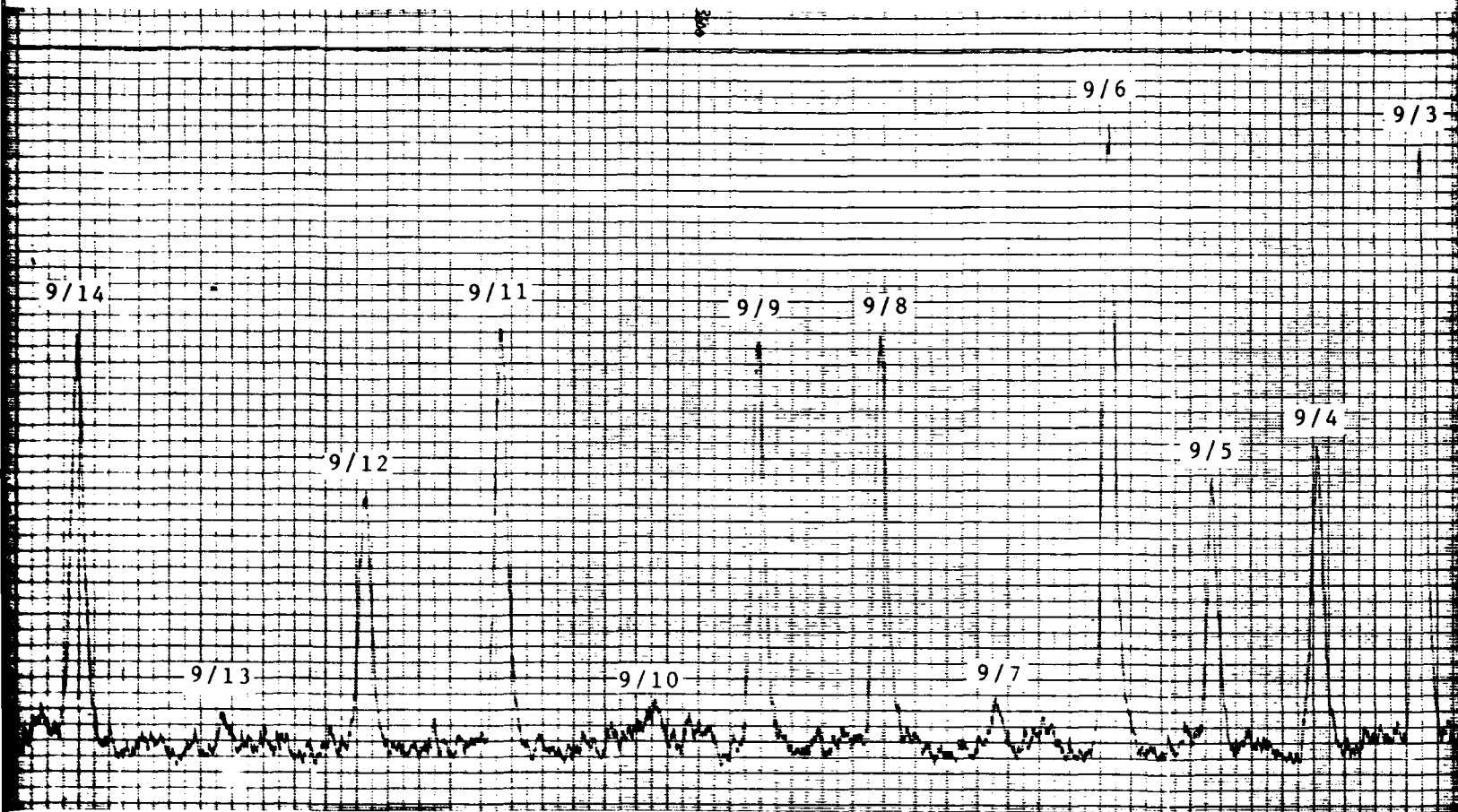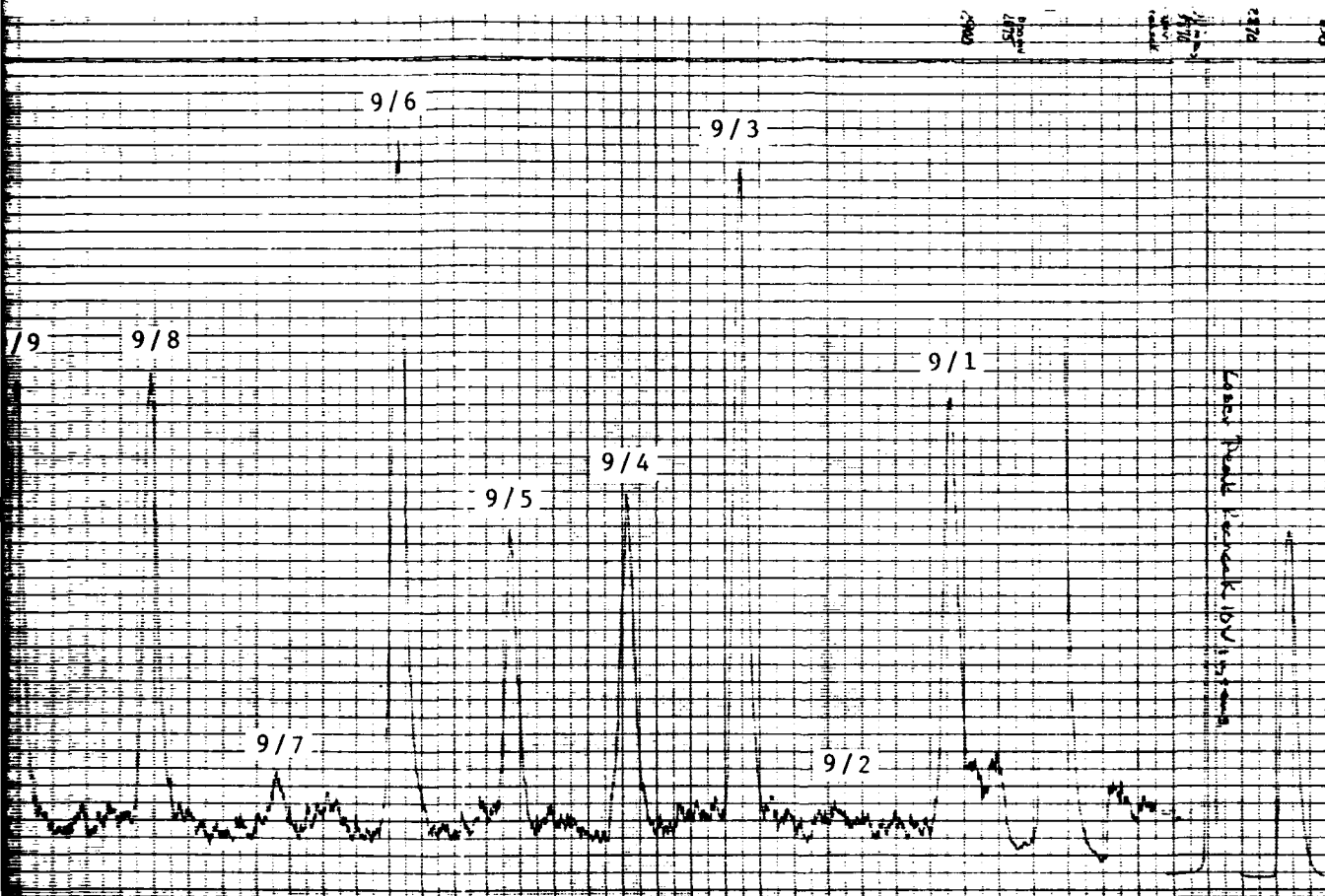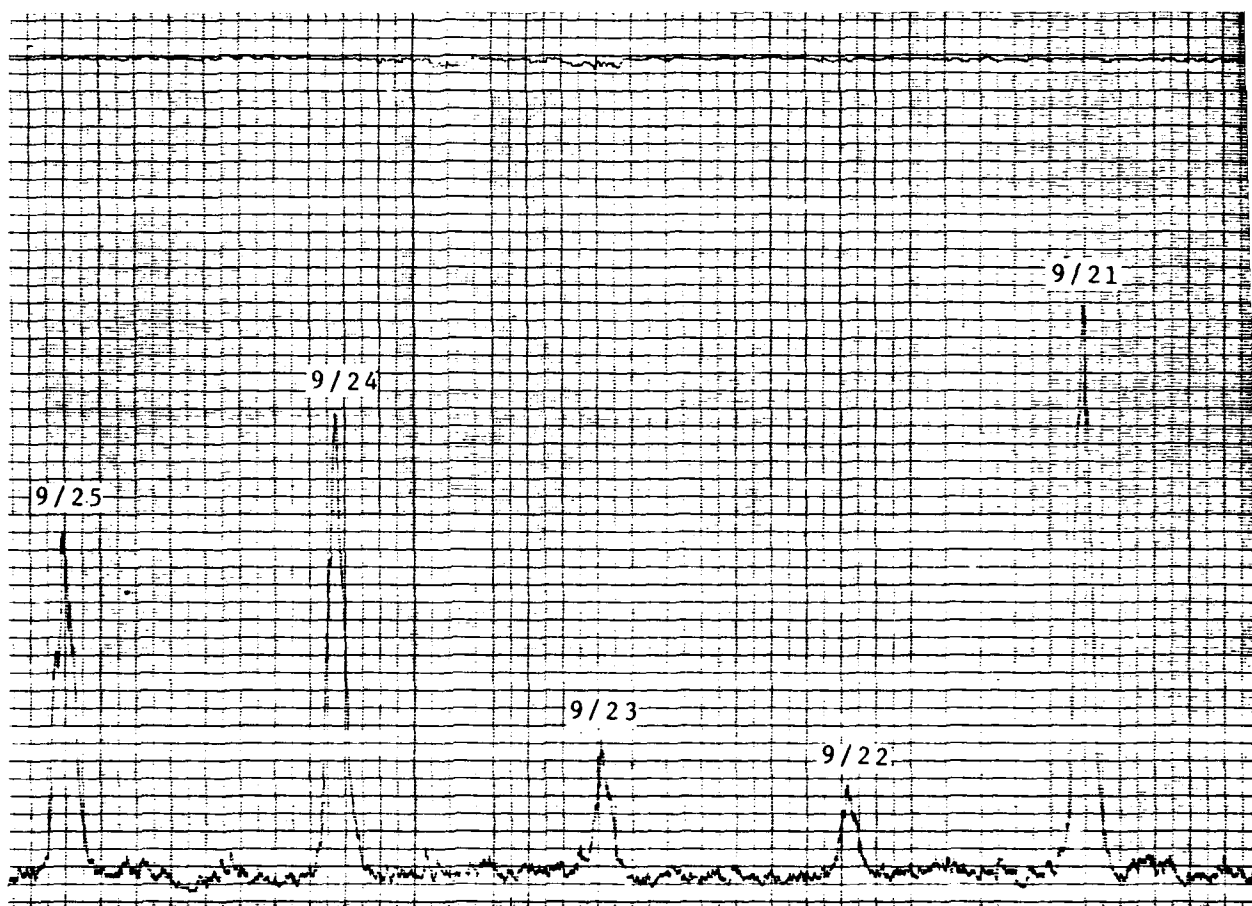
8/12

8/7

8/10

8/13

8/11

8/14

8/8

8/5

4 (3.47 torr)

3
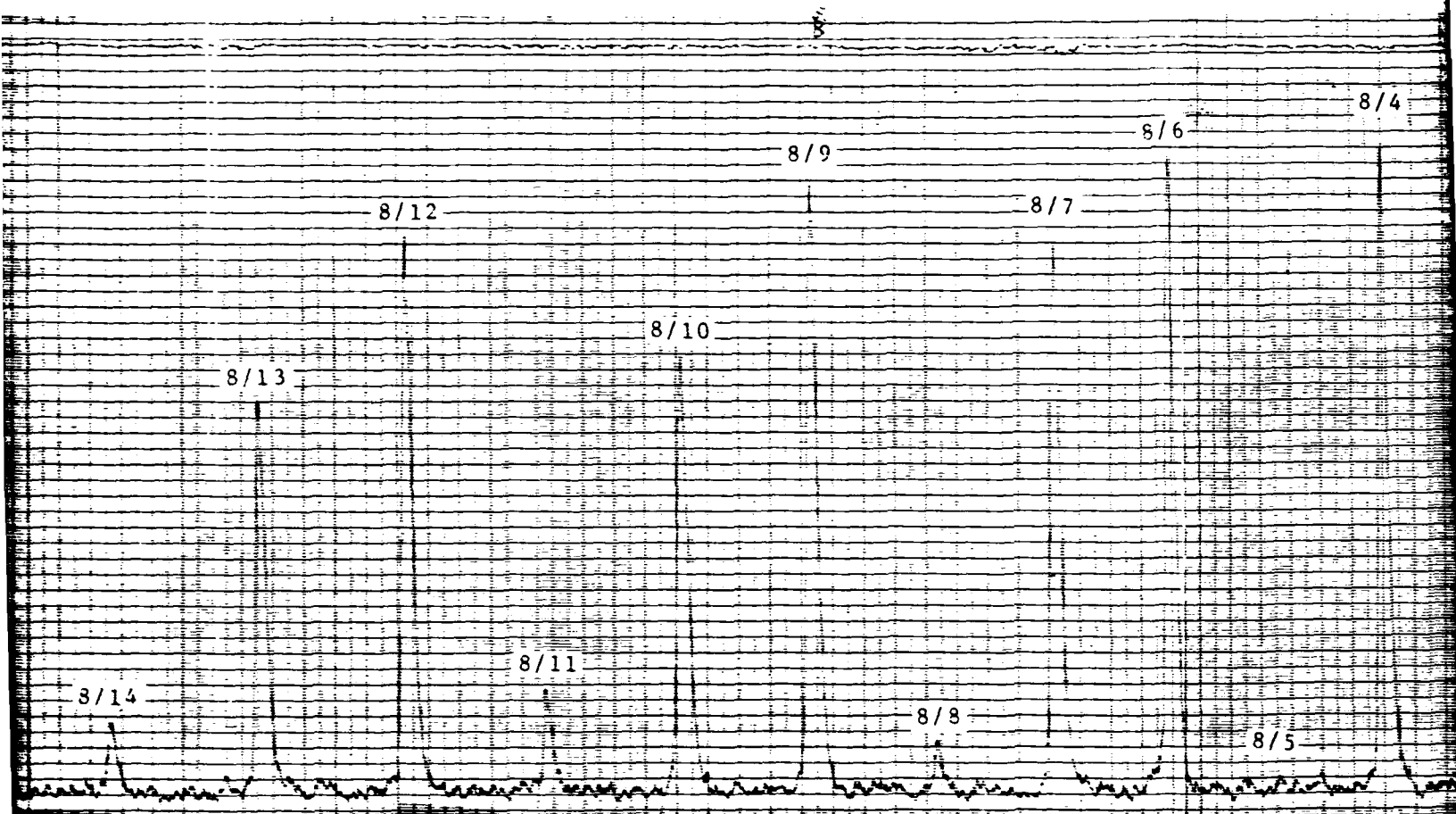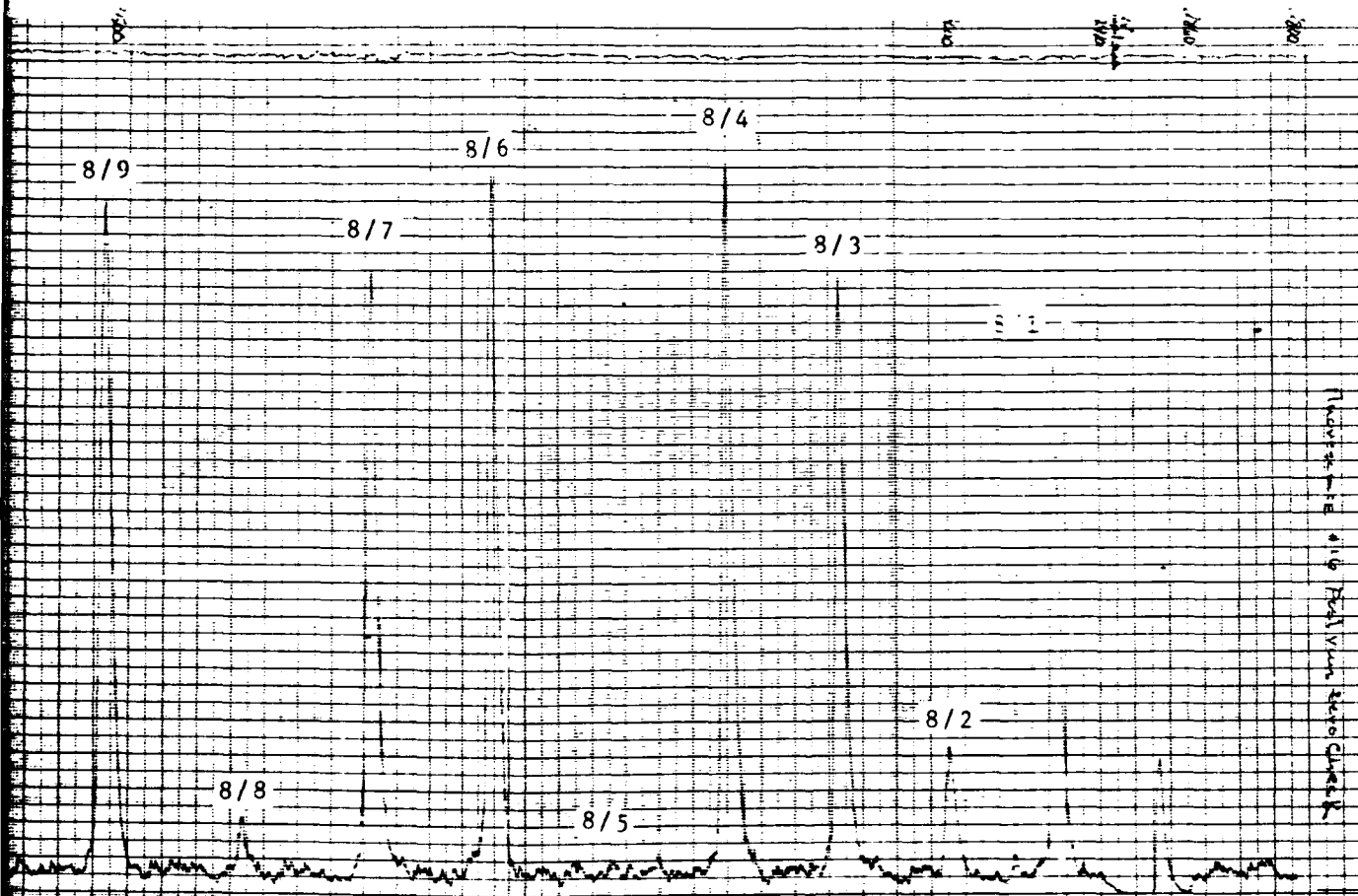
Figure 21. Fluorescence Spectrum v'=8, v"=0→24 (12.58 torr)

2

8/4

8/7 ——— 8/6

8/9

8/3

8/12 —————— 8/10

3/13

8/2

8/11

8/8

8/5

3

58
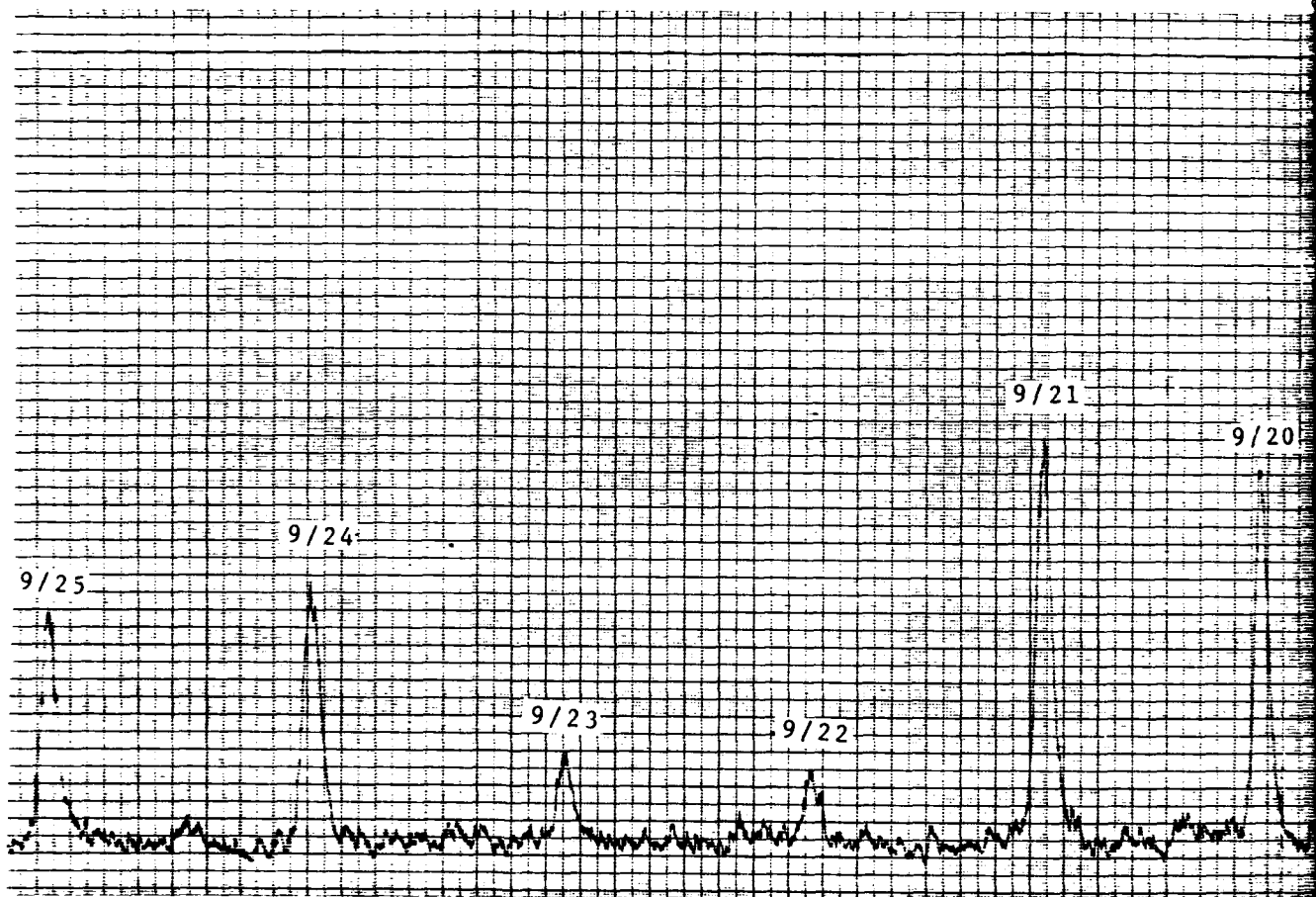
Figure 22. Fluorescence Spectrum v'=9,v"=0→25 (0.31 torr)

9/6   9/3

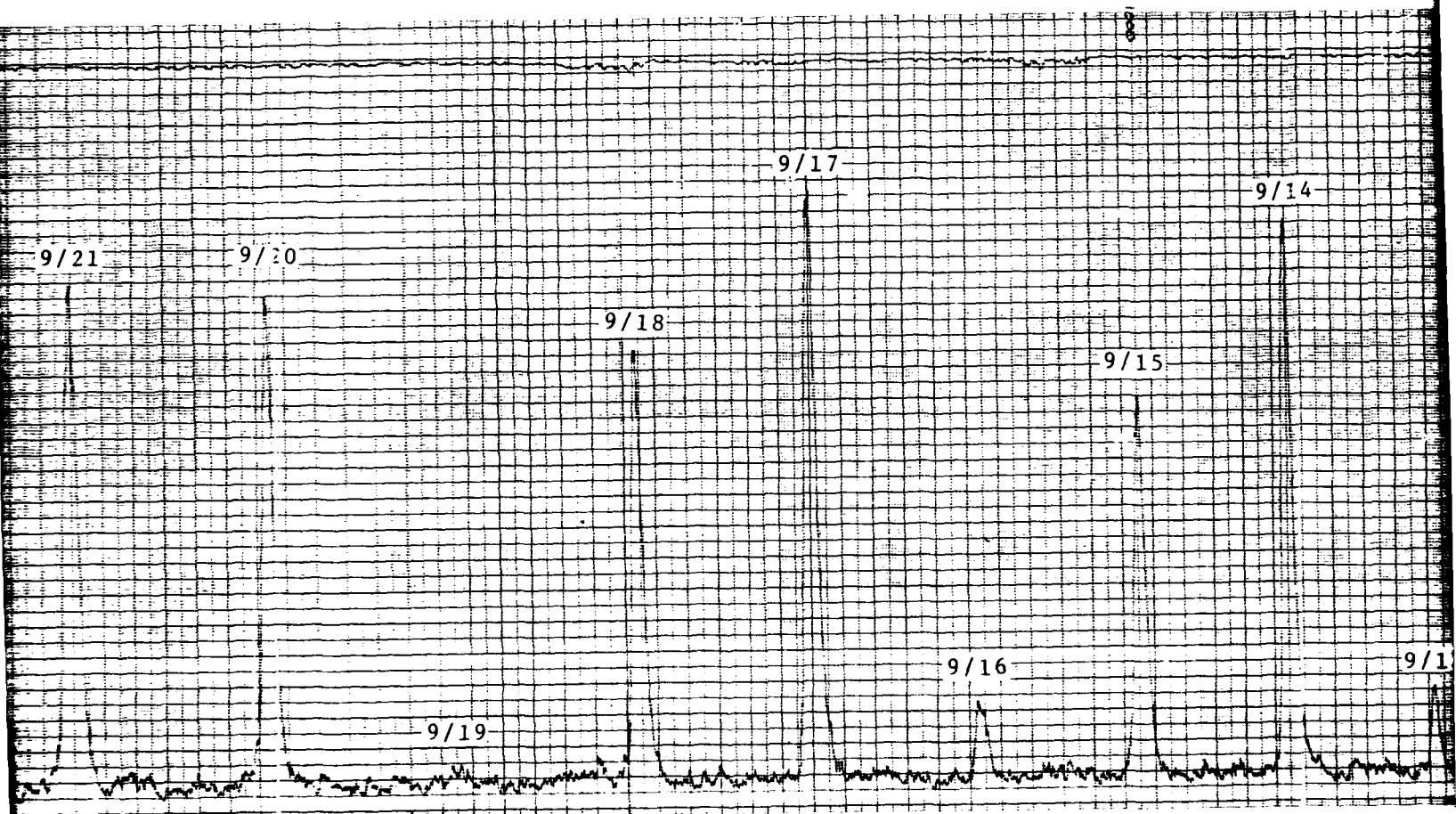9/14   9/11   9/9   9/8

9/12   9/4

9/5

9/13   9/10   9/7

)rr)

59
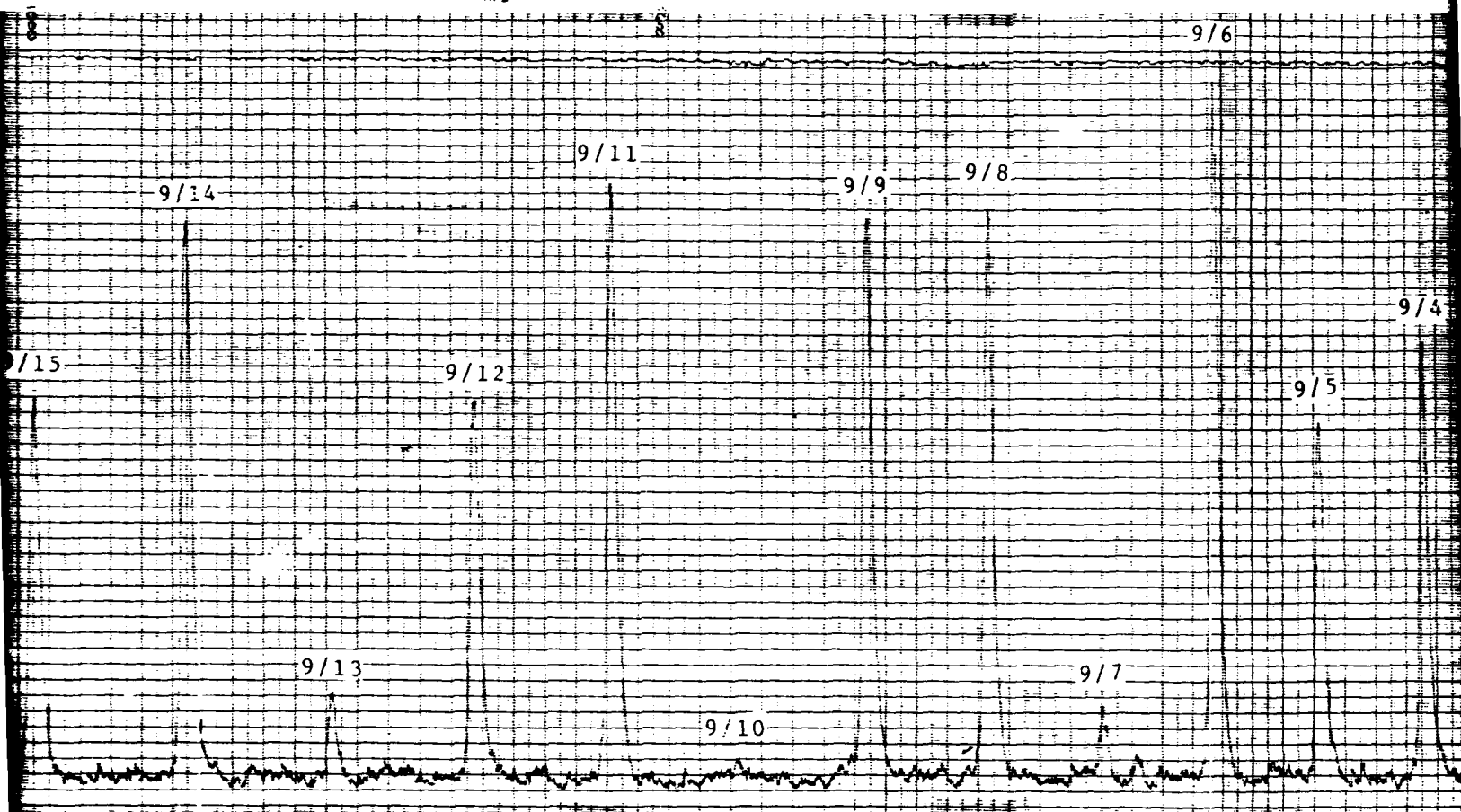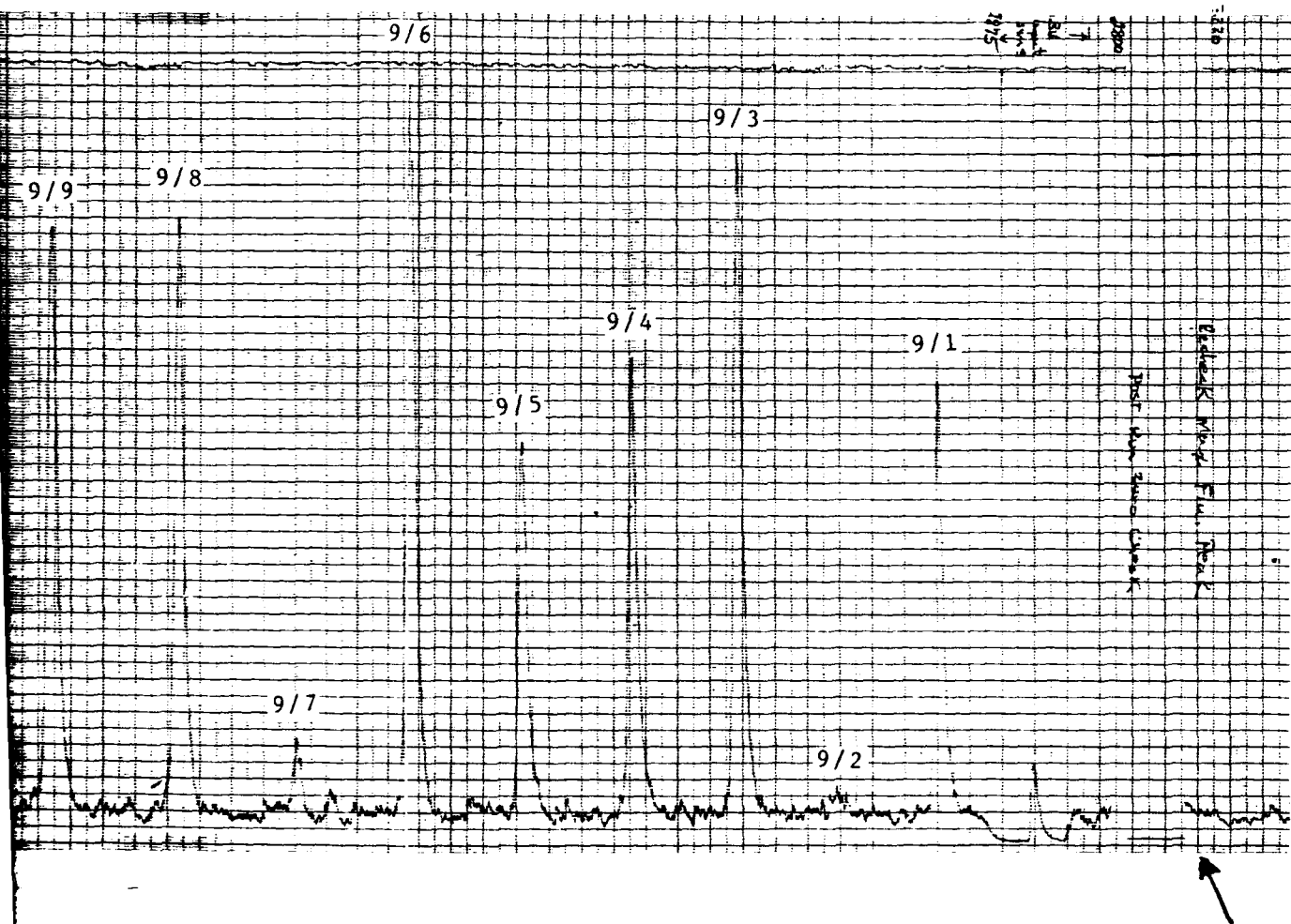
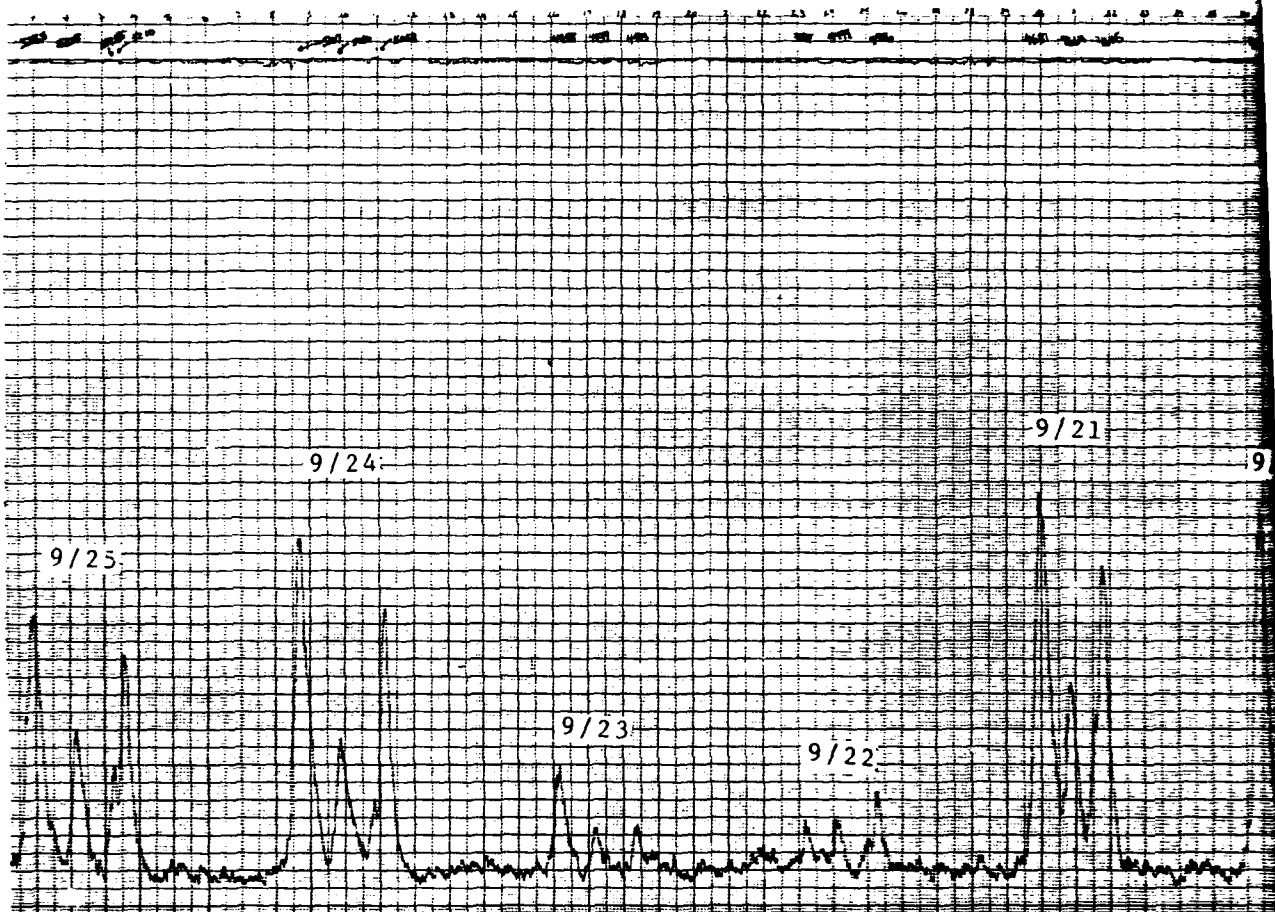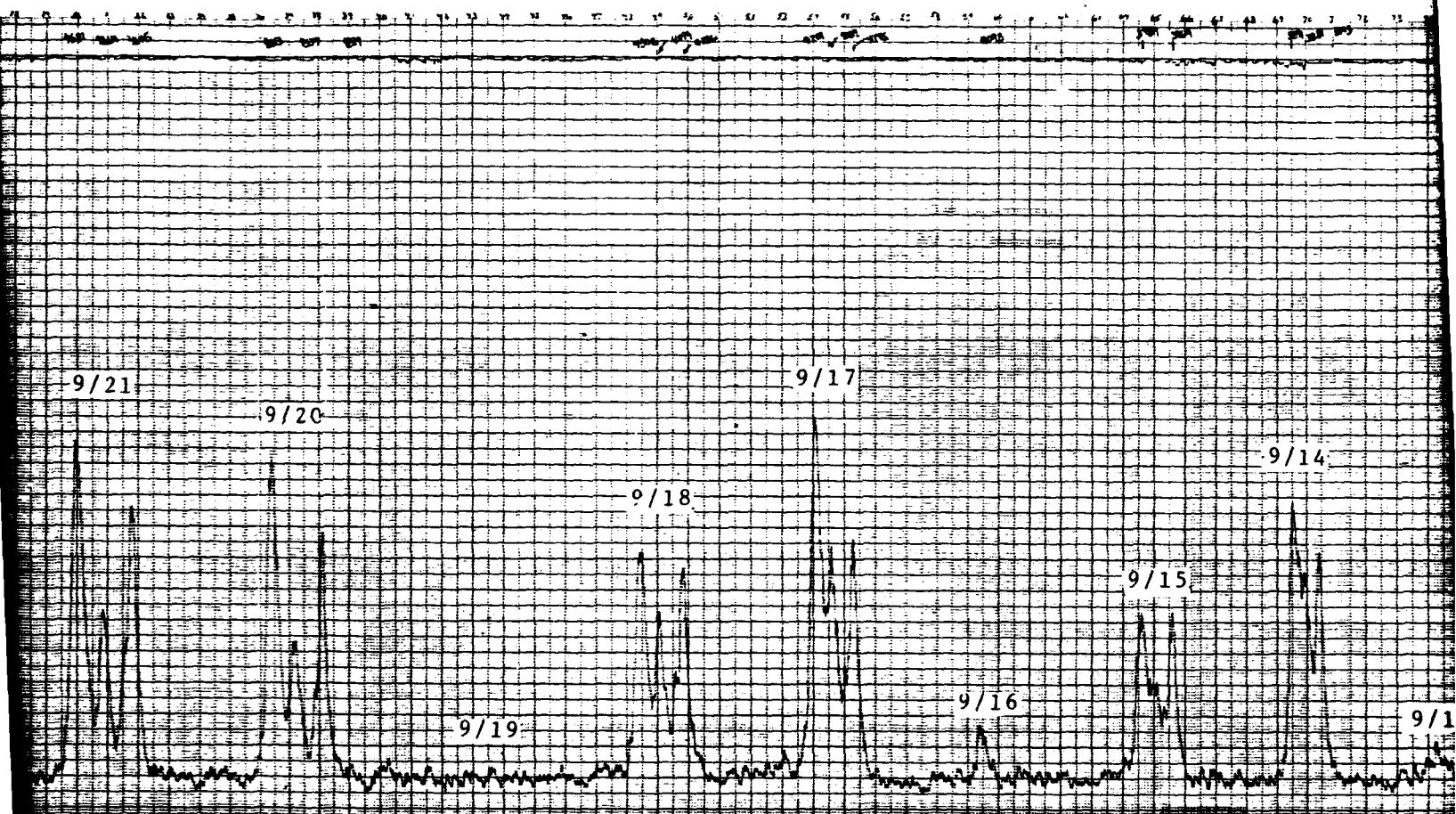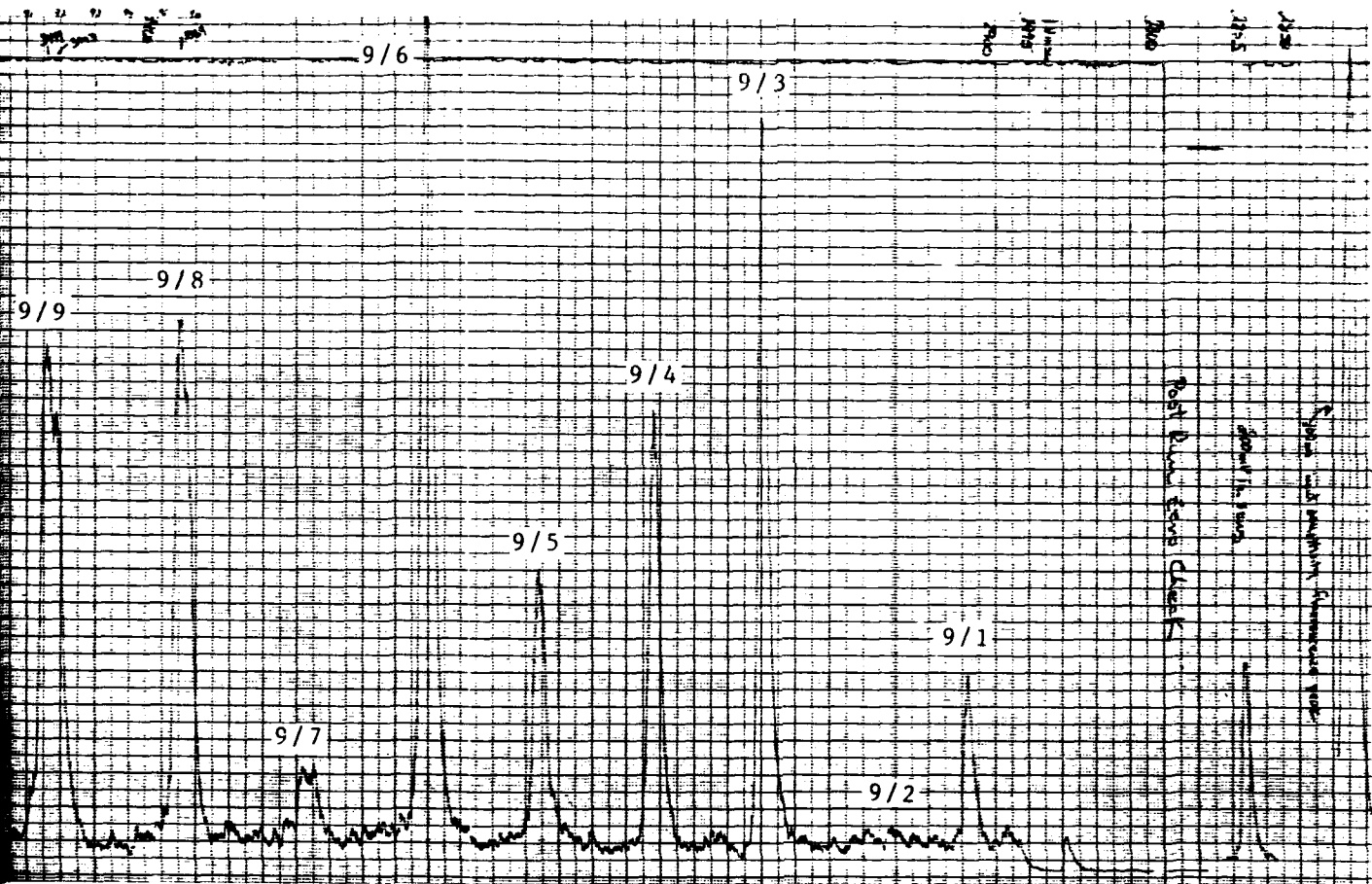Figure 23. Fluorescence Spectrum $v'=9, v''=0\rightarrow25$ (3.47 torr)

(3.47 torr)

60

Figure 24. Fluorescence Spectrum $v'=9, v''=0 \rightarrow 25$ (12.58 torr)

9/6

9/8

9/9

9/11

9/4

9/14

9/12

9/5

9/13

9/10

9/7

(8 torr)

3

Fluorescence Intensity Measurements

The excitation spectra for $(9{\rightarrow}6)$ and $(8{\rightarrow}4)$ bands are shown in Figures 25 and 26, respectively. They indicate the wavelength corresponding to maximum fluorescence intensity for $(8{\rightarrow}4)$ is 2861.4 Å and for $(9{\rightarrow}6)$ is 2830.6 Å. These correspond closely to the excitation wavelengths used for the fluorescence scans which were used to pick these two transitions because of their prominence.

Fluorescence intensity versus laser power measurements shown in Figure 27 on pages 63 and 64 exhibit the linear relationship referred to in the theory. It is evident from this plot that even partial saturation of the $(9{\rightarrow}6)$ transition did not occur at the laser power used for concentration measurements or for the higher laser powers available. The decision not to use the saturation approximations in solving the rate equations for $N_9(t)$ was made on the basis of this result.

Fluorescence intensity versus temperature measurements for the $(9{\rightarrow}6)$ transition are shown in Figure 28 on page 65. The first signs of S_2 occur between 200 and 250°C, instead of the 350–400°C reported in prior research. As shown in Figure 29 on page 65, in an equilibrium composition of sulfur vapor, S_2 starts to form near 240°C, and reaches 1% concentrations near 350°C. The results of the present work, as shown in Figure 28, indicates a more rapid increase in S_2 formation which is consistent with Robbin's earlier work (Ref 4:46). The observed fluorescence intensity had already passed its peak at 410°C and dropped to approximately 80% of that peak at 450°C, where, according to Figure 29, the equilibrium composition of S_2 is 3% of the sulfur vapor. The accelerated S_2 formation observed may have been due to the lower pressure used in this research, 3.47 torr. Near 450°C, the partial pressure of S_2 for this tube was
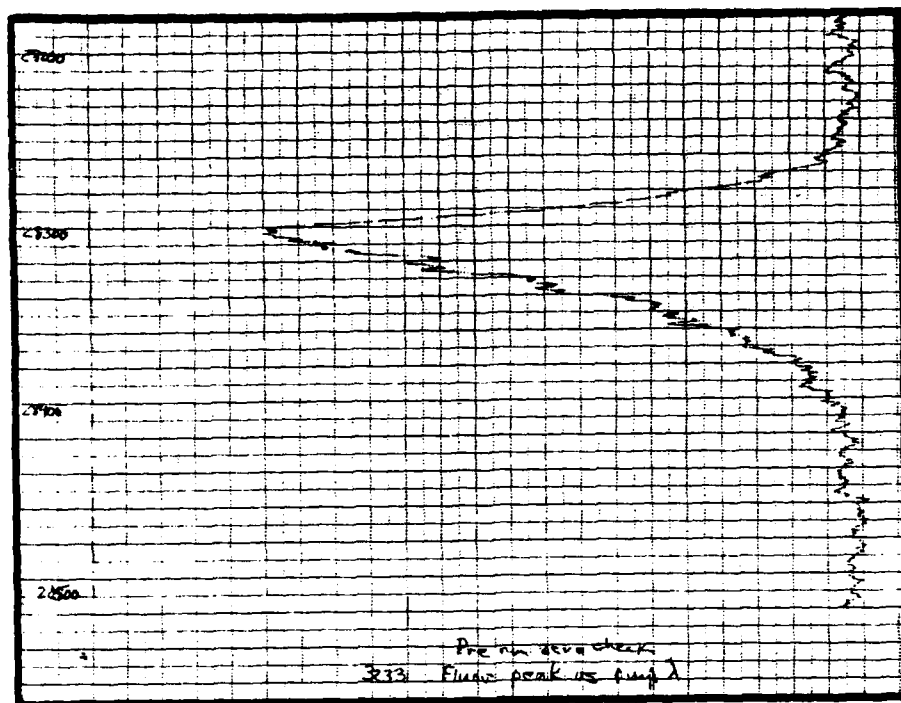
Figure 26. (9→6) Excitation Spectrum
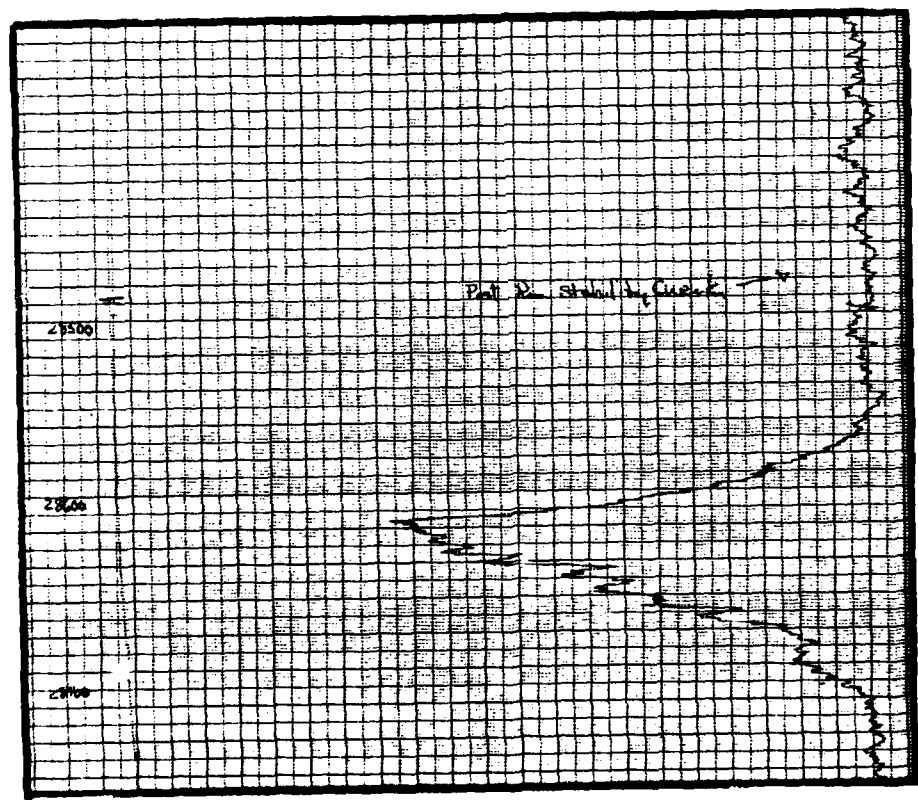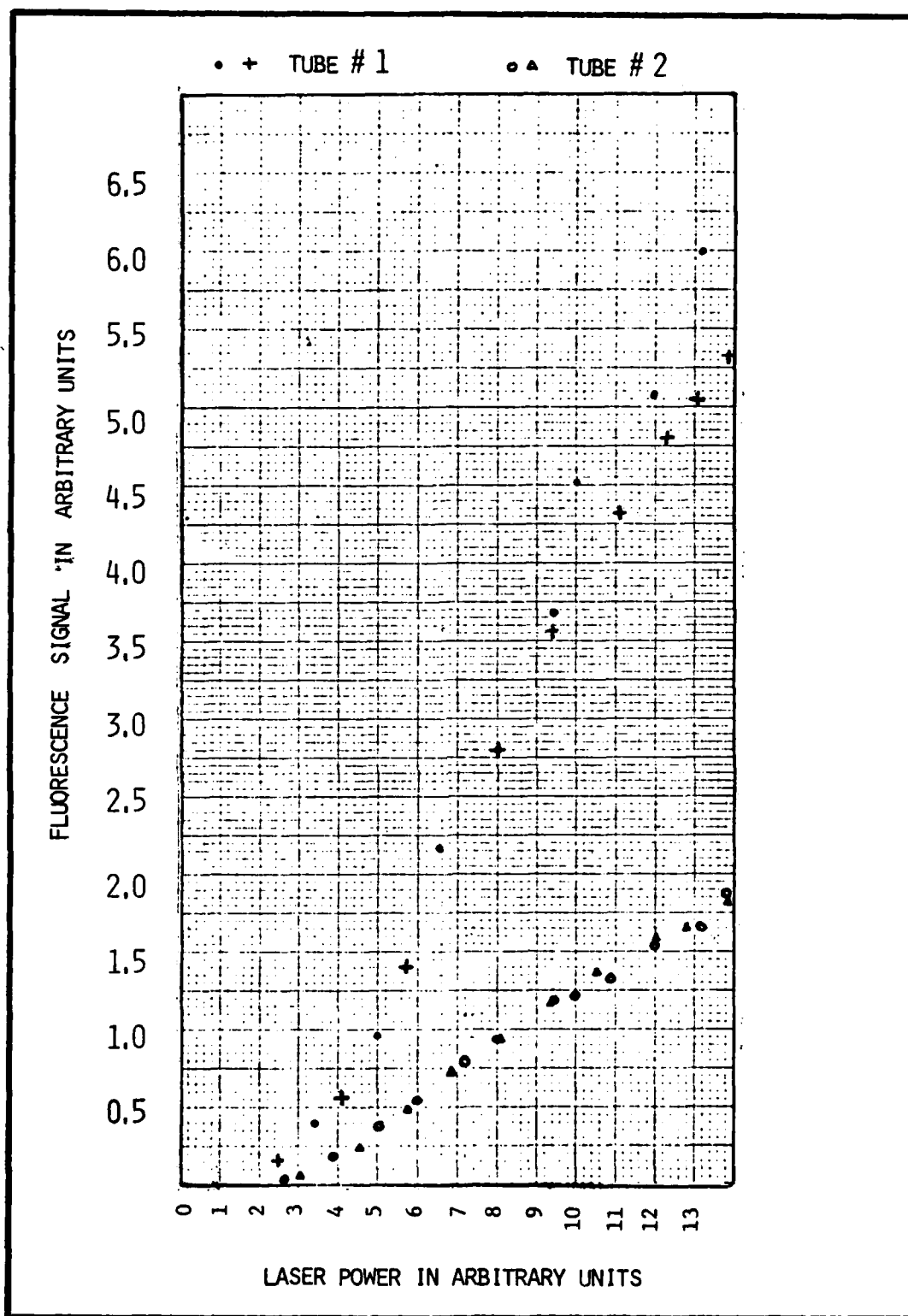

Figure 25. (8→4) Excitation Spectrum

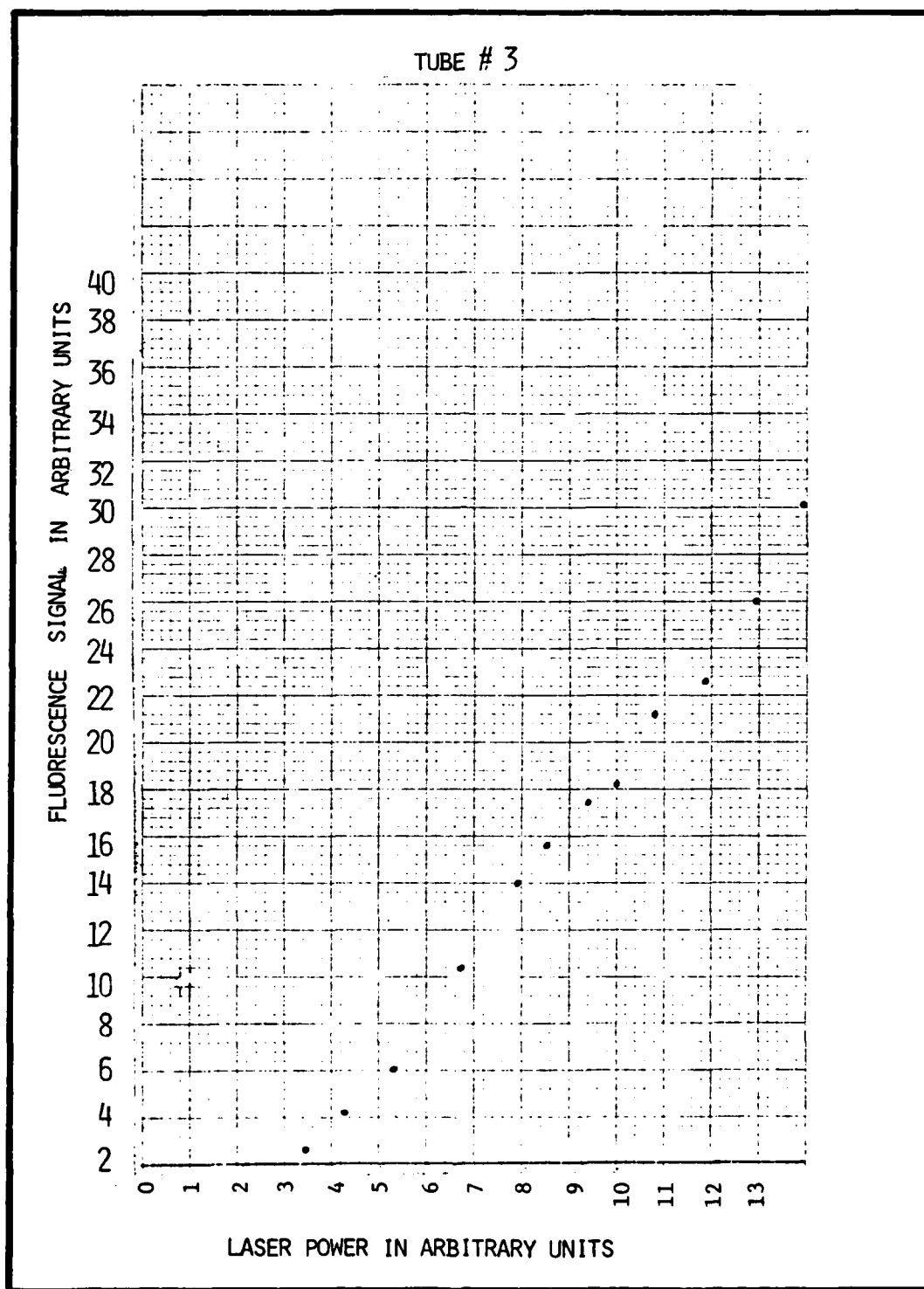Figure 27. v'=9, v"=6 Fluorescence Intensity vs Laser Power

63

Figure 27.   v'=9, v"=6   Fluorescence Intensity vs Laser Power
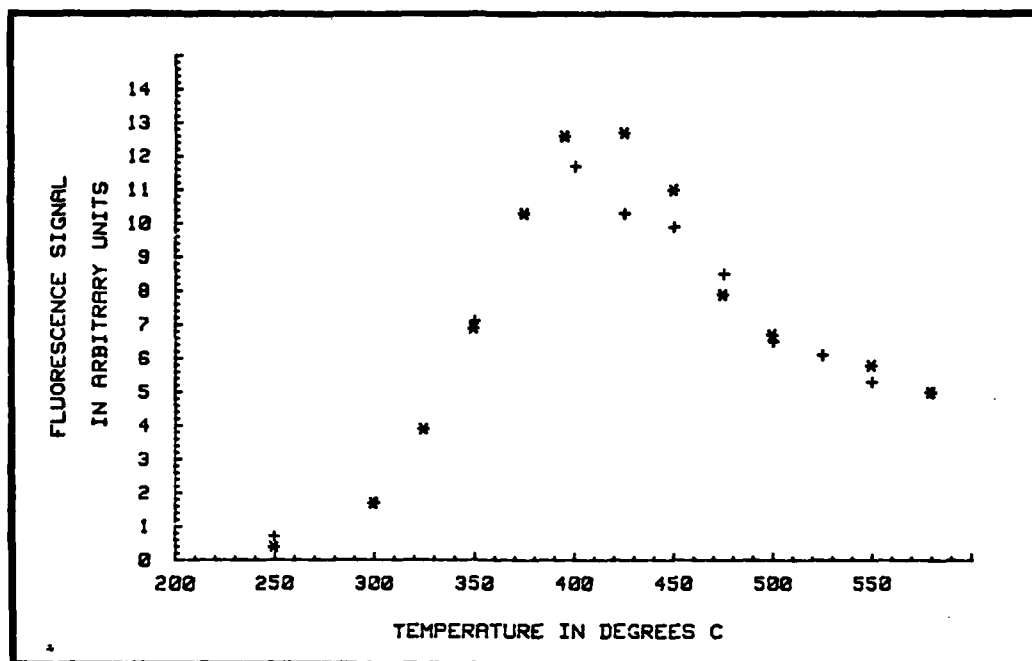
64

Figure 28.   (9→6) Fluorescence Intensity vs Temperature
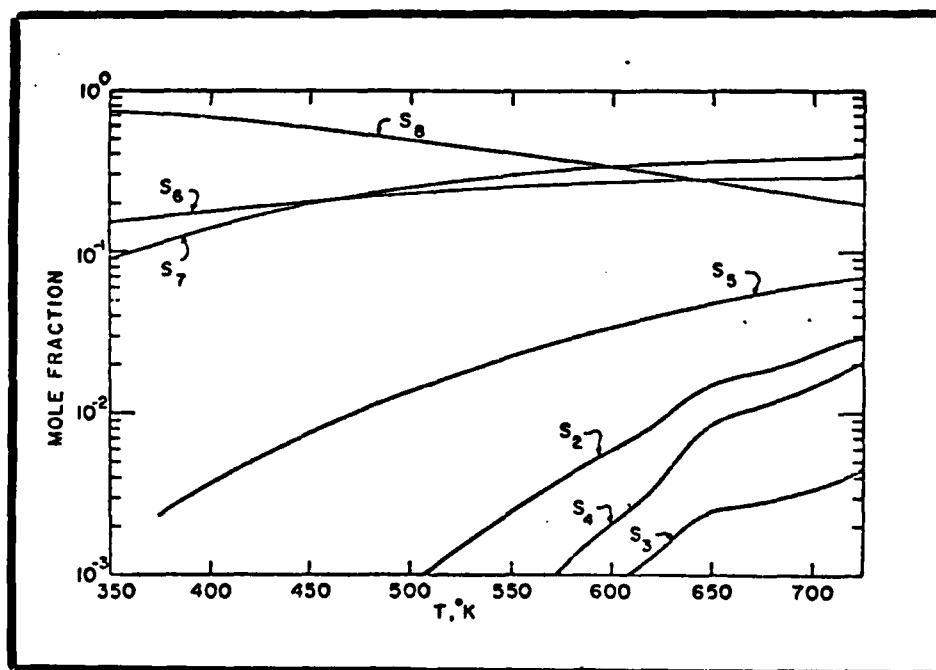

Figure 29.   Concentrations of Various Species in Saturated
Vapor for Room Temperature to Boiling Point of
Sulfur (Ref 18:149)

approximately .09 torr using .03 mole fraction of S_2 shown in Figure 29.

Four possible mechanisms which might cause the decrease in intensity with temperatures above 410°C were described by Robbins (Ref 4:45-47) and could apply here. These are discussed below. First as will be shown later in this section, the quenching rate Q_9 may be increasing due to increasing pressure. At a constant temperature, quenching can be approximated by the equation

$$Q_9 \approx q_r P \qquad (29)$$

where q_r is the quenching rate constant and P the pressure. As the pressure increases, depopulation of the $v'=9$ excited level through nonradiative means reduces the observed fluorescence. Another mechanism is the pressure dependence of sulfur vapor molecular concentrations. The concentration of each sulfur molecule (S_8, S_7, S_6, etc.) depends on both temperature and pressure. Where Figure 29 may describe the variation of the mole fractions of sulfur molecules at one pressure it does not necessarily describe the variation at a different pressure. In the present case, since the intensity is decreasing, S_2 molecules may be recombining to form different molecules, thereby decreasing the S_2 concentration. Self absorption of the fluorescent radiation is the third process that may contribute to reduction in intensity with higher temperatures. In this process a photon emitted is immediately reabsorbed by a neighboring like molecule or species which has a matching absorption wavelength. The probability of this happening increases as the number density increases. Furthermore, the reabsorbed radiation may be re-emitted in a different direction and/or at a different wavelength.

As a result, the fluorescence intensity at the original wavelength may decrease as self absorption increases. However, since the terminal state in the (9→6) transition, v''=6 is approximately 4300 cm^{-1} above the ground vibrational state, the fractional population of the v''=6 state is negligible even at 600°C. Thus, this effect can be neglected as the responsible mechanism. The fourth mechanism is the thermal distribution of the rotational levels. As shown in Figure 30 below the population of an individual vibrational-rotational level $N_{J,v}$ is greatly influenced by the temperature. If, as the temperature increases, there are fewer molecules populating the ro-vibrational levels which are within the bandwidth of the excitation beam, the fluorescence observed will decrease. (9→6) fluorescence peak scans versus temperature might verify this.
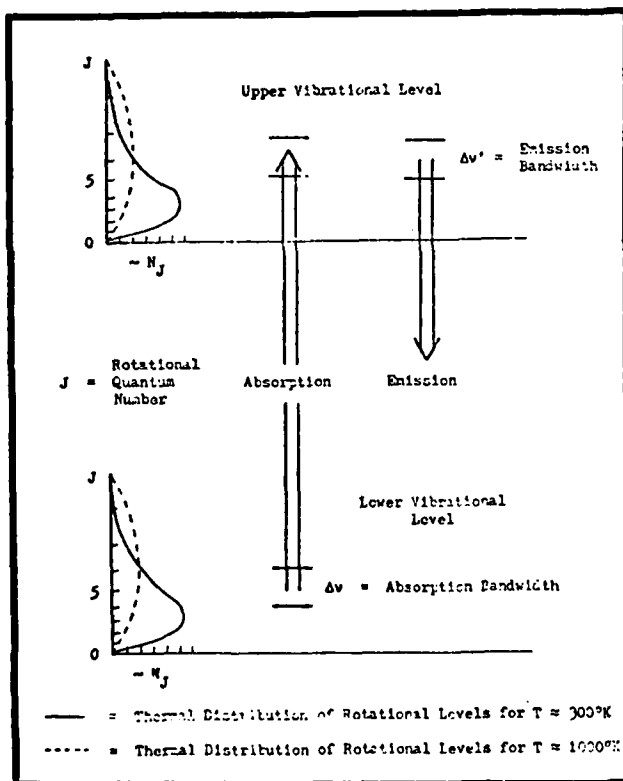

Figure 30. Thermal Distribution of Rotational Levels (Ref 4:16)

END
DATE
FILMED
83
DTIC
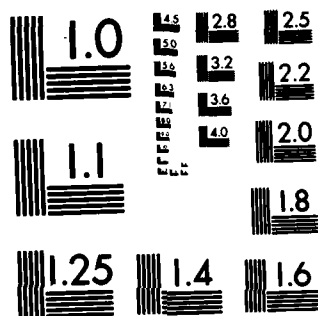
MICROCOPY RESOLUTION TEST CHART
NATIONAL BUREAU OF STANDARDS-1963-A

The seven fluorescence intensity versus pressure measurements are
listed in the table on the next page. The maximum fluorescence intensity
occurred for the 3.47 torr tube. As shown in Table V the intensity
of the fluorescence from the 12.58 torr tube was, on the average, 29%
of the 3.47 torr tube. The standard deviation for this percentage was
15.2%. A comparison of the ratio of the standard deviation to the average
percentage for tube two was .52 while that for tube three, .12. The
larger ratio for tube two may be due to absorption effects. Although
calipers were routinely used to ensure the distance "a" from a given
sample tube's front window to the observed fluorescing volume did not
change from trial to trial, small errors in placement would have been
more critical for tube two because it contained the highest pressure and
therefore the highest absorption.

One of twelve photographs used to measure the radiative lifetime
of the (9→6) fluorescent transition is shown in Figure 31 below.
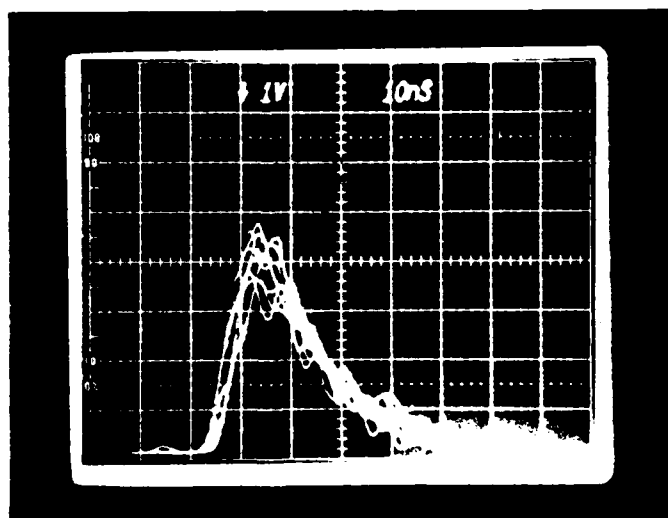
Figure 31.   Effective Lifetime Measurement

Table V

Summa v of v'=9, v"=6 Fluorescence Intensity

vs Pressure Measurements

Tube	Pressure	Trial	1	2	3	4	5	6	7	Avg	Std Dev
1	3.47		1.00	1.00	1.00	1.00	1.00	1.00	1.00	1.00	0
2	12.58		.228	.135	.136	*	.512	.406	.325	.291	.152
3	0.31		.00352	.00313	.00415	*	.00357	.00337	.00436	.00368	.00047

* Flashlamp broke during this trial.

Using these photographs the effective lifetimes listed in Table VI were determined.

Table VI Summary of Effect Lifetime Measurements

Pressure at (5 °C)	Effective Lifetime
0.31 torr	27 ± 4 nsec
3.47 torr	22 ± 3 nsec
12.58 torr	9 ± 2 nsec

Equation (9) from the theory section can be used to relate the effective lifetime τ_{eff} to τ_{rad} and quenching since the radiative lifetime τ_{rad} is the inverse of the Einstein A_{96} coefficient. Therefore,

$$\tau_{eff} = (^{1}/\tau_{rad} + A_9 + Q_9)^{-1} \tag{30}$$

Assuming A_9 remains relatively constant, the effective lifetime decreases when quenching increases. If quenching is approximated as a linear function of pressure, as in Equation (29), it becomes apparent that τ_{eff} decreases with increasing pressure. This was exactly the relationship observed in this experiment.

Figure 32 on the following page shows the Stern-Volmer plot used to determine the radiative lifetime of the v'=9 level and the quenching rate constant q. This plot is understood by considering Equation (30) in the form

$$\frac{1}{\tau_{eff}} = qP + C \tag{31}$$

PRESSURE [TORR]

INVERSE EFFECTIVE LIFETIME [X 10^7 SEC^{-1}]

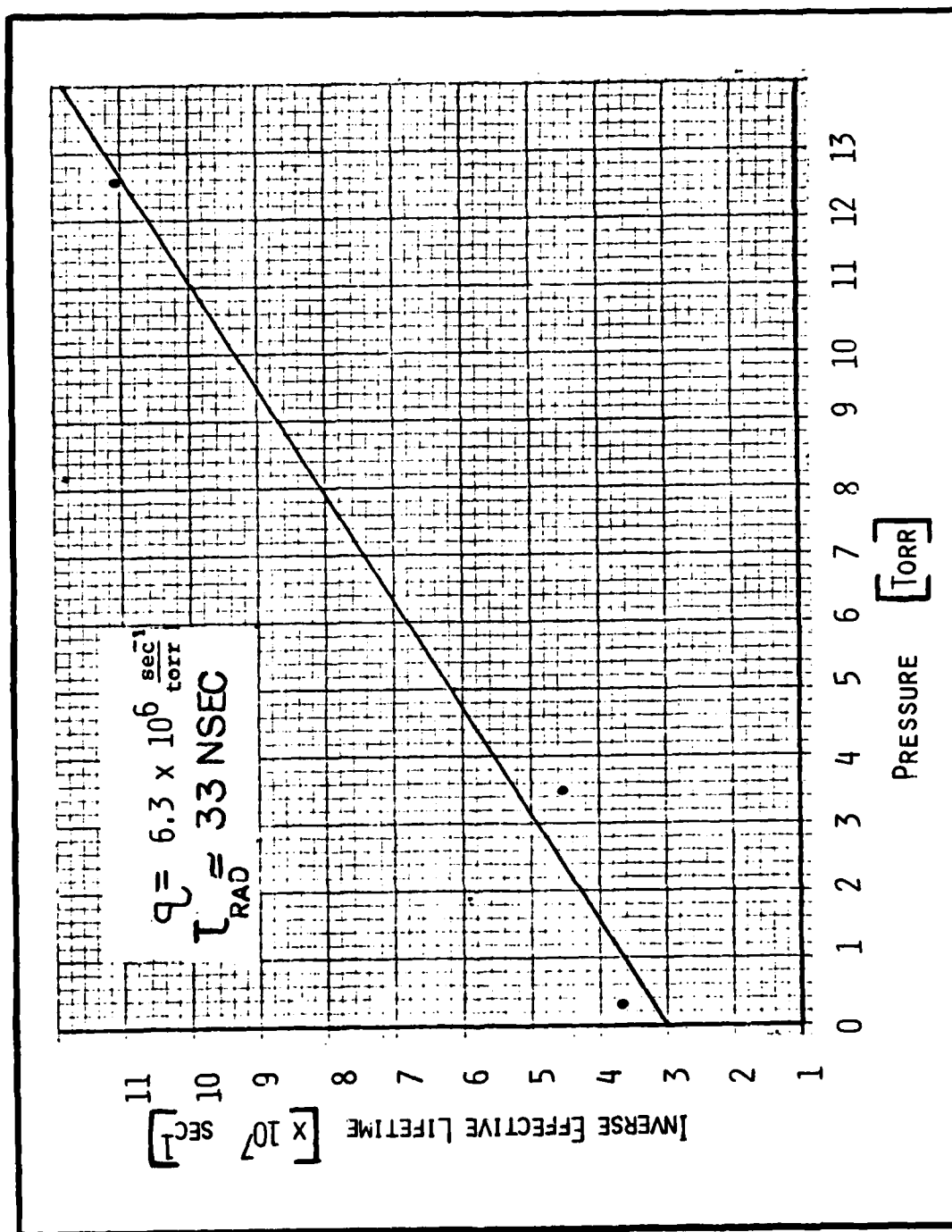$q = 6.3 \times 10^6 \; \frac{\text{sec}^{-1}}{\text{torr}}$

$\tau_{RAD} = 33 \; NSEC$

Figure 33. Stern – Volmer Plot

where

$$C = \text{constant} = \frac{1}{\text{rad}_{(9 \to 6)}} + A_9 = A_{96} + A_9 = \frac{1}{\text{rad}_{(v'=9)}} \quad .$$

In the Stern Volmer plot, the values of the inverse effective lifetime were plotted versus pressure. By taking a least squares fit line through these data points the slope, m, or as Equation (31) shows the quenching rate q, is determined. Using the quenching rate $q = 6.3 \times 10^6 \text{ sec}^{-1}\text{torr}^{-1}$ and Equation (29) the quenching rates in Table VII were determined for each of the pressures used.

Table VII.   Quenching Rates

Pressure (torr)	Quenching Q_9 (sec^{-1})
0.31	1.95×10^6
3.47	21.9×10^6
12.58	79.2×10^6

The radiative lifetime of the v'=9 level is found by finding the y intercept of the fitted line and taking its inverse. This results in $\tau_{\text{rad}_{(v'=9)}} \simeq 33$ nsec.

Self Absorption

The results of the self absorption measurement are shown in Figure 33. Because the (9→6) normalized relative intensities of the (9→5) through (9→1) transitions decreased with an increase in temperature it can be concluded that self absorption is indeed occurring.
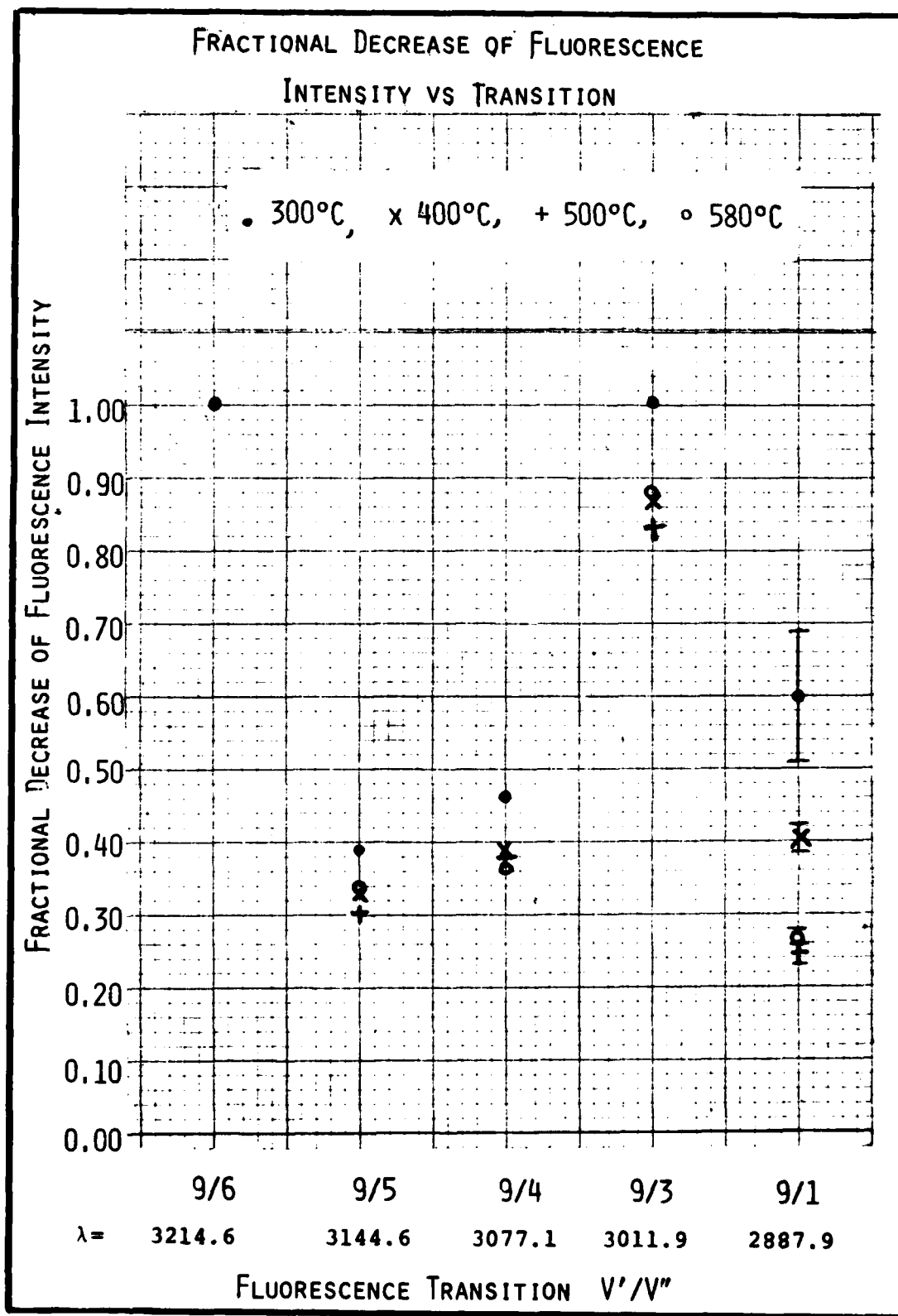
72

Figure 33. Fractional Decrease of Fluorescence Intensity vs Transition

VI Summary and Recommendations

This thesis continued the investigation of the feasibility of using laser induced fluorescence for S_2 concentration measurements of previous researchers. The ability to accurately measure S_2 concentrations would permit quantitative measurements of pumping efficiencies and lasing strengths of this potentially tunable, high-power, laser gain medium. The rate equation analysis of T. Robbins (Ref 16:11-30), modeling transitions within the $B^3\Sigma_u^- - X^3\Sigma_g^-$ system, was modified to model the v'=9, v"=6 transition at 3214.6 Å. Excitation spectra were obtained over the range of 2890 to 2810 Å clearly showing the v"=0, v'=8 and v"=0, v'=9 absorption bands. Wavelengths corresponding to the fluorescence maximum for the (9←0) and (8←0) excitation spectra were determined. These wavelengths were then used while fluorescence scans of the (8→1) through (8→24) and (9→1) through (9→25) were taken. After these broad band spectra were identified fluorescence intensity of the prominent peaks (8→4) and (9→6) versus excitation wavelength measurements were made. Further investigations of the (9→6) transition included fluorescence intensity versus temperature, laser power measurements, and pressure, effective lifetime measurements, and a quenching analysis. Data was generally taken at near 600°C to ensure a large percentage of S_2. Fluorescence intensity versus pressure measurements did, however, reveal fluorescence intensities at 12.58 torr were on the average 29% that of the intensity at 3.47 torr.

Recommendations

Many experiments which were not possible before can now be performed

on the upgraded equipment/system. Continued use of this system for
concentration measurements using laser induced fluorescence should prove
fruitful. Specific recommendations for future research of the laser
induced fluorescence technique include:

1. Installation of a Fabry-Perot etalon to reduce
   excitation beam linewidth, and therefore, increase resolution.

2. Secure an advanced model two channel boxcar integrator
   would be useful when normalizing signals.

3. Incorporate stimulated emission and rotational effects into
   the rate equation model to improve its accuracy.

4. Determine a method for taking excitation scans without beam
   walking occurring, yet not use an absorbing filter.

5. Use sample tubes which allow the same pathlength from front
   window to observed fluorescence volume to reduce absorption
   effects.

6. Secure a calibrated source or detector for the ultraviolet
   region.

7. Develop a method of heating and cooling the oven quickly.

8. Use a quartz focusing lens to saturate the transition under
   investigation.

9. Perform concentration measurements on a microwave or radiowave
   produced discharge to ensure a more exact S_2 percentage.

Bibliography

1. Leone, Stephen R. and Kenneth G. Kosnik. "A Tunable Visible and Ultraviolet Laser on S_2 $(B^3\Sigma_u^- - X^3\Sigma_g^-)$," *Applied Physics Letters*, **30**, (7): 346-348 (April 1977).

2. Peterson, Drew A. *Pure Sulfur Discharges and Associated Spectra*. MS Thesis. Wright-Patterson Air Force Base, Ohio: Air Force Institute of Technology, October 1978. (AD A064-762).

3. Peterson, D.A. and L.A. Schlie. "Stable Pure Sulfur Discharges and Associated Spectra," *Journal of Chemical Physics*, **73**, (4): 1551-1566 (August 1980).

4. Robbins, Tyrie R. *Investigation of Laser Induced Fluorescence for Concentration Measurements of Diatomic Sulfur*. MS Thesis. Wright-Patterson Air Force Base, Ohio: Air Force Institute of Technology, December 1981. (AD-A064-762).

5. Wharton, John J., Jr. *Lifetime Measurements Using Fluorescence Emission*. MS Thesis. Wright-Patterson Air Force Base, Ohio: Air Force Institute of Technology, December 1977. (AD A055-420).

6. Crosley, David R. "Laser Induced Fluorescence in Spectroscopy, Dynamics, and Diagnostics," *Journal of Chemical Education*, **50**: 446-455 (June 1982).

7. Baronavski, A.P. and J.R. McDonald. "Application of Saturation Spectroscopy to the Measurement of C_2, $^3\pi_u$ Concentrations in Oxy-acetylene Flames," *Applied Optics*, **16** (7): 1897-1901 (July 1977).

8. Baronavski, Andrew P. and J.R. McDonald. "Measurement of C_2 Concentrations in an Oxygen-acetylene Flame: An Application of Saturation Spectroscopy," *Journal of Chemical Physics*, **66** (7): 3300-3301 (April 1977).

9. Daily, John W. "Pulsed Resonance Spectroscopy Applied to
    Turbulent Combustion Flows," *Applied Optics*, 15 (4): 955-960
    (April 1976).

10. Daily, John W. "Saturation Effects in Laser Induced Fluorescence
    Spectroscopy," *Applied Optics*, 16 (3): 568-571 (March 1977).

11. Piepmeier, E.H. "Theory of Laser Saturated Atomic Resonance
    Fluorescence," *Spectrochimica Acta*, 27B: 431-443 (1972).

12. Calvert, Jack G. and James N. Pitts, Jr. *Photochemistry*. New York:
    John Wiley and Sons, Inc.

13. Herzberg, Gerhard. *Molecular Spectra and Molecular Structure,*
    Volume I: Spectra of Diatomic Molecules (Second Edition). New York:
    Van Nostrand Reinhold Company, 1950.

14. Siegman, A.E. *An Introduction to Lasers and Masers*. New York:
    McGraw-Hill Book Company, 1971.

15. Eckbreth, Alan C., Paul A. Bonczyk and James F. Verdieck. *Review*
    of Laser Raman and Fluorescence Techniques for Practical Combustion
    Diagnostics. Task I Technical Report, UTRC R77-952665-6. Ease
    Hartford, Connecticut: United Technologies Research Center, February, 1977.

16. Pedrotti, Leno S. *Laser Physics I*. PH 7.43 Course Notes. Wright-
    Patterson Air Force Base, Ohio: Air Force Institute of Technology
    Physics Department, 1982.

17. Roh, Won B., Assistant Professor of Physics. Personal conversation.
    Wright-Patterson Air Force Base, Ohio: Air Force Institute of
    Technology Physics Department, 1982.

18. Meyer, Beat, ed. Elemental Sulfur, New York; Interscience
    Publishers, 1965.

19. Gray, Dwight E., Coord. ed. American Institute of Physics Handbook
    (Third Edition). New York: McGraw-Hill Book Company, 1972.

20. Anderson, William R., David R. Crosley, and John E. Allen, Jr.
    "Franck-Condon Factors for the B-X System of S_2," Journal of
    Chemical Physics, 71 (2): 821-829 (July 1979).

21. Braune, Von H., S. Peter, and V. Neveling. "Die Dissociation des
    Schwefeldampfes (The Dissociation of Sulfur Vapor)," Zeitschrift
    fur Naturforschg, Teil 6a: 32-37 (1951).

Vita

William D. Harris, Jr. was born on July 26, 1955 at Hamilton AFB, California and graduated from high school in Commerce, Texas in 1973. He attended East Texas State University in Commerce, Texas and graduated with a Bachelor of Science degree in Mathematics with a second major in Physics in 1977. Captain Harris completed the Basic Meteorology program and received a second Bachelor's degree in meteorology from The Pennsylvania State University in 1978 and was assigned to Det 16, 9th WS, 3rd Weather Wing, (MAC) at Dyess AFB, Texas. While stationed at Dyess, he served as SAC Wing Weather Officer to the 96th Bombardment Wing (Heavy). Captain Harris entered the Air Force Institute of Technology in June 1981.

Permanent address: P.O. Box 931

Commerce, Texas 75428

REPORT DOCUMENTATION PAGE	READ INSTRUCTIONS BEFORE COMPLETING FORM

1. REPORT NUMBER	2. GOVT ACCESSION NO.	3. RECIPIENT'S CATALOG NUMBER
AFIT/GEP/PH/82D-10	AD-A124 760	

4. TITLE (and Subtitle)	5. TYPE OF REPORT & PERIOD COVERED
INVESTIGATION OF THE FEASIBILITY OF USING LASER INDUCED FLUORESCENCE FOR CONCENTRATION MEASUREMENTS OF DIATOMIC SULFUR	MS Thesis
	6. PERFORMING ORG. REPORT NUMBER

7. AUTHOR(s)	8. CONTRACT OR GRANT NUMBER(s)
William D. Harris, Jr. Captain USAF	

9. PERFORMING ORGANIZATION NAME AND ADDRESS	10. PROGRAM ELEMENT, PROJECT, TASK AREA & WORK UNIT NUMBERS
Air Force Institute of Technology (AFIT-EN) Wright-Patterson AFB, Ohio 45433	Project 2301-51-17

11. CONTROLLING OFFICE NAME AND ADDRESS	12. REPORT DATE
Aerospace Power Division/POOC-3	December, 1982
Air Force Aero Propulsion Laboratory	13. NUMBER OF PAGES
Wright-Patter AFB, Ohio 45433	89

14. MONITORING AGENCY NAME & ADDRESS(if different from Controlling Office)	15. SECURITY CLASS. (of this report)
	Unclassified
	15a. DECLASSIFICATION/DOWNGRADING SCHEDULE

16. DISTRIBUTION STATEMENT (of this Report)

Approved for public release; distribution unlimited

17. DISTRIBUTION STATEMENT (of the abstract entered in Block 20, if different from Report)

18. SUPPLEMENTARY NOTES

Approved for public release: IAW AFR 190-17 Approved for public release; IAW AFR 190-17

LYNN E. WOLAVER
Dean for Research and Professional Development
Air Force Institute of Technology (AFIT)
Wright-Patterson AFB OH 45433

16 JAN

19. KEY WORDS (Continue on reverse side if necessary and identify by block number)

Laser Induced Fluorescence
Diatomic Sulfur
Concentration Measurements

20. ABSTRACT (Continue on reverse side if necessary and identify by block number)

The feasibility of using laser induced fluorescence to measure total S_2 number densities in a laboratory environment is studied. A rate equation analysis modeling transitions within the $B^3\Sigma_u^- - X^3\Sigma_g^-$ system of S_2 is developed and applied to model the $v'=9$, $v''=6$ transition at 3214.6 Å. Excitation spectra were obtained over the range of 2890 to 2810 Å clearly showing the $v''=0$, $v'=8$ and $v''=0$, $v'=9$ absorption bands. Fluorescence scans of the $v'=8$, $v''=1$ through 24 and $v'=9$, $v''=1$ through 25 were taken. After these broad spectra were identified. further investigations of the $v'=9$, $v''=6$ transition included

DD $_{1 \text{ JAN } 73}^{\text{FORM}}$ 1473   EDITION OF 1 NOV 65 IS OBSOLETE

fluorescence intensity versus temperature, laser power, and pressure.
Additional measurements of quenching, radiative lifetime and self absorption
are made.